BIOGEOCHEMICAL AND ECOHYDROLOGIC CONTROLS ON ARSENIC MOBILIZATION IN GROUNDWATER OF THE OKAVANGO DELTA

by

HERSY J ENRIQUEZ

B.S.C.E. CALIFORNIA STATE POLYTECHNIC UNIVERSITY, POMONA

A THESIS

submitted in partial fulfillment of the requirements for the degree

MASTERS OF SCIENCE

Department of Civil Engineering
College of Engineering

KANSAS STATE UNIVERSITY
Manhattan, Kansas

2014

Approved by:

Major Professor
Dr. Natalie Mladenov

Abstract

The detrimental health effects of arsenic (As) contamination have motivated the study of As mobility around the globe. The variability in naturally occurring As concentration is due to variation in geology and climate. In arid environments with high evaporation, ecohydrology and As desorption under alkaline pH are thought to be responsible for high As concentrations. In reducing groundwater, on the other hand, microbial iron (Fe) reductive dissolution is known to release As into solution. In such environments, As-sulfide minerals precipitation and vegetation uptake could contribute to re-distribution of As. The Okavango Delta is an arid-zone wetland punctuated by ten of thousands of islands, and the reducing groundwater beneath these islands have dissolved As as high as 3000 $\mu g \cdot L^{-1}$. Ecohydrologic controls are thought to contribute to the elevated As level; however dissolution of Fe-containing sediments has been proposed as the initial step in releasing As from sediment to the groundwater. To test the consistency of the hypothesized mechanisms, four islands were sampled in January 2013. The goal of this thesis is to: 1) provide more evidence on the zones of elevated As in groundwater of four islands, 2) gain understanding on the influence ecohydrology (i.e., evapotranspiration) on high As in groundwater, 3) evaluate the sediment of microbial community composition, and 4) gain new insights into the behavior of DOM along the groundwater flow path. The findings show zones of elevated As in all four islands. The ecohydrologic controls provide information on the location of high As and solute accumulation. Microbial analyses suggest DNA sequences collected were grouped within lineages that contain organisms capable of dissimilatory Fe reduction and sulfate reduction. This supports evidence from previous study that sulfide produced by microbial sulfate reduction is available for As-sulfide mineral formation. The variation of DOM characteristics could influence As solubility and reactivity. In addition, carbonate alkalinity and increase pH

may contribute to As mobility further along the flow path. In this arid and reducing groundwater, we find that ecohydrologic and biogeochemical processes have a fundamental role in As mobility.

Table of Contents

List of Figures

List of Tables

Acknowledgements

The success and final outcome of this project required a lot of guidance and assistance from many people and I could not have completed this project without them.

I wish to express my sincerest gratitude to Dr. Natalie Mladenov for her continuous guidance and encouragement throughout my graduate studies and this research project. This research could not have been successful without the assistance of great scientists from Okavango Research Institute (ORI), Dr. Mike Murray-Hudson, Dr. Piotr Wolski, I. Mosie, Ndobano Lokae, Tshephi Mosimane. Field sampling could not had been fun and possible without the support and company of ORI. I am truly thankful to Buddhika Galkaduwa for her immeasurable help in all the analyses in their lab. This project would not have been complete without her help. I am also thankful for Dr. Siva Damaraju his assistance in the lab and Harshad for his willingness to help with Matlab and GIS. To the rest of my committee, Dr. Matthew Kirk and Dr. Ganga Hettiararchchi, I sincerely thank their guidance in making me understand this very complex project.

I would also like to thank my first mentor, Dr. Monica Palomo, who had encouraged me to pursue a graduate degree and apply to her Alma Mater, K-STATE! Thanks to my family and friends in California who were willing to listen to my complaints about Kansas' unpredictable weather. Last, thanks to Aida Guido for introducing me to Natalie, and needless to say, I would not be here at K-State if not for her.

Support for this project came from the National Science Foundation (grant NSF OISE Project #1105289). I am also grateful to the Government of Botswana for permitting this research. Without this funding and research permit, this research project would not have been possible.

Chapter 1 - Introduction

1.1 Background on Arsenic (As)

Arsenic (As) is a naturally occurring trace element and one of the most abundant elements found in our earth's crust, but a high level of As in drinking water is problematic and toxic for human consumption (Ravenscroft et al., 2009). More than 70 countries are affected by As contamination (Ravenscroft et al., 2009) either by natural or anthropogenic contamination, but the most widely-studied instances natural As contamination are Argentina, Bangladesh, Chile, China, Hungary, India (West Bengal), Mexico, Romania, Taiwan, Vietnam and many parts of the USA, particularly the southwest region (Figure 1-1). Countries affected by As contamination due to mining are Ghana, Greece, Thailand and some parts of the US (Figure 1-1).

Figure 1-1. Location of major aquifers affected by As contamination (*from Smedley and Kinniburgh, 2002*)

There are several theories regarding As mobilization (Smedley and Kinniburgh, 2002; Ravenscroft et al., 2009). This overview section focuses on the different mechanisms controlling As mobility in natural waters. The mobilization of As from sediments into groundwater and surface water is a natural process, but could be enhanced by anthropogenic activities (Neumann et al., 2010). Although most As groundwater contamination is caused by natural processes, high As levels in some parts of the world are due to human contribution, such as disposal of waste from coal and metal mining and usage of arsenical pesticide (Smedley and Kinniburgh, 2002).

The major factor affecting the fate of As in groundwater is the reduction and oxidation (redox) condition of the aquifer. In reducing groundwater, As is mostly found as As (III), the toxic and mobile form of As while As (V), which has higher affinity to sorb into sediments is more prevalent under oxidizing conditions (Ravenscroft et al., 2009; Smedley and Kinniburgh, 2002; Gao et al., 2006). Ravenscroft et al. (2009) described three main mechanisms for As mobility in groundwater. Microbial reductive dissolution is possibly the most documented As pollution mechanism in reducing aquifers. Thus, constant supply of carbon source (i.e., abundance of DOM) to the aquifer will enhance Fe-reductive dissolution resulting in As reduction. The second case is alkali desorption, the desorption of As under oxidizing conditions, and high pH. Alkali desorption of As typically occurs in high dissolved oxygen (DO), nitrate (NO_3^-) and sulfate (SO_4^{2-}) environments (Welch and Lico, 1998; Gao et al., 2006). Last, sulfide (e.g., Fe-As-sulfide minerals) oxidation typically occurs under oxidizing conditions and could release As to natural waters (Rochette et al., 2000; Fisher et al., 2008; Langer et al., 2011).

1.1.1 Health risk of elevated arsenic

Elevated As in drinking water, air and soil poses a health risk through different exposure pathways: airborne pathway, dermal pathway, and ingestion. The airborne pathway of As comes from coal-burning power stations, aerial pesticide spraying and even cigarette smoking. Among

the different exposure pathways for As contamination, drinking water contaminated by As probably poses more threat (Smedley and Kinniburgh, 2002). Drinking As-contaminated water and ingesting crops from As-contaminated soil and/or irrigated with As-contaminated water are commonly the path for As exposure in the human body. The lethal dose of As, if absorbed into human body, is 1 to 3 $mg \cdot kg^{-1}$ and the World Health Organization (WHO) sets the limit of As in drinking water at 10 $\mu g \cdot L^{-1}$. In addition, there are geographical differences on the severity on health effects of As contamination, which are influenced by variations in As concentrations, species, dietary and nutrition practices, genetics and possibly improper diagnosis of the source of contamination.. In natural water, As (III) is the more mobile and toxic species of As than As (V)

1.1.2 Sources of Arsenic

The dissolution of As to groundwater comes from various sources. The enrichment of As in sedimentary and metamorphic rocks and some consolidated sediments are higher compared to other types of rocks (Ravenscroft et al., 2009). In sedimentary rocks, the average As level measured range from 5 to 10 $mg \cdot kg^{-1}$ (Smedley and Kinniburgh, 2002; Ravenscroft et al., 2009). Unconsolidated sediments, such as alluvium and loess silts, typically contain 3 to 10 $mg \cdot kg^{-1}$ of As (Smedley and Kinniburgh, 2002). Although the concentration of As in unconsolidated soil is less than As found in sedimentary and metamorphic rocks, the concentration of As in natural waters is partly driven by the parent source.

1.1.3 Arsenic speciation in natural water

Arsenic can occur in several oxidation states (-3, 0, +3 and +5), but in natural waters, it is mostly found in inorganic form as arsenite (As^{3+}) or arsenate (As^{5+}) (Smedley and Kinniburgh, 2002; Ravenscroft et al., 2009). In addition, As generally exists as an oxyanion with water; for

example as AsO_4^{3-} for arsenate and $As(OH)_4^-$ for arsenite (Fujii et al., 1995) (Figure 1-2). Redox potential and pH are very important in predicting As speciation in natural water (Smedley and Kinniburgh, 2002). Under oxidizing condition, arsenate is most dominant. Reducing conditions, on the other hand, occur in iron (Fe) and manganese (Mn) rich environments that are low in DO and NO_3^-, and the pool of As is mostly dominated with arsenite species. Arsenite and arsenate oxyanions undergo a similar series of dissociation reactions from $H_3AsO_4^0$ to $H_2AsO_4^-$ and $HAsO_4^{2-}$ (Ravenscroft et al., 2009). The main difference between the behavior of arsenate and arsenite oxyanions is that uncharged arsenite predominates in pH less than 9.2 while uncharged arsenate occurs in extremely acidic environments (Ravenscroft et al., 2009). The ability of uncharged arsenite to stay in solution at a wide pH ranges limits its sorption affinity unlike arsenate where it predominantly exists as charged oxyanion (Ravencroft et al., 2009; Smedley and Kinniburgh, 2002). To fully understand As speciation, the potentiality of arsenite to protonate has to be considered. In reducing aquifers, extremely high levels of sulfide (S) will precipitate orpiment (As_2S_3), realgar (AsS) or other As-S minerals (Cullen and Reimer, 1989; Smedley and Kinnirburgh, 2002; Kirk et al., 2004).

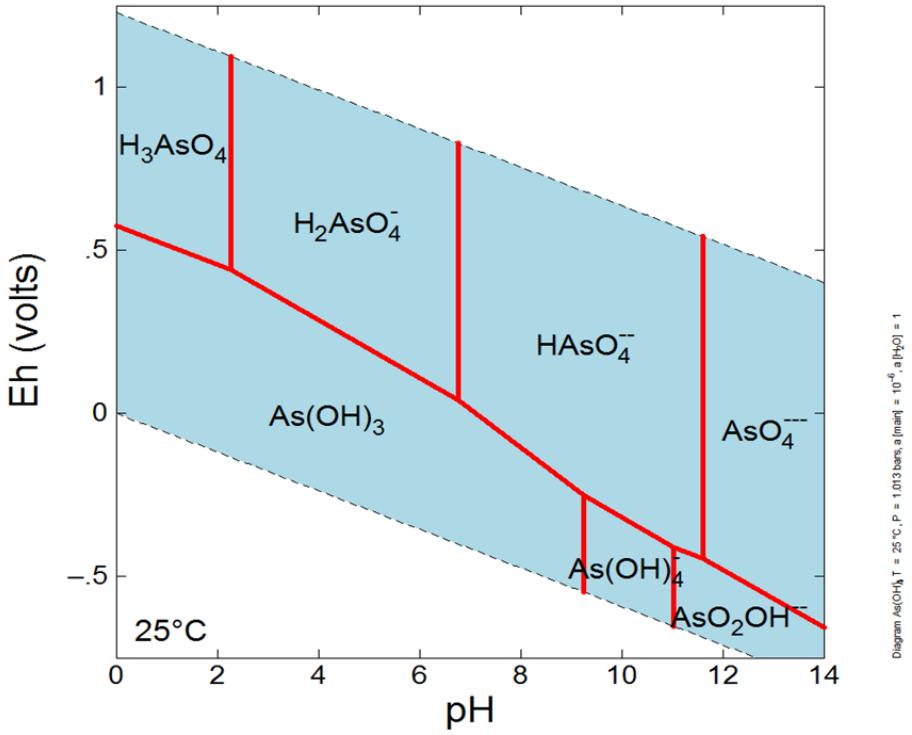

Figure 1-2. Speciation diagram of As in natural waters (*from Geochemist Workbench*).

1.2 Global Arsenic Distribution

1.2.1 Reducing Aquifers

In groundwater aquifers, there is a zonation of microbial groups capable of using certain e- acceptors (Box 1.1). The Thermodynamic ladder in geomicrobiology (Figure 1-3) of aquifers arranges microorganisms in order of most energetically favorable microbial reaction to occur (Champ and Jackson, 1979; Bethke et al., 2011). The thermodynamic ladder of geomicrobiology generally occurs in reducing aquifers, where microorganisms use the most energetically favorable e- acceptors, which are listed in order of most favorable: nitrate (NO_3^-), Fe (III), sulfate (SO_4^{2-}), and carbon dioxide (CO_2).

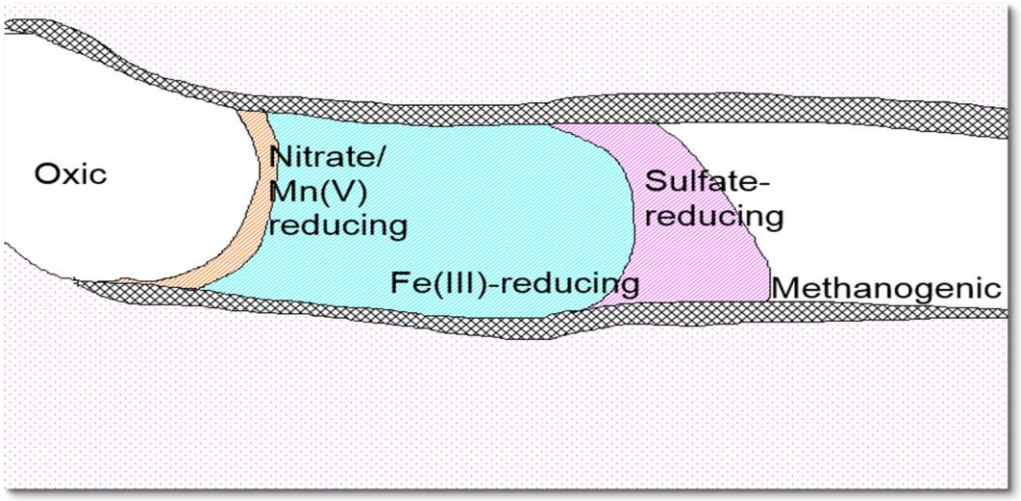

Figure 1-3. Thermodynamic ladder in Geomicrobiology
(*Adapted from Champ et al., 1979; Lovley et al., 1994*)

Microbial reductive dissolution is the main mechanism controlling As mobilization in reducing environment. The stability of As in iron (Fe)-, manganese (Mn)-, and aluminum (Al)-oxide and clay sediments (Ravenscroft et al., 2009) and abundance of organic matter (Mladenov et al., 2010) are two components in driving microbial reduction process. Microorganisms use labile organic matter as electron (e-) donors and e- acceptors (i.e., NO_3^-, Fe (III), SO_4^{2-}, CH_4) for their metabolism. Typically, As adsorbs onto iron-oxides, particularly ferrihydrite ($Fe(OH)_3$) and goethite (FeOOH). Thus the presence of Fe-respiring microbes reduces Fe (III) with sorbed As (V) to Fe (III) and also reduces As (V) to As (III). After release of As from sediments, sorbed As tends to stay in solution and accumulates over time. In aquifers with high levels of S, As tend to form orpiment (As_2S_3) or other As-S minerals (Kirk et al., 2004; Smedley and Kinniburgh, 2002; Langer et al., 2011).

Elevated As in the aquifers of the Bengal basin, particularly Bangladesh, is probably the most documented occurrence of As contamination in the world (Ahmed et al., 2004; Smedley and Kinniburgh, 2002; Zheng et al., 2004; McArthur et al., 2004; Ravenscroft et al., 2009; Mladenov et al., 2010). The range of As concentration found in aquifers of Bangladesh is from

0.5 to 2500 $\mu g \cdot L^{-1}$, which exposes 30 million people to drinking As contaminated water (Smedley and Kinniburgh, 2002). The initial hypothesis of As contamination in Bangladesh was oxidation of As-rich pyrite due to the lowering of water table by irrigation tube wells. This hypothesis was ruled out, and now the accepted interpretation is the microbial reductive dissolution of Fe oxides (Ravenscroft et al., 2009; Ahmed et al., 2004). Decomposition of soil organic matter (SOM) and oxidation of other dissolved organic matter (DOM) in the groundwater produces a strong reducing environment (Ravenscroft et al., 2009; Chin et al., 1998). Understanding the mechanisms transforming DOM (i.e., microbial processing of DOM) under reducing conditions can provide new insights into the controls on As mobilization in aquifers of Bangladesh and possibly other reducing aquifers (McArthur et al., 2004; Mladenov et al., 2010).

1.2.2 Oxidizing Aquifer

Contamination of As under reducing condition has been greatly documented, but oxidation mechanisms are also important for As mobilization (Smedley et al., 2008). The desorption of As (V) from sediments at high pH is the main control on high As levels under oxidizing conditions (Smedley and Kinniburgh, 2002; Gao et al., 2004; Ravenscroft et al., 2009). The adsorption affinity of As (V) onto Fe oxides tends to be stronger with lower pH, and it becomes unstable at pH range of 8.5 to 9.5 (Smedley et al., 2008).

The Chaco-Pampean plains aquifer is shared between Paraguay, Uruguay and Bolivia, perhaps the largest high As area in the world, extending over 1 million km^2, and the high As concentration exposes 1 million people to the health effects of As contamination (Smedley and Kinniburg, 2002). A number of documented studies measured As concentration as high as 100 $\mu g \cdot L^{-1}$ on average, and some samples are over 1000 $\mu g \cdot L^{-1}$ (Smedley et al., 2008). Accumulation by evaporation may be partially responsible for high As levels in La Pampa, Argentina (Smedley

et al., 2008). However, alkali desorption is the main mechanism in releasing As into aqueous solution because of the abundance of Fe-, Mn-, Al- oxides in sediments, which are known to be important component in the As cycle of dissolution and precipitation (Smedley et al., 2008; Ravenscroft et al., 2009). Another process that indirectly affects As release into solution is the hydrolysis of silicate minerals, such as kaolinite and other clay sediments. This process results in high carbonate concentration causing pH and alkalinity to raise thus desorbing As (V) into solution (O Sracek interview qtd. in Ravenscroft et al., 2009). Furthermore, weathering of silicate minerals, such as apatite, results in release of phosphorus (P), which is believed to outcompete As for sorption sites (Smedley et al., 2008). The presence of P thus increases the As mobility into groundwater.

1.2.3 Mixed oxidizing and reducing environment

The southwest US, particularly Nevada, California and Arizona, is the most affected by As contamination. Elevated arsenic (As) is a concern in parts of Tulare Basin of San Joaquin Valley, California, especially in drainage and shallow groundwater. The aquifer's redox condition varies with well depth characterized by proportion of trivalent As (Smedley and Kinniburgh, 2002). Desorption of As (V) from iron oxides is the main mechanism driving As contamination in shallow aquifers of Tulare Basin. In the deeper aquifers, As (III) level increase, which suggests more reducing environment (Smedley and Kinniburgh, 2002)? In more arid areas, such as Nevada and Arizona, the evaporation and transpiration is thought to control the accumulation of As in groundwater (Smedley and Kinniburgh, 2002).

1.2.4 Sulfide oxidation and mining related arsenic contamination

As-S minerals, such as orpiment or realgar, and pyrite (FeS), are often used as a gold mineralization indicator in gold mining industry (Lengke and Tempel, 2004). Oxidation of pyrite, commonly associated with mining, mineral releases solid-phase As (V) into aqueous

solution, sulfate (SO_4^{2-}) and hydrogen ion (H^+) thus decreasing the pH and the solubility of As (V) (Lengke and Tempel, 2004; Ravenscroft et al., 2009). Sulfide oxidation can also occur when rivers or wetlands are drained, which causes increase in dissolve oxygen in water (Ravenscroft et al., 2009). Shallow wells are more susceptible to As contamination by sulfide oxidation due to water fluctuation. A study made in Ghana documented As contamination due to sulfide oxidation in mining environment. The highest As concentration observed was 64 $\mu g \cdot L^{-1}$, but it was found in the more reducing condition rather than closer to the vicinity of the gold mine (Smedley and Kinniburgh, 2002).

1.3 Background dissolved organic matter (DOM)

In aquatic and terrestrial ecosystem, dissolved organic matter (DOM) is a source of organic carbon, nutrients and sulfur derived mainly from plant degradation and microbial processing (book chapters Cory et al., 2011; McKnight et al., 2001). DOM is operationally defined as all natural organic matter passing through a binder-free glass-fiber filter with an average pore size less than 0.7 μm. The most commonly studied fraction of DOM is humic substances derived from plant degradation and amino acids derived from microbial processing. Humic substances, soluble in water, can be further divided into subcategories of humic acids and fulvic acids. Fulvic acids, defined as yellow, moderate molecular weight and soluble at all pH values, are known to be the dominant fraction of DOM in the DOM pool from surface water (45-65%) and wetlands (80-90%) (Aiken et al., 1985; Thurman, 1985; McKnight et al., 2001). In groundwater, fulvic acids only accounts for 10-30% of the DOM pool and mainly comprise of microbially processed DOM (Thurman, 1985). Measurement of DOC is natural waters has been the primarily measure of DOM (Thurman, 1985). However, characterization of DOM continue to evolve from traditional techniques including: 1) stable isotopes, ^{13}C and ^{15}N, analyses, 2) bulk properties C:N ratio, and 3) measurement of amino acid, carbohydrates and lignin phenol.

1.4 Background on Study Area

The Okavango Delta is a large alluvial fan located in the northwestern region of Botswana, Africa. Although the river does not discharge to a lake or an ocean, the delta-like features of this alluvial fan warrants the misnomer term delta. The Okavango River, which feeds most of the delta's water inflow, is unregulated thus maintaining a natural hydrologic regime. Over the years, increased population and thriving tourism industry delimited the delta for conservation and regulation. The Ramsar List of Wetlands of International Importance (Box 1) named the Okavango as the world's largest Ramsar site, which includes Okavango River, the entire delta, Lake Ngami and parts of the Kwando and Linyanti river system. Most recently, the Okavango Delta was listed as the 1000th World Heritage Site, and it is expected that this status will promote conservation of the ecosystem for years to come. The main threats to the area come from possible water extraction from the Okavango and Kwando rivers and their tributaries by the surrounding countries of Angola, Botswana, Namibia, and Zambia.

Box 1. *Ramsar List of Wetlands of International Importance*

Wetlands are vital to human life, and the consequences of the loss and degradation of wetlands could induce climate change, flooding, drought, pollution and species loss. Today, over half of the world's wetlands have already been destroyed which started the Convention on wetlands or commonly called Ramsar Convention. The chief objective is to "develop and maintain an international network of wetlands which are important for the conservation of global biological diversity and for sustaining human life through the maintenance of their ecosystem components, processes and benefits/services." www.ramsar.org

1.4.1 Location, vegetation, climate

The catchment of the Okavango River and delta are shared between three countries. The delta is annually flooded by water from the Angolan Highlands and inundates an area between 4000 km^2 and 13 000 km^2 (McCarthy et al 2007). The water enters the delta through the panhandle, which is confined by the graben structure, and loses confinement as water enters the delta proper. The Okavango Delta is situated in a semi-arid region that experience large annual fluctuation, and October being the hottest month and July as the coldest with maximum temperatures of 35^oC and 25^oC respectively. The Angolan Highlands, which is 600 km away from the delta, receives an approximate annual precipitation of 1,300 mm while the semi-arid region of Botswana accounts for 475 mm annually (Ramberg and Wolski, 2008). The hydrological inputs to the delta are 58% discharge from the Okavango River, 42% from rainfall, 1-2% leaves the delta through surface water outlet (Ramberg and Wolski, 2008). About 98-99% of water input is eventually lost by evapotranspiration that can lead to aqueous solution in surface water, soil water and shallow groundwater. Total dissolved solids (TDS) accumulation due to evapotranspiration, which is referred to as evapoconcentration, accounts to approximately 380,000 tons of TDS (composed mainly of calcium, magnesium and silica) annually, and only 5.5% of this is removed via surface water outlet (Ramberg and Wolski, 2008; McCarthy and Ellery 1998).

The delta is divided in three physiographical regions, a) panhandle, b) permanent swamps on the upper reach of the alluvial fan, and c) seasonal swamps on the lower part of the alluvial fan (Ellery et al 1993). The annual discharge to delta range from 6.0 x 10^9 to 1.64 x 10^{10} m^3 causing seasonal floods, which increases water level in the panhandle of up to 2 m and inundating the seasonal floodplain (McCarthy 2006). The major components of the delta are channels, wetlands and islands, which covers the area of almost 40 000 km^2 and about 150,000

islands ranging in size from small, irregular islands to large islands (Ramsberg and Wolski, 2008; Gumbricht et al, 2004). Initiated by termite mound, growth of the island has been hypothesized to be a result of termite activity and dust deposition (Ca) (60-70 % of islands volume) and chemical precipitation (<40 % of islands' volume) (McCarthy et al 2012). The islands were made up of medium to fine-grained sandy soils and constitute about 5% of the permanent swamp and 25% of the seasonal swamp (Gumbricht et al., 2004). Gumbricht et al. (2004) hypothesized that islands formation was due to physical and biological processes and could grow laterally and vertically by chemical precipitation and dust accumulation.

Dependent on vegetation cover and distribution, islands were delineated as Grassland islands, formed from regular flooding, and Salt islands, dominated by salt crusts or having a central salt crust partially surrounded by riparian woodland (Gumbricht et al., 2004). Salt islands are prominent in the lower reach of the delta, and the zonation of plant species is attributed to proximity to water source and water chemistry beneath the islands. On these islands, the island fringe is characterized by tall, dense woodlands, containing mainly evergreen trees and other woody plant species. The island interior, however, is virtually barren with sparse coverage of grass and trona (sodium-carbonate) encrusted soil (Ellery et al., 1993). The barren island interior is mainly attributed to the increasing salinity of the water beneath the island.

1.4.2 Solute transport beneath the islands of the Okavango Delta

The groundwater in the Okavango Delta is usually shallow, and evapotranspiration intensifies groundwater salinity and can trigger geochemical reactions, including mineral dissolution and precipitation. The transpiration by island vegetation causes a local lowering of the groundwater table affecting groundwater salinity beneath the islands of the Okavango Delta (McCarthy et al 2012). Studies have indicated that the islands act as a sink for solutes, impacting growth of the island through chemical precipitation and maintaining low solute loading in the surface water (McCarthy et al., 2012; Geiske, 1996; Ramberg and Wolski, 2007; Bauer-Gottwein et al., 2006). Gumbricht et al. (2004) and McCarthy et al. (2010) have hypothesized that the islands started as termite mounds and, because of mineral precipitation, the island grew over a period of time. Ultimately, as the density of groundwater increases, the brine becomes unstable leading to density fingering as suggested by Gieske (Zimmerman et al., 2006; Gieske, 1996). This solute transport mechanism therefore plays an important role in the salt balance of the whole Okavango delta.

Chapter 2 - Motivation

Natural As groundwater contamination in Africa lacks detailed documentation. Although the natural As contamination occurs in a small portion of the continent, evidence of the presence or absence of natural As contamination is not well-documented (Ravenscroft et al., 2009). The Okavango Delta is a relatively pristine wetland with very high evapotranspiration and DOM-rich surface water replenishing groundwater with DOC (Mladenov et al., 2008). Insights from this unique ecosystem could enhance our knowledge in developing a more efficient and sustainable design of constructed wetlands to treat water contaminated with trace elements. In addition, anthropogenic sources of organic carbon, such as landfill leaching and leaching of hydrocarbons from other sources, are likely promoting reductive dissolution of naturally occurring As in situ (Harte et al., 2012). Understanding the relationships between As and DOM may inform our understanding of As mobilization. In reducing groundwater environments with high amounts of DOM, elevated As may become an issue that can impact nearby drinking water supply.

Further understanding the role of microorganisms and DOM as controls on As distribution could give way to new solutions for treating groundwater As, particularly in areas with a large populations affected with As in their water supply. It has been suggested that stimulation of microbial SO_4^{2-} -reduction may be a way to inhibit As contamination in aquifers with limited SO_4^{2-}, which can precipitate As to form orpiment or other As-S minerals thus sequestering As (Kirk et al., 2004; Smedley and Kinniburgh, 2002). This could be sustainable and inexpensive remedial method for As contamination as long uncertainties regarding As-S precipitation are addressed. Therefore, what we learn from the Okavango Delta about the interactions between DOM, microbes, and metalloids in saline groundwater will aid scientists

and water managers in Botswana and also be broadly applicable to other arid-zone wetlands around the world.

Chapter 3 - Influence of evapotranspiration on the biogeochemical processes beneath the islands of the Okavango Delta

3.1 Introduction

In semi-arid regions, redox processes and evapotranspiration play an important role in the mobilization of As in groundwater. The Okavango Delta is situated in a semi-arid region that is known to have evapotranspiration exceeding precipitation (McCarthy and Ellery 1995; Ramberg and Wolski, 2008). The hydrological inputs to the delta are 58% discharge from the Okavango River originating from the Angolan Highlands and 42% from rainfall, while 1-2% leaves the delta through a surface water outlet, the Thamalakane River (Ramberg and Wolski, 2008). About 98-99% of the water input is eventually lost to evapotranspiration that can lead accumulation of total dissolved solids (TDS) in surface water, soil water and shallow groundwater. The concentrating effects of evapotranspiration (evapoconcentration) on TDS accumulation, composed mainly of calcium, magnesium and silica, accounts for approximately 380,000 tons annually, and only 5.5% of this is removed via the surface water outlet (Ramberg and Wolski, 2008; McCarthy and Ellery 1998).

It has been proposed that the groundwater of the Okavango, a generally reducing shallow aquifer, dissolves geogenic arsenic, transported from the Angolan Highlands, producing concentrations as high as 3000 $\mu g \cdot L^{-1}$ as a result of Fe-reductive dissolution and evapoconcentration (Huntsman-Mapila et al 2006). In other environments, such as the Bengal Basin, the high As level in groundwater is a combination of biogeochemical and hydrologic

processes (Harvey et al., 2006; Stute et al., 2007). As is released from the sediments via Fe-reductive dissolution (Ahmed et al., 2004; Ravenscroft et al., 2009; Smedley and Kinniburgh, 2002) and further mobilized by the local groundwater flow regime. In such environments, microbial reduction of sulfate (SO_4^{2-}) could precipitate As-S minerals contributing to the sequestration of As in groundwater (Smedley and Kinniburgh, 2002; Kirk et al., 2004; Langer et al., 2011).

Evapoconcentration and microbial Fe reduction are known to be controlling As mobilization in the groundwater of the southwest region of US (Gao et al., 2004; Welch and Lico, 1998; Smedley and Kinniburgh, 2002). The sources of As are variable and include As adsorption and desorption under the mixed reducing and oxidizing condition of the aquifer in the southwest region (Smedley and Kinnibugrh, 2002). In the Carson Desert, Nevada, largely reducing and lateral groundwater flow aquifers, known to have less intense evapotranspiration, contain higher As than that can be explained by evapoconcentration, and which may instead evolve from a combination of evapoconcentration and redox reactions (prevalent in reducing aquifer) (Welch and Lico, 1998). In the mixed reducing and oxidizing aquifer of the Tulare Basin, California, desorption of As from Fe oxide becomes more favorable at pH higher than 7 and is strongly influenced by evapotranspiration (Gao et al., 2004; Smedley and Kinnibrugh, 2002).

In the Chaco-Pampean plains aquifer, alkali desorption under oxidizing condition is posed to be the main mechanism in releasing As into aqueous solution because of the abundance of Fe-, Mn-, and Al- oxides in sediments, which are known to be important components in the As cycle of dissolution and precipitation (Smedley et al., 2008; Ravenscroft et al., 2009). Another process that indirectly affects As release into solution is the hydrolysis of silicate minerals, such as kaolinite and other clay sediments. This process results in high carbonate concentration

causing pH and alkalinity to rise thus desorbing As (V) into solution (Ravenscroft et al., 2009). Weathering of silicate minerals with phosphorus (P) inclusions, such as apatite, results in release of P, which is believed to outcompete As for sorption sites (Smedley et al., 2008). Presence of silicic acid (H_4SiO_4), PO_4^{3-}, DOM and HCO_3^- may be also enhancing desorption of As (III) and As (V) through competition for sorption sites (Smedley and Kinniburgh, 2002).

The quality and quantity of water inflow to the Okavango Delta, a closed system wetland, is very susceptible to changes in evapotranspiration and climate. In environments with known high evapotranspiration and mixed reducing and oxidizing aquifer, increasing evapotranspiration rate could enhance the mobility of As and other trace metal contaminants (e.g., uranium). Although many studies have been conducted over the past few years, much still remains to be know about the biogeochemical processes controlling As distribution in groundwater (Ahmed et al., 2004; Smedley and Kinniburgh, 2002; Ravenscroft et al., 2009), the role of hydrology in the spatial distribution of As (Stute et al., 2007; Harvey et al., 2006) and the contribution of anthropogenic activities, such as over extraction due to irrigation (Smedley and Kinniburgh, 2002; Ravenscroft et al., 2009; Stute et al., 2007). The development of the Maun Groundwater Development Project (MDGP; Department of Water Affairs (DWA), 2003) is expected to provide water for the growing population of the City of Maun, Botswana. This new groundwater extraction has raised the issue of elevated As in groundwater affecting surrounding populations (Huntsman-Mapila et al., 2006).

In this study, I hypothesized that the role of microorganism in releasing As into the groundwater is more important in the islands' fringe compared to the islands' center. The dense vegetation at the island's edge is expected to have high amount of nutrients in order for plants to grow, and microorganisms are likely to be more active in this zone than in zones with barren

surfaces (i.e., islands' center) (Mubyana et al., 2003). Thus, evaluating the microbial community composition will improve our knowledge of the role of microorganisms in As mobilization.

The goals of this study are to better evaluate the roles of microbial communities along the groundwater flowpath to provide insight into the governing biogeochemical processes and build on the hypotheses posed by Mladenov et al (2013) that: *1)* at the high EC center zone evapoconcentration controls As accumulation; and *2)* at the low EC fringe zone redox processes and microbial activity enhance As release. In addition, reactions affecting As desorption and adsorption (i.e., competitive interaction, increasing alkalinity and ionic strength and sediment weathering) are evaluated to further understand the mechanisms responsible for As release. To evaluated if the influence of evapoconcentration and biogeochemical processes on As mobilization is similar throughout the Okavango Delta, we studied four islands along the lower reach of the Boro Channel, two of which have been previously studied (i.e., New Island by Mladenov et al. (2013) and Camp Island by Huntsman-Mapila et al. (2011)) and two islands that are located in a seasonal floodplain east of Camp Island (Palm Island and One Tusk (OT) Island).

3.2 Methods

3.2.1 Site Description and Field Sampling

3.2.1.1 Study sites

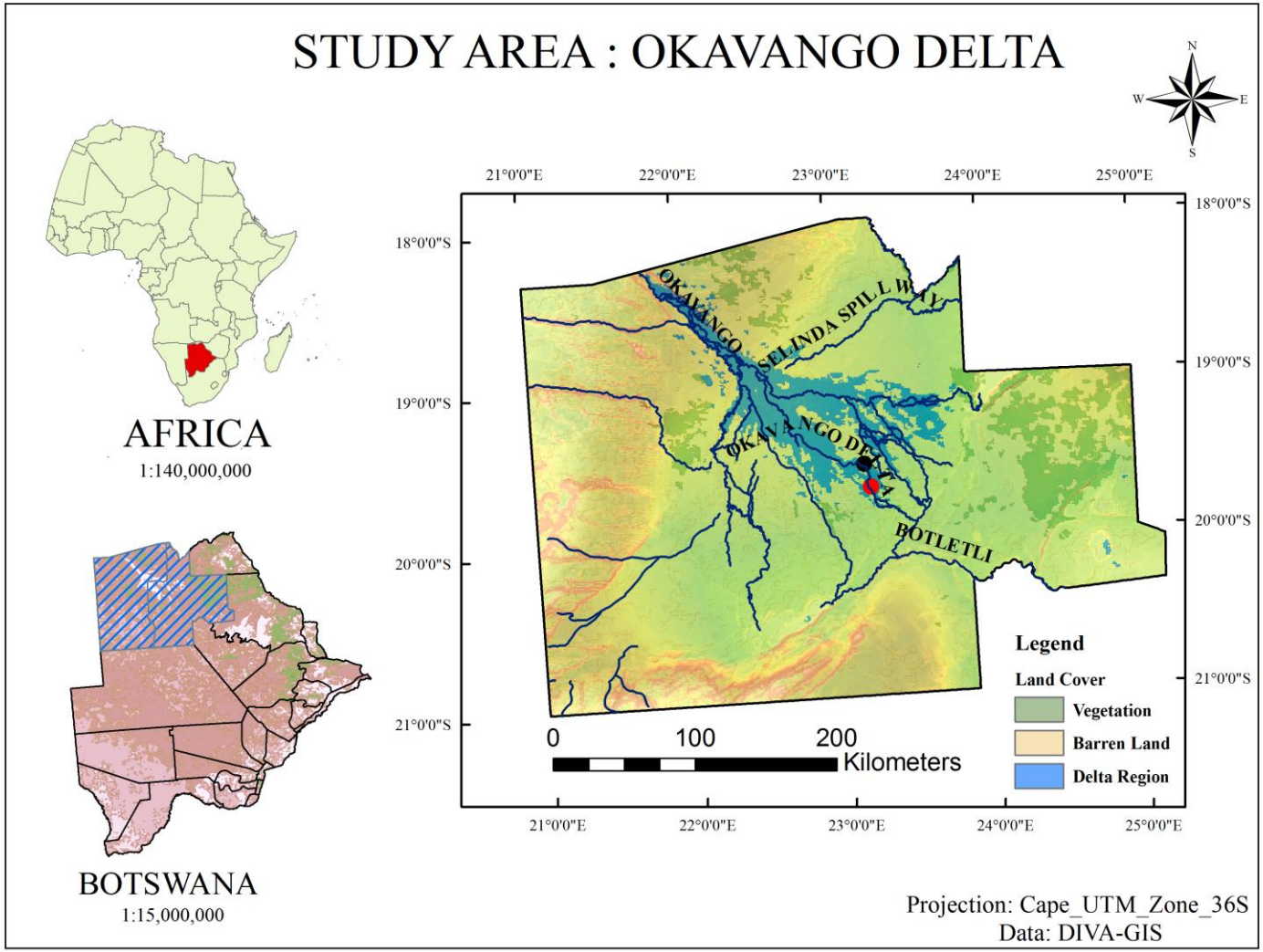

Figure 3-1. Study area. Black circle shows the location of Camp Island, Palm Island and One Tusk Island. Red circle shows the location of New Island. (*Cartography credit: Harshad Kulkarni*)

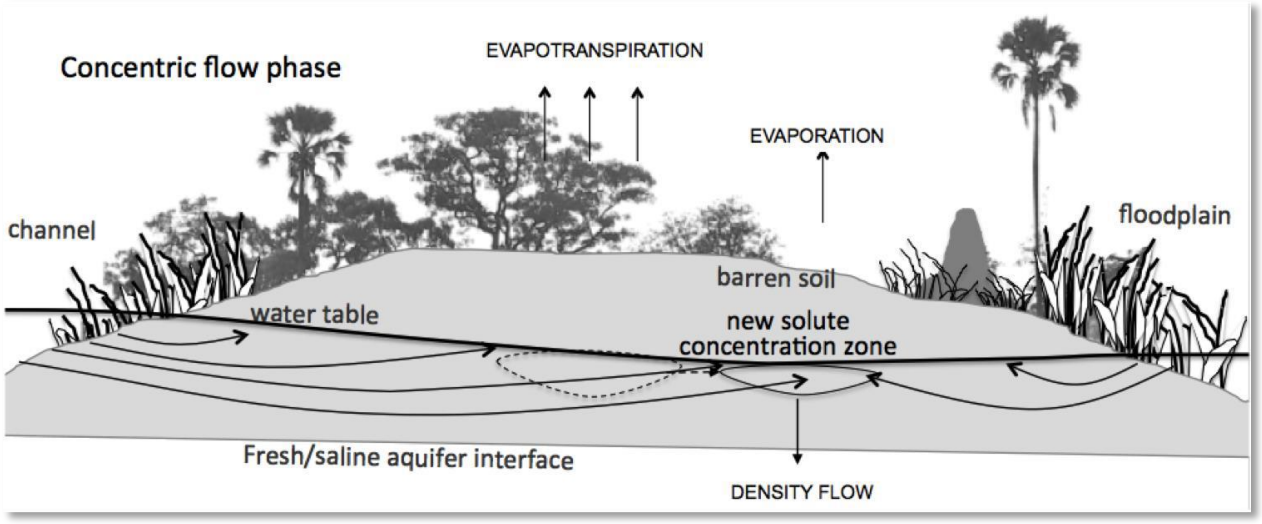

Figure 3-2. Schematic of groundwater flow driven by evapotranspiration and accumulation of inorganic ions and DOC beneath the island's center. *(Adapted from Mladenov et al., 2013)*

The Okavango Delta contains tens of thousands of islands. As proposed by Ellery and McCarthy (1994), the overall conceptual hydrology and geology of the Okavango delta is that the islands are slightly elevated and surrounded by permanent swamp and/or seasonal swamp. Tall, dense woodlands, mainly evergreen trees, characterize the islands with woody plant species in the island fringe. The island interior, however, is virtually barren with sparse coverage of grass and trona (sodium-carbonate) encrusted soil (Ellery et al., 1993). The barren island's interior is mainly attributed to the increasing salinity of the water beneath the island. The process of islands acting as sinks for solutes to keep surface water fresh has been studied extensively (Geiske, 1996; Zimmerman et al., 2006; McCarthy et al., 2010; Ramberg and Wolski, 2008; Bauer-Gottwein et al 2004). The shallow groundwater table of the Okavango Delta is more susceptible to evapotranspiration fluxes (Bauer et al., 2007). High evapotranspiration rate is the main driving force of the groundwater flow beneath the islands of the delta (Wolski and Savinje, 2006; Figure 3). Evapoconcentration triggers density driven flow and numbers of geochemical processes including mineral precipitation and CO2 de-gassing (Bauer-Gottwein et al., 2004).

We studied four different islands along the lower reach of the Boro channel and seasonal floodplain (i.e., Camp Island, New Island, Palm Island and One Tusk Island) (Figure 3-1).

Camp Island, the research station for the Okavango Research Institute (ORI), is located on the Boro channel reach and is known to have dissolved As concentrations as high as 3000 $\mu g \cdot L^{-1}$ in groundwater beneath the interior of the island (Huntsman-Mapila et al 2011). Camp Island is the largest island investigated in this study with a salt-crusted and barren center, and it's the island fringe is characterized by thriving vegetation and salt-crusted and barren center indicating high salt concentration in groundwater (Figure 3-3).

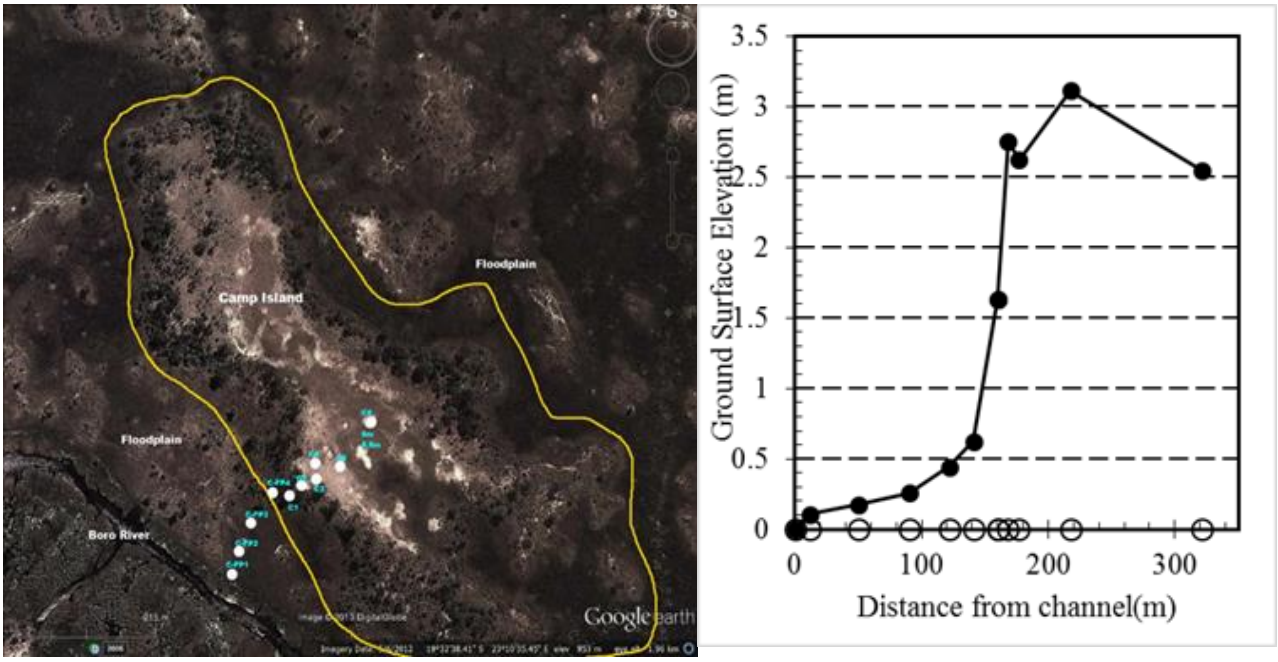

Figure 3-3. Plan and profile view of Camp Island. The aerial photo (left) shows the groundwater sampling point along the west-east transect. The profile view (right), surveyed from western shore to center of the island (Camp 6), showing groundwater table is expected to be at the same elevation as the surface water.

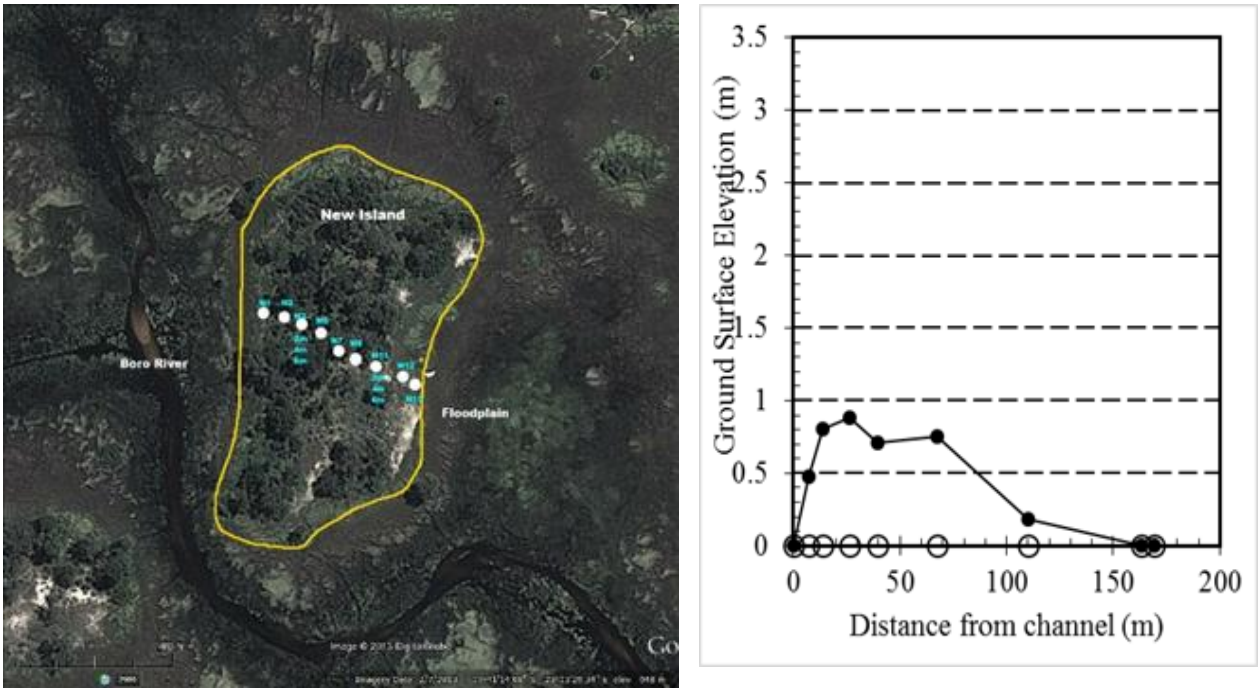

Figure 3-4. Plan and profile view of New Island. The aerial photo (left) shows the groundwater sampling point along the west to east transect. The profile view (right), surveyed from western shore to the edge near floodplain surface water, showing groundwater table is expected to be at the same elevation as the surface water.

New Island is about 80 m by 200 m in area (Figure 3-4) and is partially encircled by the Boro Side Channel (Figure 3-8). This island has been observed to have high dissolved solids compared to other islands (Bauer-Gottwein et al., 2007; Mladenov et al 2013). The higher groundwater elevation on one side of the island results in asymmetrical flow (Figure 3-3). The shift in the location of the area with highest solute concentration was a result of the shift of the highest zone of evapotranspiration (Bauer-Gottwein et al., 2007; Mladenov et al 2013). Palm and One Tusk Islands are located on a seasonal floodplain east of Camp Island. Palm Island, which is about the same size as New Island (Figure 3-9) is characterized by sparse distribution of vegetation (i.e., palm trees and salt tolerant grass) (Figure **3-5**). One Tusk Island is the smallest island among all the islands investigated in this study with sparse vegetation including rain tree (Figure 3-5).

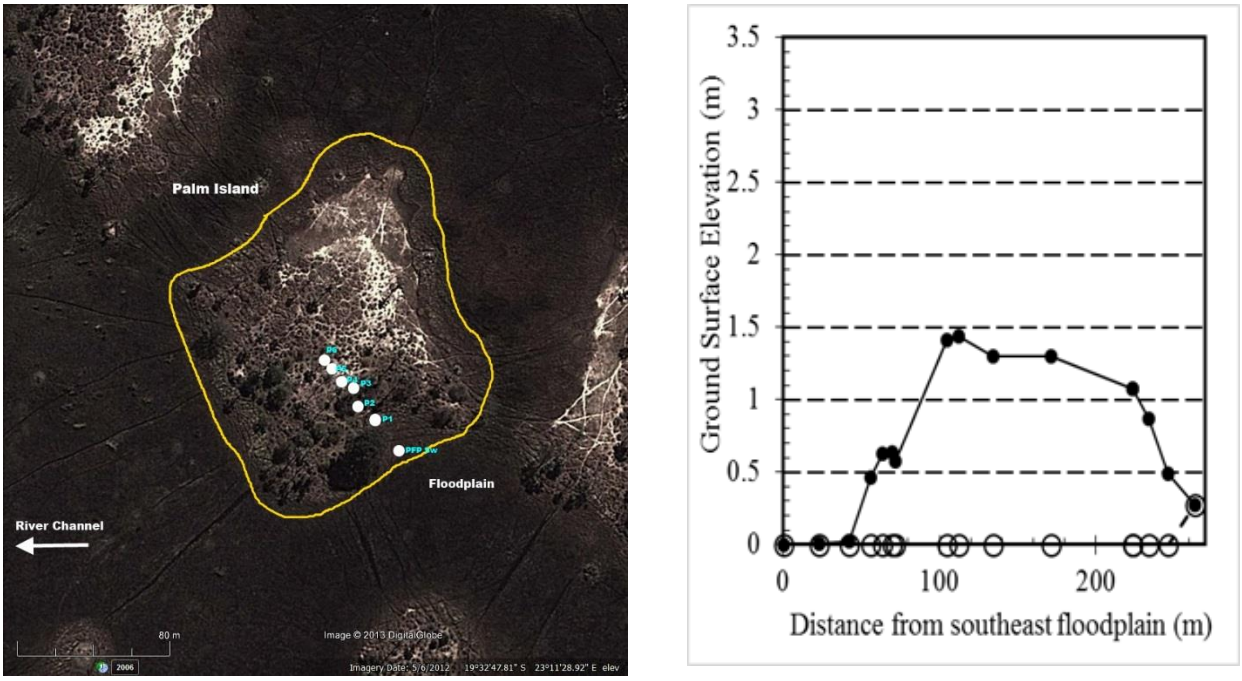

Figure 3-5. Plan and profile view of Palm Island. The aerial photo (left) shows the groundwater sampling point along the southeast-northwest transect perpendicular to the hypothesized groundwater flow path. The profile view (right), surveyed from southeast to northwest floodplain, showing groundwater table is expected to be at the same elevation as the surface water.

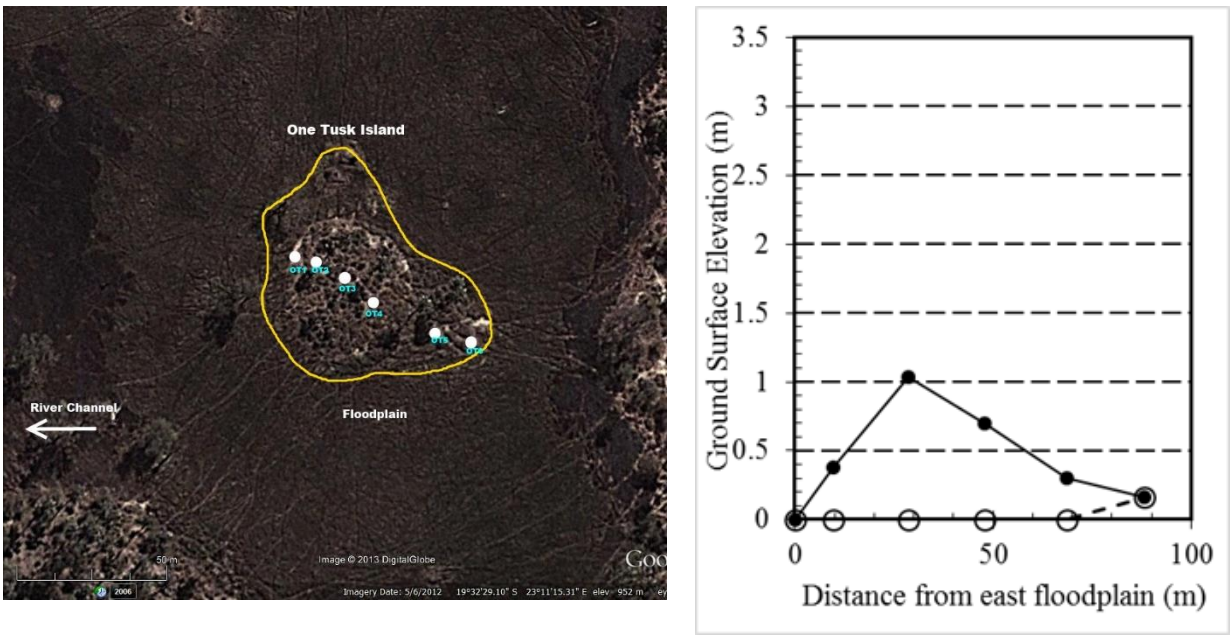

Figure 3-6.. Plan and profile view of One Tusk Island. The aerial photo (left) shows the groundwater sampling point along the southeast-northwest transect perpendicular to the hypothesized groundwater flow path. The profile view (right), surveyed from southeast to

northwest floodplain, showing groundwater table is expected to be at the same elevation as the surface water.

Figure 3-7. Camp Island fringe zone

Figure 3-8. Boro Side Channel adjacent to New Island photo taken from island's fringe.

Figure 3-9. Palm Island photo taken from floodplain.

3.2.1.2 Sample collection and preparation

Shallow wells were hand-augered to a depth between 1.5m and 2.5m below the soil surface (~0.3 m below the groundwater table). The ~50 mm diameter PVC pipes were hand sawn with slits of about 5cm in length around the pipe until about 0.3 m from the bottom (Figure **3-11**). A fitted mesh cover was secured around one end of the pipe and rinsed before installation. The piezometer was purged three times with a peristaltic pump (Figure **3-10**).

Figure 3-10. Piezometer drilling. Left photo: Hand drilled piezometer. Right: Peristaltic pump used for purging the well and sampling.

Figure 3-11. PVC pipe (~50mm diameter) with slits and then covered with mesh forgroundwater sampling.

Groundwater samples were collected in triplicate after 24 hours of drilling in a pre-rinsed and pre-combusted serum bottles (Figure 3-12). Two serum bottles were filled and crimp sealed immediately and another set of groundwater was collected with plastic bottles. In Camp Island, there were no samples collected for alkalinity or anions at wells Camp FP1-FP4 and Camp 1-5. Fluorescence and absorbance measurements were collected using filtered and acidified (with HCl) samples for samples Camp FP1-FP4 and Camp 1-5. A complete set of analyses was carried out for Boro River surface water adjacent to Camp Island and for groundwater at Camp 6 (6m and 8.5m depth).

Figure 3-12. Groundwater sampling after purging well three times.

Surface water were collected with large buckets and serum bottles were submerged in the bucket for sampling (Figure 3-9).Surface water samples were collected in triplicate in pre-combusted and pre-rinsed serum bottles ~10cm below the water surface. Surface water samples were collected from the Boro channel adjacent to Camp Island, the Boro Side Channel near New Island, and a floodplain adjacent to Palm and New Islands.

Figure 3-13. Floodplain surface water sampling.

Sediment samples were collected with airtight plastic core samplers from sediments recovered at about 2 m and immediately placed in zipped-tight bags with oxygen absorbing packet inclusions. We also collected surface soil samples with zipped-tight bags.

Figure 3-14. Split Core used for sediment sampling.

All surface water, groundwater, sediment samples and vegetation samples were transported in a portable refrigerator to the Okavango Research Institute within 24 hours. The triplicate samples we collected were filtered, unfiltered and filtered and acidified with HCl (Figure 3-15). Unfiltered samples were collected for backup. Samples in crimp-sealed serum bottles were filtered through pre-combusted 0.7 µm glass fiber filters (GFF) under a portable anaerobic glove bag purge and filled with N_2 gas. The samples collected with plastic bottles were filtered with 0.7 mm nominal pore size glass fiber filters and acidified to pH ~2 with hydrocholoric acid (HCl). All surface water and groundwater samples were shipped on ice to Kansas State University (KSU) Civil Engineering Department and kept at 4^{o}C until analysis. All sediment samples were shipped on ice to the KSU Agronomy department and kept at -20^{o}C.

Figure 3-15. Samples collected. Left photo shows filtered–acidified and crimp-sealed samples (minimize oxygen exposure). Right photo shows solid phase extraction (SPE) filtered samples for As speciation.

3.2.2 Water Analyses

3.2.2.1 In-Situ water analyses

The pH of groundwater was measured with a Fisher Scientific AP60 pH meter, calibrated with pH 4, 7 and 10 standards. Electrical EC (EC) was measured with YSI 30 Conductivity meter, calibrated with Conductivity Calibration solution of 1,000 µS/cm at 25^{o}C. Dissolved

oxygen (DO), calibrated with the local elevation (~900 m), was measured with YSI 55 DO meter. Oxidation and reduction potential (ORP) was measured in the field with YSI pH 1000 pH and ORP meter.

3.2.2.2 Arsenic Speciation

At the Okavango Research Institute (ORI) Laboratory Facility, we slowly filtered a ~10 mL of the filtered-acidified samples through solid phase extraction (SPE) cartridges (Waters Corporation, Milford, MA) in a portable anaerobic (N_2 gas-filled) glove bag. The SPE cartridges traps As (V) and the ~10mL SPE-filtered contains only As (III). We then analyzed the SPE-filtered and SPE-unfiltered water samples using a graphite furnace atomic absorption spectrometry (GF-AAS) (Varian Inc.) in the KSU agronomy soil chemistry laboratory. Ten micro-liter of 1000 $mg \bullet L^{-1}$ Ni was used as the modifier to enhance the signal (absorbance) of As in GF-AAS. The filtered-acidified (SPE-unfiltered) samples analyzed with GF-AAS measured total As concentration, and the SPE-filtered samples measured As (III) concentration; thus As (V) concentration is the difference between total As and As (III). For quality control/assurance, a blank and a NIST standard for trace elements in waters (SRM 1643e) were used and 116% As recovery was achieved for NIST sample. Every sample was analyzed in duplicate. The spiked recoveries were in the range of 93-102%.

3.2.2.3 Fe^{2+} analysis

An aliquot of a filtered and HCl acidified sample was used for colorimetric determination of soluble Fe^{2+} by the phenanthroline method described by Greenberg et al., 1992. In the KSU CE Environmental Engineering Laboratory, sample handling and color development were carried out in an anaerobic glove box. We transferred ~2 mL of the filtered samples into a 25mL volumetric flask. We then added 1 mL of 0.015 M 1,10-O-phennanthroline regent and 2 mL of 5*M* Ammonium acetate to the sample and mixed well. The mixture pH was brought to pH range

of 3-5 by adding 6M of HCl. The volume of the mixture was brought to 25mL with ultra pure water and transferred in crimp-sealed serum bottle to maintain anaerobic condition. We analyzed the mixture using a Beckman UV–visible DU 800 spectrophotometer in the KSU Agronomy Soil Chemistry Laboratory. Ferrous ammonium sulfate (FAS) was used to prepare fresh iron standards and the procedure of color development for standards was followed similar to that of samples. Finally, Fe^{2+} concentration of samples was measured using UV-visible spectrophotometer at 510 nm wavelength.

3.2.2.4 Total dissolved ion analysis

The filtered-acidified samples were measured for total elemental analysis (B, Na, Mg, Ca, S, and K) using a Varian 720-ES ICP-optical emission spectrometry (ICP-OES) in the KSU Agronomy Soil Chemistry laboratory. We further filtered the filtered-acidified samples with 0.45 µm syringe filters before running the analysis. For anions measurement, filtered samples were furthered filtered through 0.20 µm syringe filters. Anions (F^-, Cl^-, NO_2^-, Br^-, NO_3^-, PO_4^{3-}, and SO_4^{2-} were analyzed on an ion chromatograph (ICS-1000, Dionex Corporation).

3.2.2.5 Total Organic Carbon

Total organic carbon (TOC), assumed to be all dissolved organic carbon, and total nitrogen (TN) were measured from samples filtered and acidified (with HCl at the ORI laboratory). The highly colored and extremely high conductivity samples were diluted 1:100. We then analyzed the samples using a Shimadzu TOC-L TOC/TN analyzer with high salts kit and sparged for 5 minutes with ultra-high purity air to remove inorganic carbon.

3.2.2.6 Alkalinity

We used the Gran alkalinity titration method to measure alkalinity in our filtered samples. A ~10mL aliquot of our filtered samples was titrated with 0.02 N of H_2SO4 (0.2 N for highly alkaline samples) using the Fisher Scientific bottle top digital burette for more volume accuracy.

The pH meter was calibrated with standards of pH 4, 7 and 10. We constantly measured pH during titration and brought pH to 4.5. About 6 data points listing acid volume added and corresponding pH were recorded prior to reaching pH ~4.5 and 6 more data points were recorded after pH 4.5. We used the USGS alkalinity calculator (http://or.water.usgs.gov/alk/) and entered our acid concentration, temperature, sample volume, pH and acid volume and checked the "gran alkalinity" box.

3.2.3 Sediment sample analyses

Sediment samples were hand homogenized in the anaerobic N_2 gas chamber. A portion of the sediment samples was homogenized and separated into two 15 mL sterile falcon tubes in an anaerobic chamber with sterile surfaces for sediment chemical analysis and microbial analysis. Sediment samples were analyzed for As and Fe content after digestion with aqua regia using a GF-AAS (As) or ICP-OES (Fe). The total elemental concentrations in the soils were determined using modified aqua regia digestion procedure described by Premarathna et al., 2010. In brief, approximately 0.5 g of finely ground soil was predigested with0.5 mL of H_2O_2 for 10 min at room temperature. Another 2.5 mL of H_2O_2 was added and allowed to react for 12 h at room temperature, after which the tubes were heated on a digestion block at 90 ^{0}C until the volume was reduced to ~1 mL. After cooling, the soils were digested using 5 mL of aqua regia (1:3 HNO_3/HCl) using the tube soil digestion procedure (75^{0}C for 30 min, 100 ^{0}C for 30 min, 110 ^{0}C for 30 min, and 140 ^{0}C until the acid volume decreased to <1 mL), then made up to 20 mL using 0.1% HNO_3, filtered, and analyzed for total As using GF-AAS and other elements (Al, Si, S, and Fe) using ICP-OES. A standard reference soil (NIST 2711a-Montana II) was also digested in duplicate along with sediment samples as a quality assurance/quality control (QA/QC) sample to evaluate the digestion and analytical procedures. Ten micro-liter of 2000 $mg{\cdot}L^{-1}$ Pd was used as the modifier to enhance the signal (absorbance) of As in GF-AAS.

Recovery of As in NIST standard was 99%. Every sample was analyzed in duplicate, analytical blanks and spiked samples were also included. The spiked recoveries were in the range of 88-91%.

3.2.4 Microbial Analysis

We selected soil samples from New island wells 1, 3, 5, 7 11, 12 and termite mound (TM) and Camp island wells 2 and 5 for microbial analysis. Mladenov and collaborators (2013) collected New 3 and New 11 soil samples on October 2011 and kept them frozen at -20^{o}C. We collected soil samples from approximately 2m depth of which same depth of groundwater was sampled. We selected this sample set because of their wide range of salinity, dissolved As, and DOC concentration. New 11 and Camp 5 had the highest EC, which reached 4,900 μS/cm and 30,000 μS/cm for New and Camp Island respectively. Further, previous study has reported As concentration of 186 ug/L for New Island (Mladenov et al 2013) and 3,200 $\mu g \cdot L^{-1}$ for Camp Island (Huntsman-Mapila et al 2011). New 1, 3, 5, 7, and Camp 2 were collected near the island's fringe, and EC in these locations ranged from 560-1430 μS/cm, a typical range for river and streams. We included New 12 and TM in this set because New 12 had relatively high DOC concentration and New TM had been reported to have more intense amino acid-like fluorescence, which indicate microbially-derived DOM (Mladenov et al., 2013).

We extracted DNA from 300 mg of soil samples for New 3, 7, and 11, Camp 2 and 5 and 600 mg of soil samples from New 1,5,11, 12 and TM. We extracted total community DNA using the PowerSoil DNA Isolation Kit (MoBio, California, USA) applying an alternative protocol according provided by the manufacturer to limit DNA shearing during extraction. The quality and quantity of the extracted DNA was determined using NanoDrop Spectrophotometer of 1-2 μL of aliquot. The extracted DNA was sent to MR DNA sequencing lab (Shallowater, TX) for amplicon pyrosequencing. Extracted DNA was amplified by PCR using HotStarTaq Plus

Master Mix Kit (Qiagen, Valencia, CA). PCR products were purified using Agencourt Ampure beads (Agencourt Bioscience Corporation, MA, USA). Samples were sequenced using Roche 454 FLX titanium instruments and reagents as per manufacturer's protocol.

Sequences were processed using a propriety analysis pipeline (mrdnalab.com, MR DNA, Shallowater, TX). Short sequences <200 bp, sequences with ambiguous base calls and holypolymer runs exceeding 6bp were removed. Operational taxonomic units (OTU) were aligned using the GreenGenes database, classified with BLASTn and compiled into taxonomic level.

3.2.5 Fluorescence spectroscopy

To support our microbial analysis, some absorbance and fluorescence spectroscopic analysis is discussed here. All Excitation-Emission Matrix (EEM) spectra and absorbance were collected using Aqualog Fluorometer (Jobin Yvon Horiba).

Filtered and crimp-sealed samples were transferred from a crimp-sealed bottle under anaerobic chamber and immediately measured for fluorescence and absorbance. Strongly absorbing samples (typically high DOC samples) were diluted with ultra-pure water 10^{-2} at 1.5 seconds integration. Absorbance with 3nm increment from 240-600 nm excitation wavelengths was collected without dilution. EEMs were collected at an increment of 3nm excitation wavelength over 250-400 nm range and 10 nm emission wavelength over 350-600 nm. EEMs were inner-filter corrected and intensities were normalized to the area under the Raman peak (excitation=~397 nm). Blank samples were subtracted from each sample EEM using ultra-pure water. Corrections and normalization and calculations of fluorescence indices (FI, B:α and HIX) and UV 254 were performed in Matlab. Fluorescence index (FI) provides information on the degree of degradation (McKnight et al 2001; Cory and McKnight 2005), Humification Index (HIX) provides information on the humification extent (Zsolnay et al 1999), and Freshness Index

(from now will be referred to as $\beta:\alpha$) indicates if a DOM is recently produced (Parlanti et al.,2009).

3.2.6 Saturation Index Calculations

Saturation Index (SI) were calculated with respect to calcite $CaCO_3$, dolomite $CaMg(CO_3)_2$ and siderite $FeCO_3$ using Geochemist Workbench 10.0 with the fundamental equation:

$$SI = log\ Q - log\ K = log\ (Q/K)$$ where

Q (reaction quotient) = product/reactant; and

K (equilibrium constant) = product/reactant at equilibrium.

The log K values used for this study were:

$Ca^{2+} + HCO_3^- = CaCO_3 + H^+$ $\quad$ log K = -1.7130

$Ca^{2+} + Mg^{2+} + 2\ HCO_3^- = CaMg(CO_3)_2 + 2\ H^+$ $\quad$ log K = -2.5207

$Fe^{2+} + CO_3^{2-} = FeCO_3$ (precipitated) $\quad$ log K = 10.45

The saturation of a solution with respect to a mineral is mathematically expressed by SI values. If a solution has an SI value < 0 (negative), the solution is undersaturated with respect to the mineral, and supersaturated with respect to the mineral if SI > 0 (positive). A solution is in equilibrium with respect to the mineral if the SI=0.

3.3 Results

3.3.1 Sediment Characterization

Soil samples collected at the soil surface and at groundwater table depth (approximately 2m) and analyzed for Al, Si, Mn, Fe, and As showed distinct zones of high solute concentration and low solute concentration, which are reflected in the water and sediment chemistry (Figure **3-16**).

The highest sediment Al, Fe and As are located at the zone of high solute concentration and the lowest concentrations of these inorganic elements are at the beginning of the flow path,

closest to the surface water (Figure **3-16**). The % TOC in sediment is also highest at the zone of high solute concentration (Figure **3-16**).

The elevation of the islands was found to be highest at well locations with highest EC, sediment As and Fe (Figure **3-16**). The ground surface elevation (with respect to the surface water elevation) illustrates that the highest point in each island (Figure 3-3 to Figure 3-6.) was located at the point of high EC in groundwater. The maximum elevation of Camp Island was 3.5 m above the surrounding channel. Palm, New and One Tusk islands' maximum elevation was at 1.5m, 1m and 1 m, respectively, above the surrounding surface water or floodplain. Sediment As, Fe and Al concentrations were highest at the highest ground surface elevation and groundwater EC. In all the islands, sediment Si content was highest in the seasonal floodplains adjacent to islands. At the highest point of elevation in all of the islands, carbonate minerals were observed in the surface soils. An acid test, which looks for the release of CO_2 (g) after applying concentrated hydrochloric acid to the soil, was performed and confirmed the presence of carbonate minerals on sediment from Camp 3 and Camp 4.

The saturation index values indicated supersaturated with respect to calcite ($CaCO_3$), dolomite (Mg-$CaCO_3$) and siderite ()There were no values for SI for piezometers Camp FP1-FP4 and Camp 1-5 due to lack of alkalinity measurement. At New Island, New 3, 7, 9, 11 and 12 had SI values >1 for calcite, dolomite and siderite (Table A-4). At Palm Island, Palm 3, 5 and 6 had SI values > 1 for calcite, dolomite and siderite (Table A-4). At One Tusk Island, all wells had SI values >1 for calcite and dolomite and the SI values for siderite were >1 at OT 1, 2 and 3 (Table A-4).

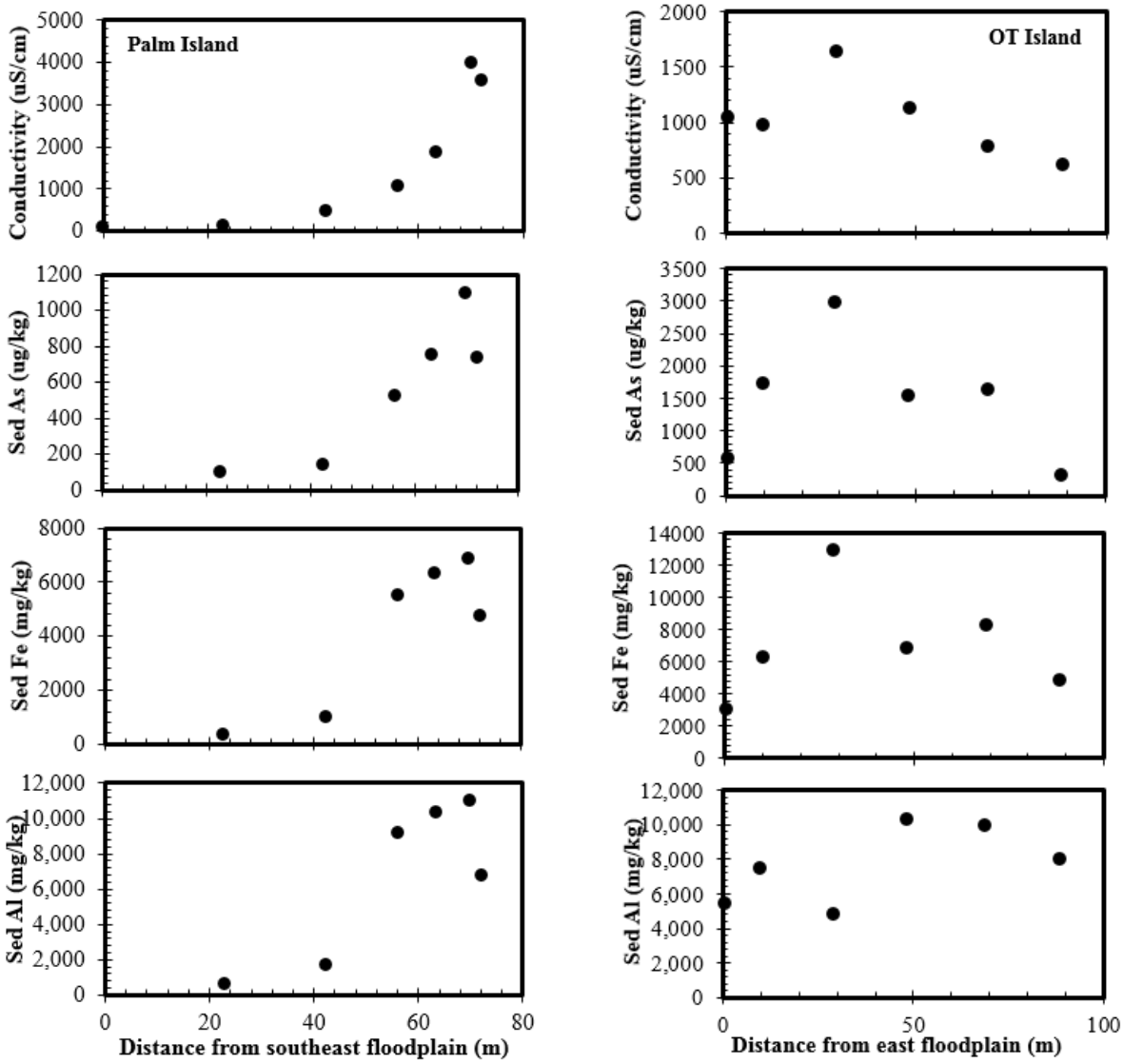

a) Palm Island

b) One Tusk Island

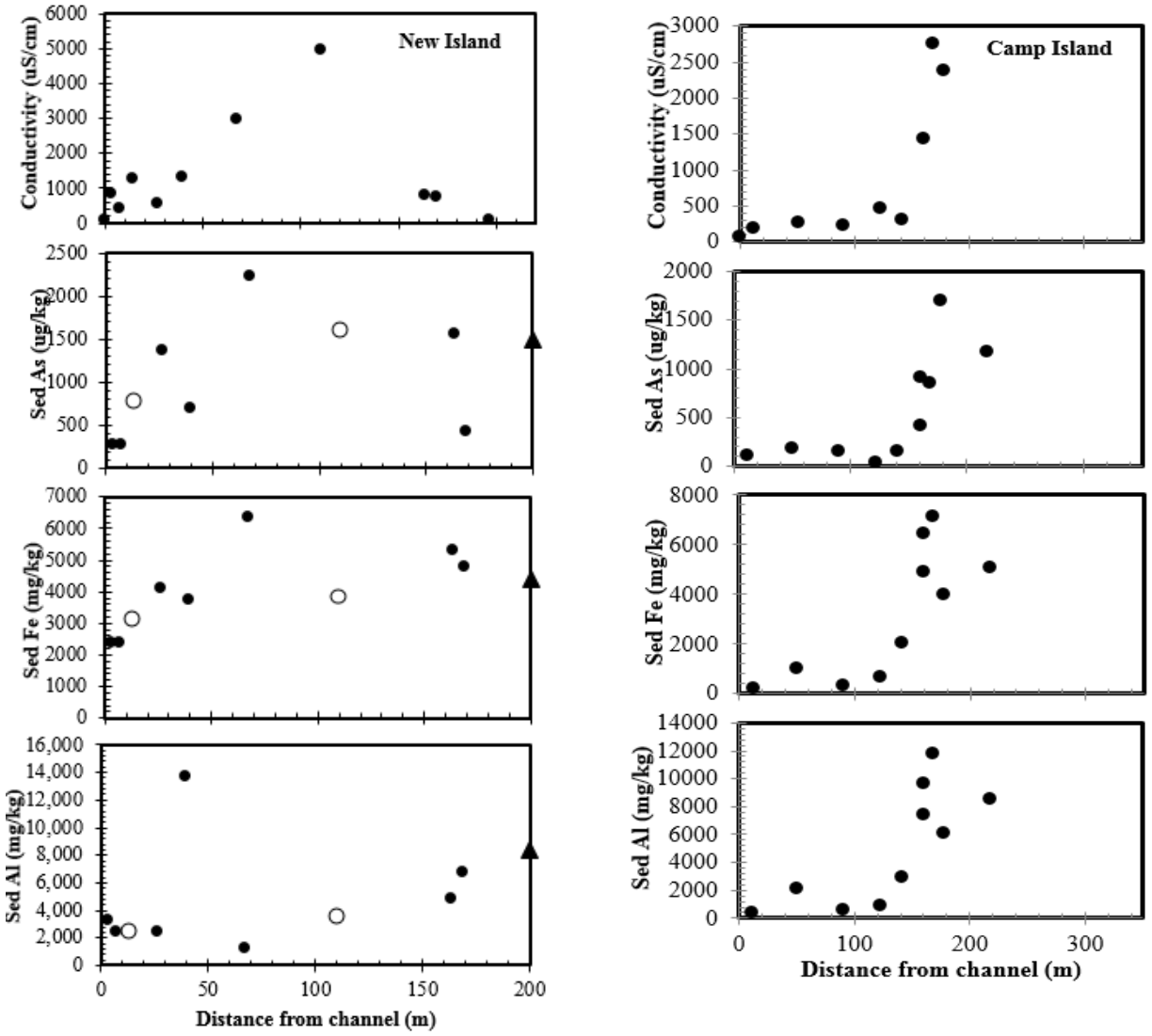

c) New Island d) Camp Island

Figure 3-16. Sediment chemistry. Spatial distribution of As, Fe and TOC in the sediment for each island. In new island, soil samples from October 2011 (unfilled circle) and termite mound (triangle) were included.

3.3.2 Spatial distribution of solutes and DOM

3.3.2.1 Camp Island

Camp Island is a salt island dominated by a barren, salt-crusted center and partially surrounded by riparian woodland. The island transect from west to east with the Boro River on the western part of the island. The surface water, the Boro River had the lowest EC (77 μS/cm), pH was nearly neutral (pH 6.76), and As concentration was 2 $\mu g \cdot L^{-1}$. The EC values for floodplain piezometers (ranging from range from 196-475 μS/cm for FP1 – FP4; Figure 3-17;Table A-6) were substantially greater than the surface water. The As concentration in floodplain groundwater remained below 10 $\mu g \cdot L^{-1}$ in piezometers located between 0 and 122 m east of the Boro River.

In the piezometers located at Camp 1-4, EC values ranged from 1430 to 2390 μS/cm (Figure 3-17) ranged from 1430 to 2390 μS/cm (Table 3-2). Compared the surface water As concentration, the concentration of As increased by a factor 300 in Camp 4, located 177 m from the western shore.

In the center zone, the EC had increased significantly, and reached a near-seawater EC of 30,740 μS/cm (seawater EC=50, 000 μS/cm) and As concentration of 4050 $\mu g \cdot L^{-1}$ (Table A-6). SO_4^{2-} was notably high in Camp 6 with a concentration of 2377 $mg \cdot L^{-1}$ (Figure 3-17).

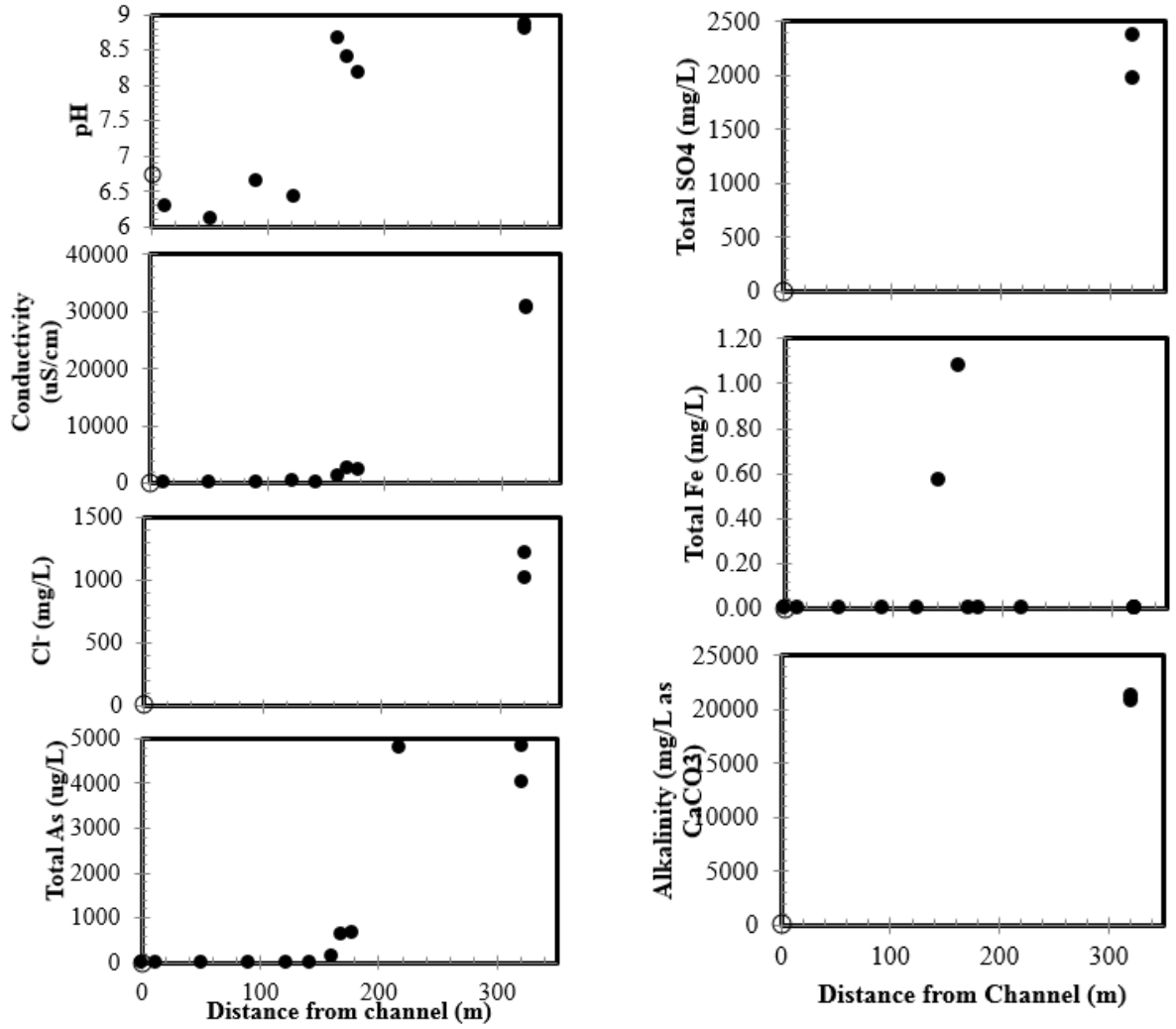

Figure 3-17. Camp Island: changes in groundwater chemistry (pH, conductivity, Cl, As, Fe, SO4 and alkalinity along the groundwater flow path. Surface water (unfilled triangle) is also included in this figure

3.3.2.2 New Island

New island is located in the lower part of the River (Figure 3-4. The Boro Side Channel adjacent to New Island had an EC of 114 μS/cm, which was substantially higher than in the Boro River near Camp Island (Figure 3-18). The EC in the floodplain was 95 μS/cm, which was lower than the Boro Side Channel. The surface waters in both Boro Side Channel and the floodplain were found to have similar As, Fe, SO_4^{2-} concentrations (Table A-7. **Ph**; Figure 3-18).

In groundwater, the island fringe bordering the Boro Side Channel was characterized by low EC, Cl^-, SO_4^{2-} and As. New 1, 2, 3, 5 and 7 had the lowest As concentrations, ranging from 2 to 11 $\mu g \cdot L^{-1}$, fairly low SO_4^{2-} concentrations, ranging from 1.39 to 2.09 $mg \cdot L^{-1}$ (Table A-7. Ph) and the highest Fe concentrations, ranging from 4.2 $mg \cdot L^{-1}$ and 10 $mg \cdot L^{-1}$.

The high EC zone at New 11 had the highest solute concentrations. At New 11, EC values reached 4950 μS/cm, and the pH was 8.03, compared to the nearly neutral surface water (Table 3-2) The concentration of As was 150 $\mu g \cdot L^{-1}$ at New 11, which was higher than in surface water. Compared to Cl^-, which increased by a factor of 46 from surface water to New 11, As increased by a factor of 63 (Table 3-1). SO_4^{2-} was also highest at New 11 with a concentration of 13 $mg \cdot L^{-1}$, which increased by a factor of 10 (Table 3-1).

Table 3-1. Ratio of groundwater: channel for Camp, New and Palm and ratio of groundwater: lowest Cl concentration (OT1) for One Tusk Island.

Sample ID	Cl	DOC	Total As	SO42-	Alkalinity	Ca2+
Boro Channel near camp	1.0	1.0	1.0	1.0	1.0	1.0
Camp FP	-	1.0	0.3	-	-	1.1
Camp FP 1	-	1.3	1.6	-	-	2.4
Camp FP2	-	1.8	1.5	-	-	4.5
Camp FP3	-	1.8	1.8	-	-	4.0
Camp FP 4	-	3.1	3.3	-	-	1.0
Camp new 1	-	2.9	4.2	-	-	0.1
Camp new 2	-	5.8	72	-	-	0.1
Camp new 3	-	5.9	303	-	-	0.0
Camp 4	-	10	313	-	-	1.2
Camp 5	-	29	2225	-	-	1.0
Camp 6 (6m)	94	27	1875	1036	316	-
Camp 6 (8.5m)	130	28	2546	1338	324	-
Boro channel	1.0	1.0	1.0	1.0	1.0	1.0
New 1	0.8	2.2	2.0	2.6	7.4	4.7
New 2	0.6	2.4	1.1	1.1	4.0	63
New 3	5.3	19	3.4	1.2	10	10
New 5	6.5	2.3	0.6	7.5	4.7	6.2
New 7	6.9	2.1	1.8	1.9	10.6	1.4
New 9	58	3.7	16	2.0	26	0.4
New 11 (2m)	63	5.1	46	9.5	47	10
New12	17	2.5	2.6	1.0	8.8	2.0
New 13	1.9	2.9	14.1	1.1	6.5	11
NEW FP SW	1.0	1.4	0.8	1.2	0.9	1.6
OT 1	1.0	1.0	1.0	1.0	1.0	1.0
OT 2	7.1	0.9	4.1	1.0	0.8	1.0
OT 3	15	0.8	2.3	1.1	1.4	1.5
OT 4	6.1	0.5	0.9	1.4	0.9	2.3
OT 5	3.4	0.5	0.5	1.6	0.7	1.1
OT 6	2.7	0.5	0.4	1.0	0.5	1.5
Palm FP SW	1.0	1.0	1.0	1.0	1.0	1.0
Palm 1	0.8	0.8	0.4	1.0	1.4	2.3
Palm 2	3.2	0.9	2.6	2.5	4.3	0.5
Palm 3	2.4	0.8	4.8	2.2	9.6	1.4
Palm 4	4.6	0.9	4.2	1.5	23	0.9
Palm 5	47	0.9	53	5.8	46	0.2
Palm 6	7.8	0.7	22	4.9	34	0.1

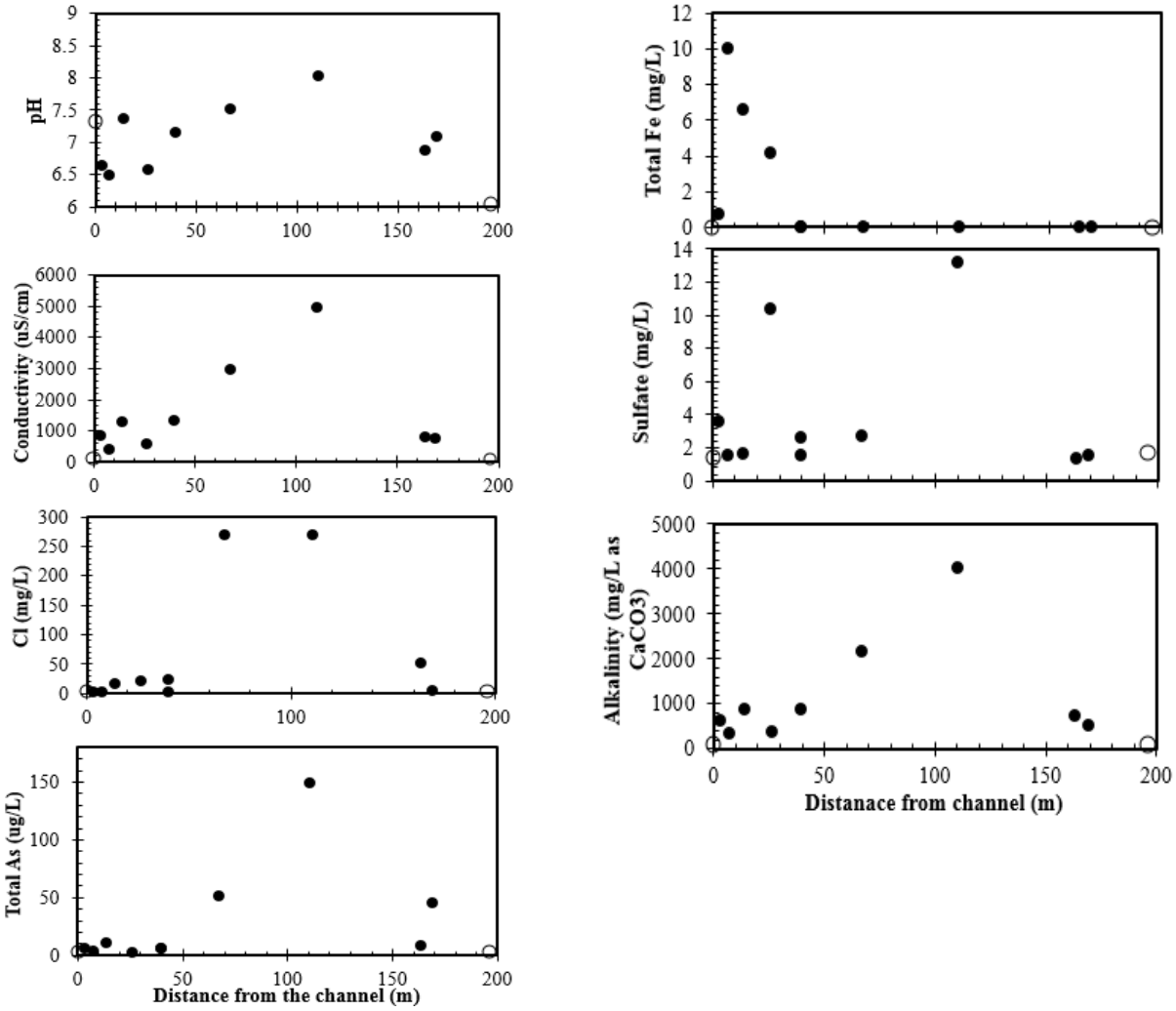

Figure 3-18. New Island: changes in groundwater chemistry (pH, conductivity, Cl, As, Fe, SO4 and alkalinity along the groundwater flow path. Boro channel and floodplain surface water (unfilled circle) are included in this figure

3.3.2.3 Palm Island

Palm Island has an area of approximately 16,500 m^2 and is surrounded by seasonal floodplain. During the high flood season, the floodplain is inundated by water, moving in a southwest-northeast direction (Murray-Hudson, personal communication). The piezometers in the fringe zone, including Palm 1, 2, 3 and 4, had EC values between 140 μS/cm and 1865 μS/cm and total As concentrations similar to New island, ranging from 1 to 13 $\mu g \cdot L^{-1}$ (Table A-8). Total dissolved Fe concentration was undetectable in groundwater throughout the whole transect.

The EC values in Palm 5 and 6 were 3976 μS/cm and 3580 μS/cm respectively, which delimited the high EC center zone of the island. Palm 5 had the highest EC (3976 μS/cm; Table 3-2), Cl (92 $mg \cdot L^{-1}$) and total dissolved As (143 $\mu g \cdot L^{-1}$). The groundwater to surface water (GW:SW) ratio for As in Palm 5 (53) increased more than the GW:SW ratio of Cl^- (47) (Table 3-1).

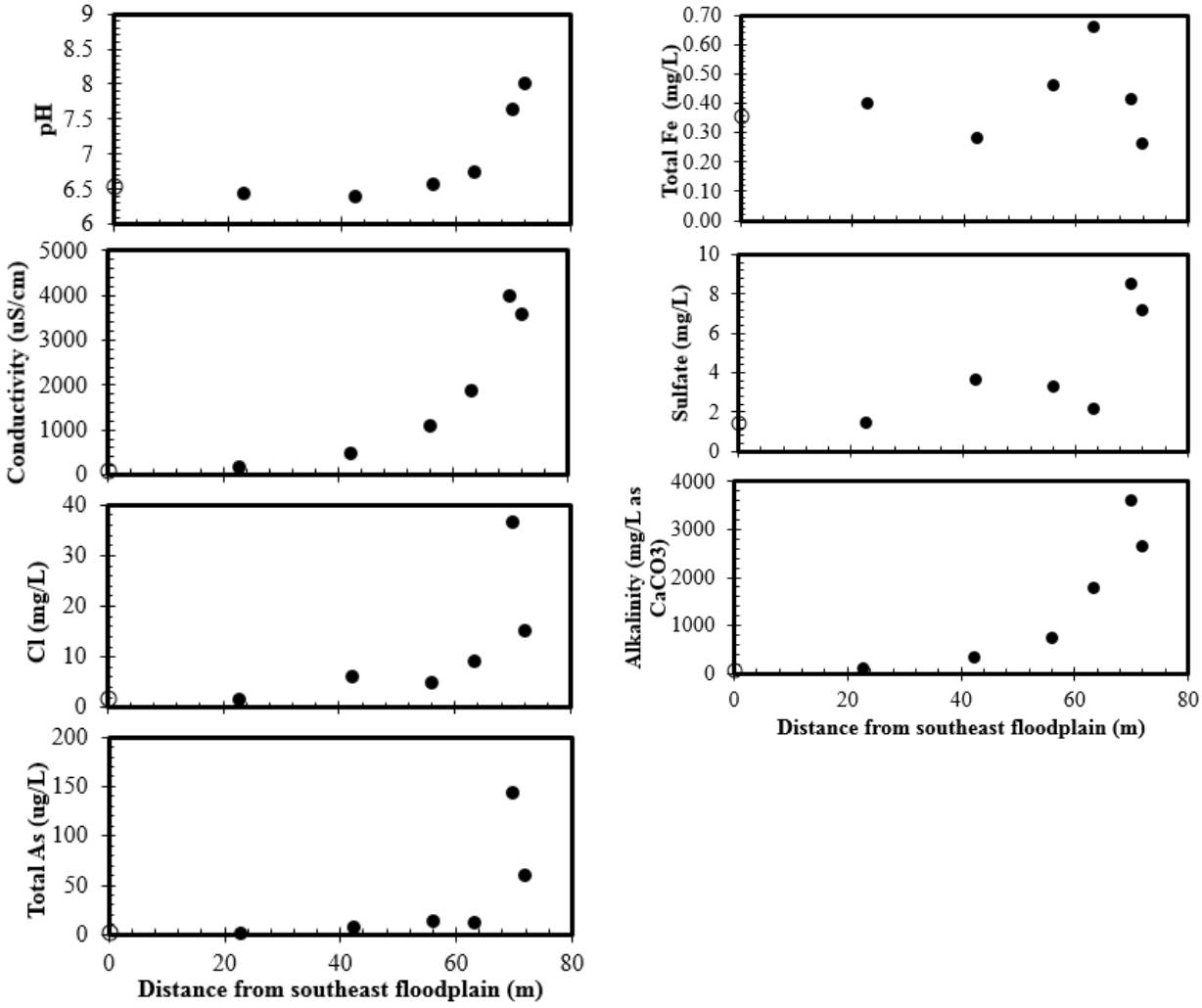

Figure 3-19. Palm Island: changes in groundwater chemistry (pH, conductivity, Cl, As, Fe, SO4 and alkalinity along the groundwater flow path. Floodplain surface water samples are depicted by the unfilled circle.

3.3.2.4 One Tusk (OT) Island

The area of One Tusk Island is the smallest compared to the other three islands discussed thus far, and it is surrounded by a seasonal floodplain, which was dry during sampling. At One Tusk Island, the groundwater from the southeast-northwest transect was characterized by low total Fe with the highest concentration of 0.95 $mg{\cdot}L^{-1}$ at OT 2. In general, the groundwater EC was lower than Camp, New, and Palm Islands, with the highest values (1656 μS/cm) found at OT 3. Overall, the highest As concentrations were also the lowest of all islands, with the highest concentration (39 $\mu g{\cdot}L^{-1}$) occurring at OT 2. The highest As concentration and EC were found at OT 2 and OT 3, respectively, which are about 20 m apart (Figure 3-6.). Piezometers OT 1, 4, 5, and 6 had EC values ranging from 630 to 1137 μS/cm (Figure 3-20; Table 3-2).

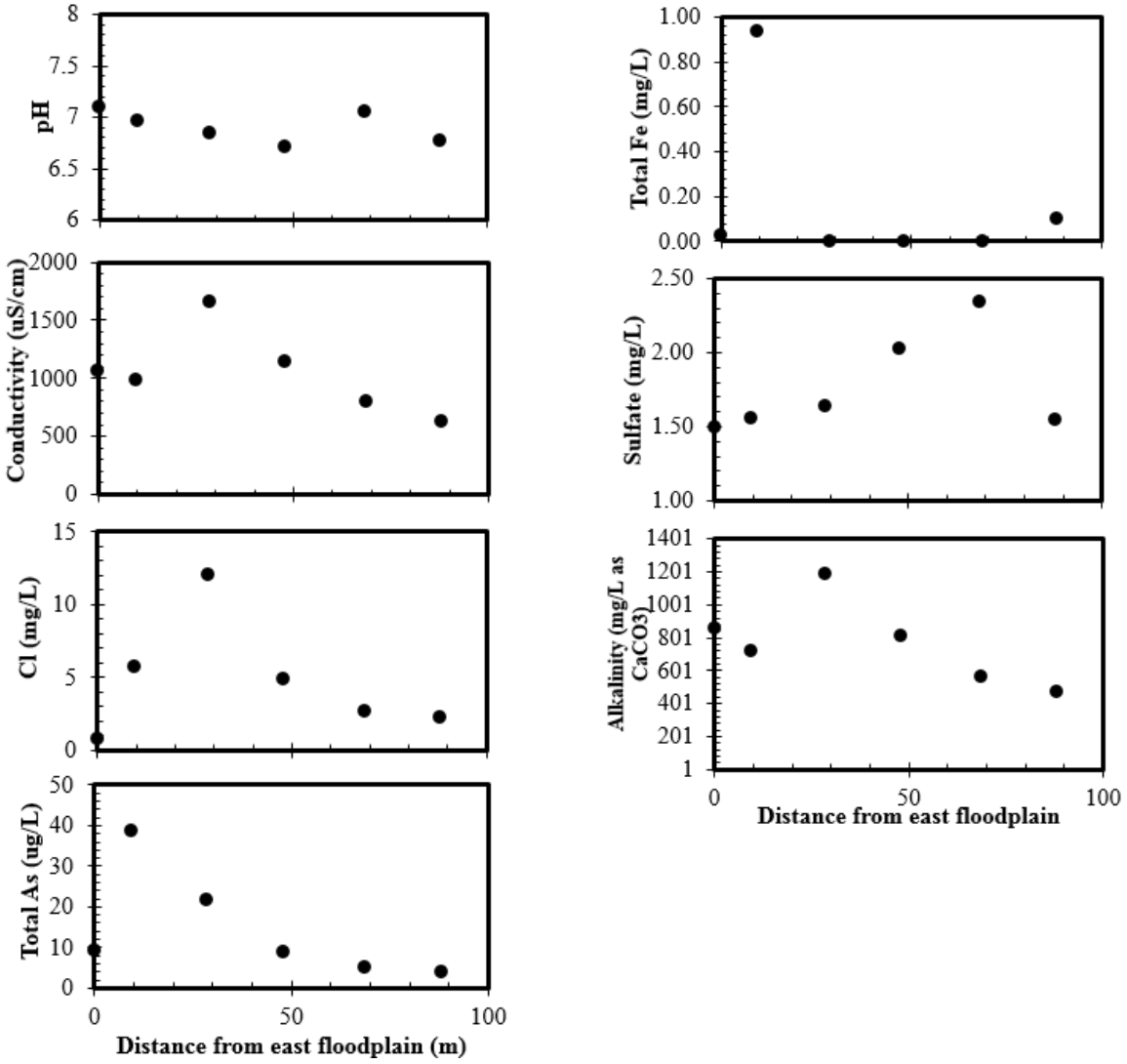

Figure 3-20. One Tusk Island: Changes in groundwater chemistry (pH, conductivity, Cl, As, Fe, SO4 and alkalinity along the groundwater flow path.

Table 3-2. Table Summary of Minimum, Average and Maximum value for the phusical and chemical properties for each island

Sample ID	Camp Island			New Island			One Tusk Island			Palm Island		
	Min	***Ave***	***Max***	***Min***	***Ave***	***Max***	***Min***	***Ave***	***Max***	***Min***	***Ave***	***Max***
Conductivity (uS/cm)	77.4	6346	30930	95	1291	4950	630	1045	1656	102	1600	3976
pH	6	7.5	9	6	7	8	7	7	7	6	7	8.0
d18O	-3	-2.4	-2	-2	1	3	-1	1	4	-6	0	2.9
d D	-28.4	-23.2	-19.6	-25.7	-3.4	10.5	-16.5	-2.8	5.6	-43.0	-6.7	15.5
Eh (V) (As^{5+} /As^{3+})*	-0.2265	-0.05	0.089	-0.12	-0.04	0.012	-0.012	0.004	0.020	-0.097	-0.011	0.072
Eh (V) (NO3-/NO2-)*	0	-	0	0.38	0.41	0.45	0.40	0.41	0.42	0.37	0.42	0.44
Ionic strength (molal)*	8.40E-04	4.64E-02	2.98E-01	1.46E-03	1.42E-02	5.06E-02	1.11E-02	1.59E-02	2.12E-02	1.47E-03	1.77E-02	4.49E-02
Alkalinity (mg•L-1 CaCO3)	66	14083	21348	76	980	4021	471	768	1185	78	1325	3593
B (mg•L-1)	0.02	0.17	0.68	0.00	0.09	0.20	0.00	0.03	0.11	0.00	0.22	0.79
Na (mg•L-1)	5.0	53	112	6.8	68	112	11	60	108	9.9	62	114
Mg (mg•L-1)	0	2.49	12.63	0	10	24.7	10	23	46	0	19	40
S (mg•L-1)	0	147	517	0	0.229	2.55	0	0	0	0	0.53	2.2
K (mg•L-1)	3.55	42	275	4.76	40	204	10	36	55	4.2	118	293
Ca (mg•L-1)	0	15	66	6.45	39	100	82	110	172	5.6	35	99
Total Fe (mg•L-1)	0	0.12	1.1	0.00	1.8	10.02	0	0.18	0.94	0	0	0
Fe(II) (mg•L-1)	0.48	1.3	2.6	0.36	1.6	12	0.32	0.57	0.84	0.26	0.52	1.5
Fluoride (mg•L-1)	0.36	3.0	5.94	0.27	1.49	9.44	0.1	0.53	0.78	0.29	0.98	1.9
Chloride (mg•L-1)	21	748	1209	1.85	56	270.9	0.81	4.75	12	1.5	11	37
Nitrite (mg•L-1)	0	1414	4240	0	1.07	1.63	0.8	0.93	1.08	0	0.82	1.1
Bromide (mg•L-1)	0	0	0	0	0.72	2	0	0.15	0.9	0	0.38	0.93
Nitrate (mg•L-1)	0	17	51.41	0	2.32	10.67	0	0.98	2.05	0	2.95	8.8
Phosphate (mg•L-1)	0	3.3	9.97	0	0.4725	1.81	0	0.39	1.43	0	0.12	0.84
Sulfate (mg•L-1)	1.5	1451	2377	1.39	3.61	13.18	1.49	1.8	2.3	1.4	3.9	8.5
Total As Conc. (µg/L)	0.64	1478	5499	2.11	25	149.98	4	15	39	1.1	34	143
As(+3) conc. (µg/L)	0	1082	3981	0	9.39	94.8	0	8.0	32	0	13	51
As(+5) conc. (µg/L)	0	396	1695	0.38	15.4	55.19	0	6.53	11	0	21	92
Calcite log Q/K	0.015	0.0148	0	0.005	2.8	12	1.6	2.9	3.76	0.013	1.5	3.9
Dolomite log Q/K	0	-	0	0.000	469	4247	3.5	32	91	0.000	264	813
Siderite log Q/K	0.086	76	120.4	0.027	13	71	0.33	1.0	1.595	0.041	2.8	11
DOC (mg•L-1)	8.0	85	233	8.9	35	166	11	17	25	24	28	33
TN (mg•L-1)	0.30	4.97	24	0.55	1.5	3.2	0.45	0.82	1.3	1.00	1.3	1.5
UV 254	-	3.14	12	0.25	0.71	1.8	0.22	0.38	0.57	0.34	0.5	0.84
SUVA (L/mg-m)	-	3.44	8.7	1.0	2.3	4.6	1.8	2.2	2.5	1.4	1.9	2.7

3.3.3 Microbial Community

To investigate the microbial community inhabiting the soils of the Okavango Delta, amplicon pyrosequencing was conducted. Pyrosequencing is a cost-effective DNA analysis of a complex genome. Pyrosequencing generated between 785 (Camp 5) and 1922 (New 3) bacterial sequence counts and between 2183 (Camp 5) and 14261 (New 3) archaeal sequences (Table 3-3).

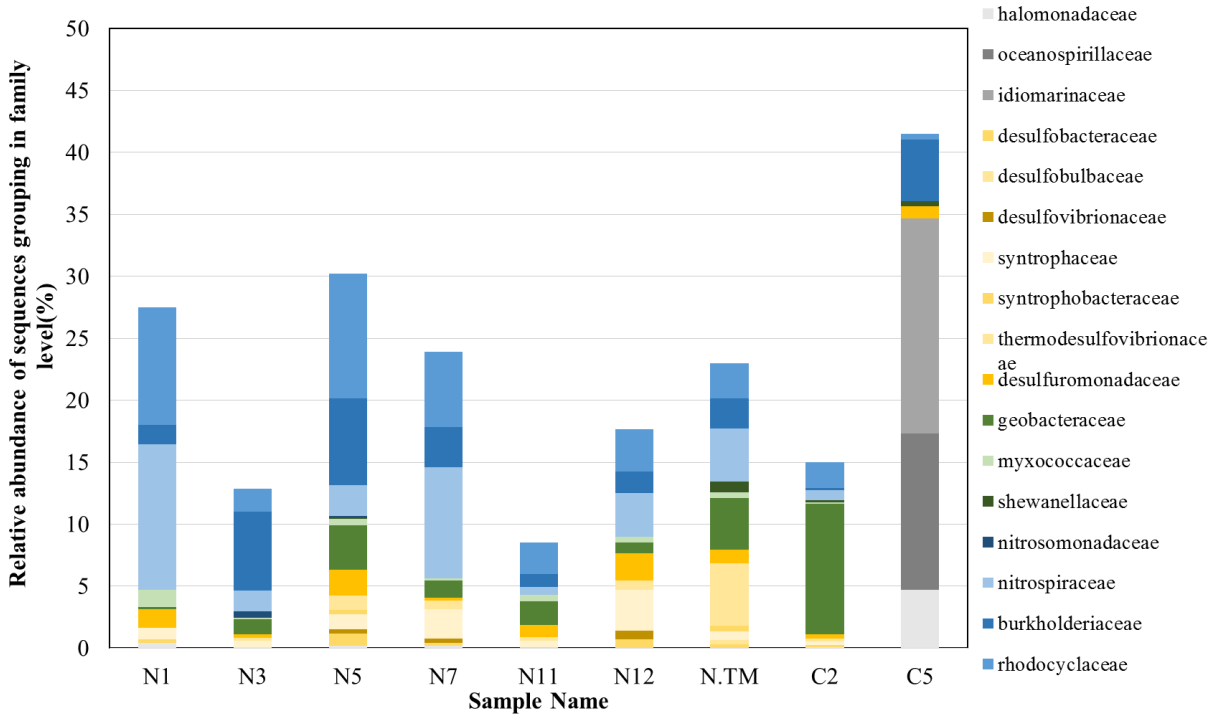

Figure 3-21. Relative abundance of sequences grouping in families capable of nitrate/nitrogen (blue), iron (green) and sulfate reduction (yellow) and sequences grouping as halophilic (gray)

At New Island, the two most abundant phylogenic groups in each soil sample were *Proteobacteria* (up to ~71% relative abundance at phylum level) and *Actinobacteria* (up to ~16% relative abundance at phylum level) (Figure 3-22). At New 1, 23% of the relative abundance was

represented by sequences grouping in families capable of reducing nitrate. The relative abundance of nitrate reducers was lowest at New 11 (4.2%) (Table 3-3). Sequences grouping in families capable of sulfate reduction were highest at New TM (8% relative abundance at family level) (Table 3-3). The relative abundance of sequences grouping in class level as gamma (γ)-proteobacteria was found to be highest at New 11 with 50% (Figure 3-22). The relative abundance of sequences grouping as delta (δ)-proteobacteria were found highest at New 5 and New 12 with 10% (Figure 3-22). Methane producing archaea were found to be present in all the soil samples. At the order level, methane-producing archaea were found highest at New 7 (~24% relative abundance) and New 12 (~25% relative abundance), and lowest at New 11 (~7% relative abundance). The highest relative abundance of sequences grouping as methanogens was *Methanosarcinales* (up to ~18% relative abundance) in all soil sample (Figure 3-23).

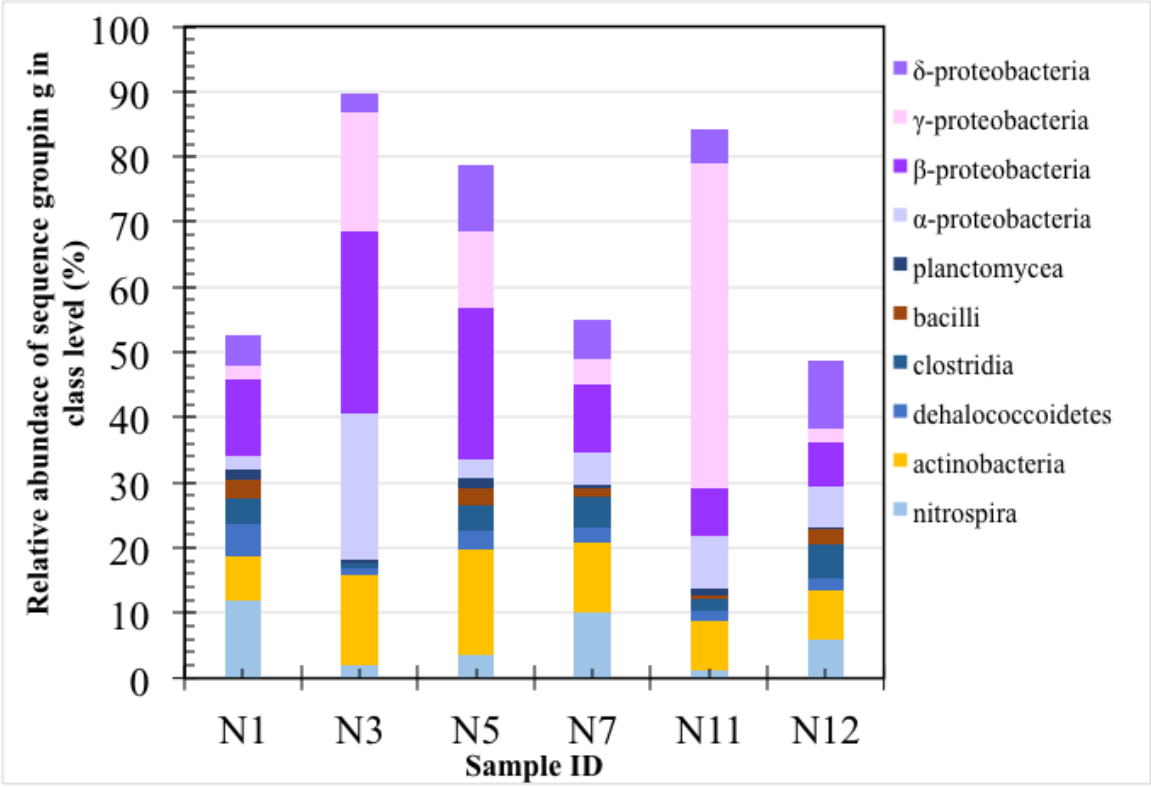

Figure 3-22. New Island: Relative abundance of sequences grouping in class level. *Note: the most abundant (unclassified sequences and relative abundance of sequences are >5% included.*

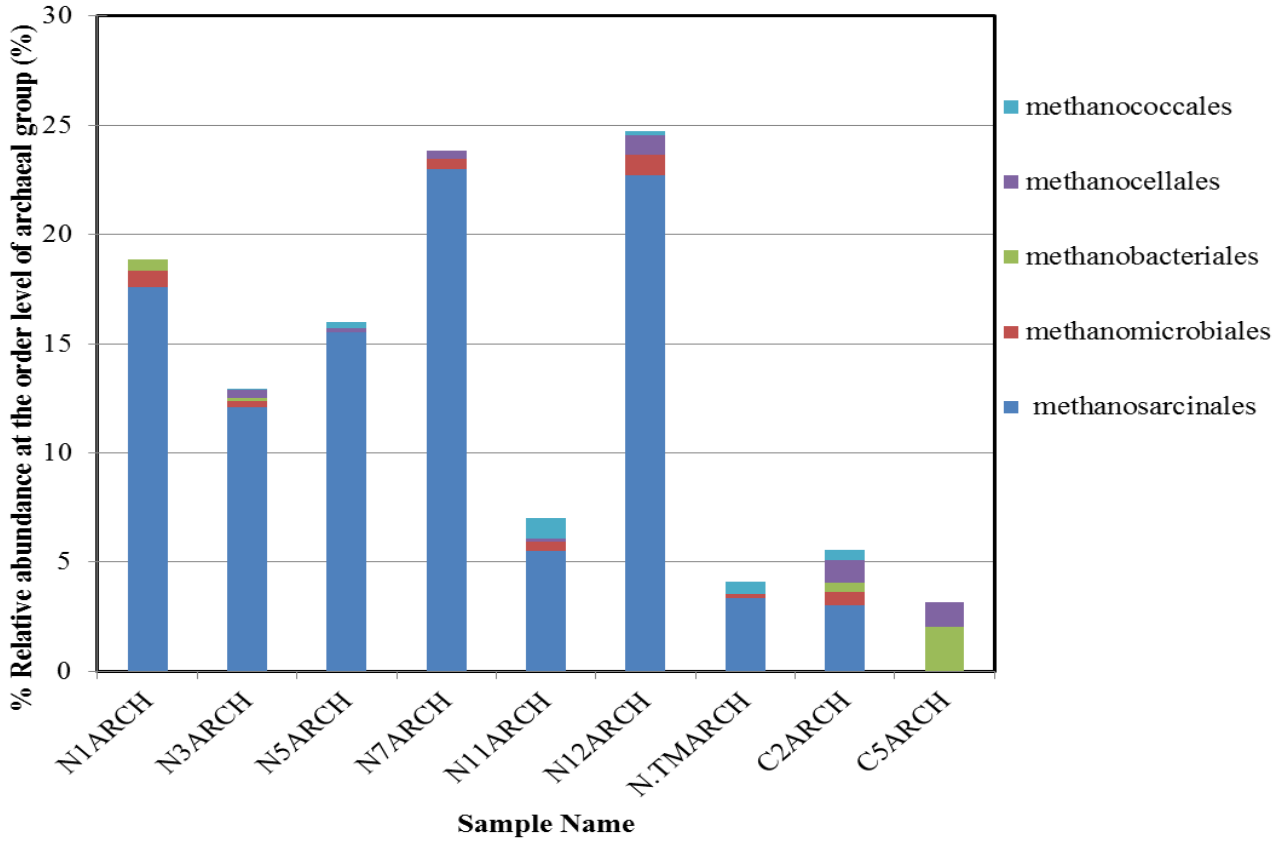

Figure 3-23. Relative abundance of archaea sequences grouping in order level, capable of producing methane.

At Camp Island, sequences grouping in phylum groups from *Fusobacteria* (~60% relative abundance) and *Proteobacteria* (~19% relative abundance) were dominant at Camp 2 soil samples whereas *Proteobacteria* (~78% relative abundance) and *Firmicutes* (~9% relative abundance) were dominant at Camp 5 (Figure 3-23. **Relative abundance of archaea sequences grouping in order level, capable of producing methane.**). At the family level, 11% relative abundance of sequences grouping in families capable of iron reduction was found in Camp 2 soil samples. In the subclass of *Proteobacteria*, the relative abundance of sequences grouping as *δ-Proteobacteria* was high at Camp 2 whereas the relative abundance of sequences grouping as γ-

Proteobacteria was at Camp 5. High *Halophiles* dominated the Camp 5 (35% relative abundance at the family level) soil samples (Table 3-3).

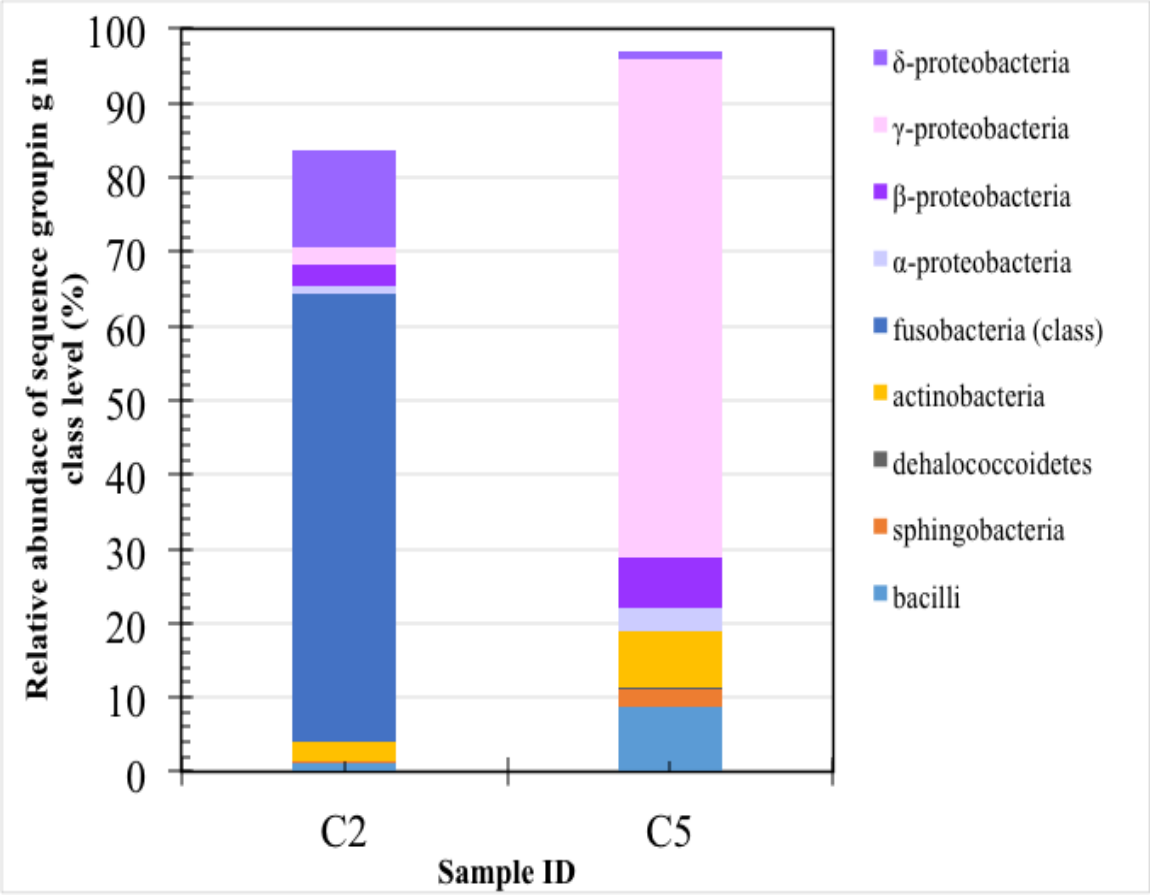

Figure 3-24. Camp Island: Relative abundance of sequences grouping in class level. *Note: the most abundant (unclassified sequences and relative abundance of sequences are >5% included.*

Table 3-3. Bacterial sequence counts at the family level for each soil sample. The total bacterial sequence counts include sequences not listed below.

Family	N1	N3	N5	N7	N11	N12	N.TM	C2	C5
Halophile									
Halomonadaceae	4	1	2	2	0	0	0	2	37
Oceanospirillaceae	0	0	0	0	0	0	0	0	99
Idiomarinaceae	0	0	0	0	0	0	0	0	136
SO_4^{2-} reducing bacteria									
Desulfobacteraceae	3	1	10	3	1	8	3	4	0
Desulfobulbaceae	0	0	0	0	0	0	3	0	0
Desulfovibrionaceae	0	0	3	4	0	7	0	0	0
Syntrophaceae	9	10	12	28	6	36	6	7	0
Syntrophobacteraceae	0	0	4	0	0	0	4	0	0
Thermodesulfovibrionaceae	0	4	11	8	3	8	45	6	0
Desulfuromonadaceae	14	5	21	3	11	24	10	8	8
Fe-reducing bacteria									
Geobacteraceae	2	24	36	16	21	9	37	258	0
Myxococcaceae	13	2	5	2	6	5	4	3	0
Shewanellaceae	0	0	1	0	0	0	8	3	3
Nitrate reducing bacteria									
Nitrosomonadaceae	0	10	1	0	0	0	0	0	0
Nitrospiraceae	113	32	25	106	7	38	38	20	0
Burkholderiaceae	15	123	70	38	12	19	22	5	39
Rhodocyclaceae	91	35	100	71	28	37	25	51	4
Aerobic									
Streptomycetaceae	36	29	32	51	15	39	19	6	8
Comamonadaceae	2	301	31	2	38	0	0	3	10
Bacillaceae	25	0	15	15	6	24	22	27	62
Pseudomonadaceae	2	152	59	3	274	10	12	19	88
Unclassified	43	7	16	38	11	47	36	3	2
Total bacterial sequence count	*959*	*1922*	*996*	*1176*	*1118*	*1080*	*892*	*2443*	*785*

Table 3-4. Methane-producing archaeal sequences count at the order level. The total archaeal sequences count include sequences not listed below.

Order level	N1	N3	N5	N7	N11	N12	NTM	C2	C5
Methanosarcinales	237	1727	326	246	368	371	51	362	0
Methanomicrobiales	10	36	0	5	29	16	3	77	0
Methanobacteriales	7	23	0	0	0	0	0	50	44
Methanocellales	0	54	4	4	9	14	0	128	25
Methanococcales	0	7	6	0	63	3	8	52	0
Total archaeal sequences count	1347	14261	2101	1069	6708	1635	1521	12086	2183

3.4 Discussion

3.4.1 Influence of Chemical Precipitation on Sediment As Concentration

The groundwater table beneath the islands of the Okavango is normally shallow allowing evaporation of water from the aquifer and transpiration from surrounding vegetation. This drives lateral flow of groundwater from surface water toward island interiors (Figure 3-2). Concentration by evapotranspiration (evapoconcentration) is known to drive several geochemical reactions resulting in chemical precipitation and ultimately, island growth and formation (Bauer-Gottwein et al., 2007; McCarthy et al., 2012). In the four islands studied in this paper, accumulation of solutes and high EC occurs in the center zone. Similarly, the sediment chemistry reveals accumulation of some elements (Al, Fe, As) in the center zone (Figure 3-16). Mineral precipitation due to increasing salinity towards the interior of the islands has been known to maintain the low solute concentration in the surface water ((McCarthy et al., 2011; Bauer-Gottwein et al 2007; Ramberg and Wolski, 2006). Camp Island and Palm Island are predominantly covered with salt-crusted surface and devoid of vegetation (Figure 3-3). Among the four islands studied, Camp Island is the largest in area with raised topography (up to 3 m above adjacent surface water) and almost barren soil in the interior of the island compared to the other three islands. Until now, it has been concluded that the sediments in the high EC center

zone are dominated by inorganic carbon (Mg-rich carbonate mineral) (McCarthy et al., 1993; McCarthy and Ellery, 1995; Ramberg and Wolski, 2008). The TIC content we measured in island soils (ranging from 0 % to 1.4 %) was higher compared to the values reported in other studies, which ranged from (0 % to 0.4 %; Huntsman-Mapila et al., 2002). In our study, the high sediment TOC and TIC in the high EC center zones of all four islands confirms the presence of both inorganic and organic carbon, and suggests that the organic carbon pool may also be contributing to island formation. New Island has a wide coverage of trees and shrubs in the fringe zone and interior of the island (Figure 3-4). Sequestration of As by soil organic matter has been suggested as an important removal method for dissolved As (Langer et al., 2011). However, Mladenov et al. (2013) suggested that sequestration of As by soil organic matter (SOM) was not likely to be a major pathway for As removal because of the low SOM content in the Okavango Delta compared to peat lands. Our results are in agreement with Mladenov et al. (2013) because our sediment TOC, ranging from 0.2 to 2.61 $mg \cdot kg^{-1}$, is lower than the global average (~5$mg \cdot kg^{-1}$ in sediment); therefore, sequestration of As by SOM is less likely. We did, however, find evidence of As uptake by vegetation at all four islands. A study conducted with wetland plants submerged on a mine tailing (rich in sulfides), having 152 $mg \cdot kg^{-1}$ of As, found leaves of *Salix* (willow tree) with 700 $\mu g \cdot kg^{-1}$ As, which is in the same range as our study (Stoltz and Greger, 2001). In our study, at One Tusk Island, rain tree leaves accumulated 1665 $\mu g \cdot kg^{-1}$ of As, where the underlying sediment As max concentration was 2997$\mu g \cdot kg^{-1}$. At New Island, a salt-tolerant grass in the eastern floodplain contained 1767 $\mu g \cdot kg^{-1}$ As, where the underlying sediment As max concentration was 1562 $\mu g \cdot kg^{-1}$. Interestingly, Stoltz and Greger (2001) found that roots contained much greater As content of 276 $mg \cdot kg^{-1}$ in *Eriophorum angustifolium* (tall cottongrass)

roots. Future measurements of As in roots at our sites are needed to further evaluate the role of plant As uptake in the fate of As in the Okavango Delta.

3.4.2 Spatial distribution of physical and chemical properties in surface water and groundwater

3.4.2.1 Surface water

The lateral direction of the groundwater flow provides constant replenishment of island groundwater from recharging surface water adjacent to the islands (Ramberg and Wolski, 2006). The infiltration of surface water due to evapotranspiration maintains the low solute and As concentrations in the surface water and keeps the Okavango Delta from becoming a great salt lake system (Ramberg and Wolski, 2006). The As concentration in the Boro Channel (~3 $\mu g \cdot L^{-1}$) was at the higher end of the As concentration range measured in major rivers (1 to 3 $\mu g \cdot L^{-1}$; Ravenscroft et al., 2009).

3.4.2.2 Low conductivity fringe zone

A high density of vegetation and low solute concentration in groundwater characterizes the low conductivity fringe zone. In this zone, microbial activity may be substantial because of high DOC concentration (>5$mg \cdot L^{-1}$) and nutrient loading from surface water infiltration and lateral transport. The vegetation at the island's fringe, more clearly delineated in Camp Island (Figure 3-3) than the other islands, is a result of nutrient inputs from surface water to groundwater in this nutrient-poor wetland (Krah et al., 2006). At New Island, a large area of trees and shrubs dominated the whole island, whereas in Palm Island and Camp Island trees and shrubs were more robust in the fringe zone than in the center zone. One Tusk Island, on the other hand, had no distinct zone of robust vegetation, but rather sparse coverage of trees and shrubs was observed. Island size has been used to speculate about the age of islands (Gumbricht et al.,

2004) and may suggest that One Tusk Island is a young island, which has not yet developed a clearly delineated center zone of high solute concentration.

During the flood season (April to September), infiltrating floodwaters supply dissolved N and P to the islands' fringe for biological and microbial processes (Krah et al., 2006). From our microbial analysis, the maximum number of sequences generated by pyrosequencing DNA analysis was measured at New 3 (20 m from the western shore of new island), and may be related to greater nutrient availability in this zone. The higher number of sequences may, to some extent, also result from the constant DOM loading that maintains more diverse microbial communities (Bethke et al., 2011; Flynn et al., 2013). The constant DOM loading allows more thermodynamically favorable microbial metabolism to proceed (Bethke et al., 2011; Kirk et al., 2004; Jin and Bethke 2009). In aquifers with high DOM loading, the oxidized species will be reduced by microbes following this sequence: O_2, NO_3^-, Mn (IV), Fe (III), SO_4^{2-} and CO_2 (Champ and Jackson, 1979; Chapelle and Lovley, 1992). In New and Camp Island, the relative abundance of nitrate reducers and iron reducers (Figure 3-21) is highest in the fringe zone (Camp 2, New 1, 2 3 and 5), where DOM was replenished by adjacent surface water. The high dissolved Fe (II) and low nitrate throughout New Island and Camp Island, suggest an active metabolism by nitrate and iron reducers. The fresh source of carbon, largely after flooding, likely creates a more favorable environment for nitrate reducers to reproduce. Ultimately, nitrate gets depleted and the carbon source reduces to a level not favorable for nitrate reducers' metabolism. Microbial iron reduction becomes more energetically favorable, outcompeting nitrate reducers for the carbon energy source.

The high DOC concentration also helps maintain reducing conditions and sustains microbially mediated metal reduction. Reductive dissolution of Fe oxide minerals may be an

important mechanism releasing As into the groundwater, according to Huntsman-Mapila et al. (2006) and Mladenov et al. (2013). There is a positive correlation between the Fe and As concentration in sediments, which may support that Fe-reductive dissolution releases As. The high dissolved Fe concentration and high relative abundance of microorganisms capable of Fe (III) reduction in the fringe zone of both New Island and Camp Island further support a mechanism of As release by reductive dissolution of Fe oxide minerals. In groundwater, re-oxidation of Fe (II) during the flood season and re-sorption of As into Fe oxy(hydro)oxides may occur (Hunstman-Mapila et al., 2006). In addition, the groundwater in the islands' center zone was supersaturated with respect to siderite ($FeCO_3$), triggered by high pH and alkalinity, and may be responsible for the low dissolved Fe in groundwater. Identifying the mineralogy of the sediments in the main island zone would provide more definitive support for reductive dissolution as the mechanism releasing As to the groundwater.

3.4.2.3 High conductivity center zone

The islands of the Okavango Delta have been known to be major sinks for solutes. A high conductivity center zone with high arsenic concentration has been proposed to be present in most of the islands in the delta (Mladenov et al., 2013). Our results showing groundwater high As zones corresponding to high EC zones are consistent with this notion. In addition to high EC, high concentrations of Cl^- and other conservative ions characterize this zone and reflect the major influence of evapotranspiration on the location of solute accumulation. In other aquifers with lateral flow, such as the Carson Desert, Nevada, the high As appears to be attributed not only to evapotranspiration but also to dissolution, desorption adsorption or re-absorption of mobilized As under oxidizing condition (Welch and Lico, 1996). In this study, the data points above the evapoconcentration line (Figure **3-25**) are from Camp Island and Palm Island, where

high As may be due to dissolution and formation of complexes (e.g., thioarsenic and As-NOM complexes). Further, alkali desorption of As may also occur due to changes in pH and ionic strength or competitive interactions with other inorganic ions (e.g. dissolved silica and PO_4^3) and humic substances (Mladenov et al., 2013). At Camp Island (Camp 6) and Palm Island (Palm 5), where pH is as high as 8.5, As increased more than Cl^- and the high As concentrations may have been a result of As desorption at high pH (from pH 8 to 10; Dixit and Hering, 2003). There may also be a competitive interaction between As and humic substances, which is dependent on the pH and ionic strength of the solution (Thanabalasingam and Pickering, 1986; Grafe et al., 2001). At higher pH, humic substances dissociate and become negatively charge (Essington, 2004), which enables humic substances to bind to positively charged surfaces of clays and metal-(hydro)oxides (Stevenson, 1982).

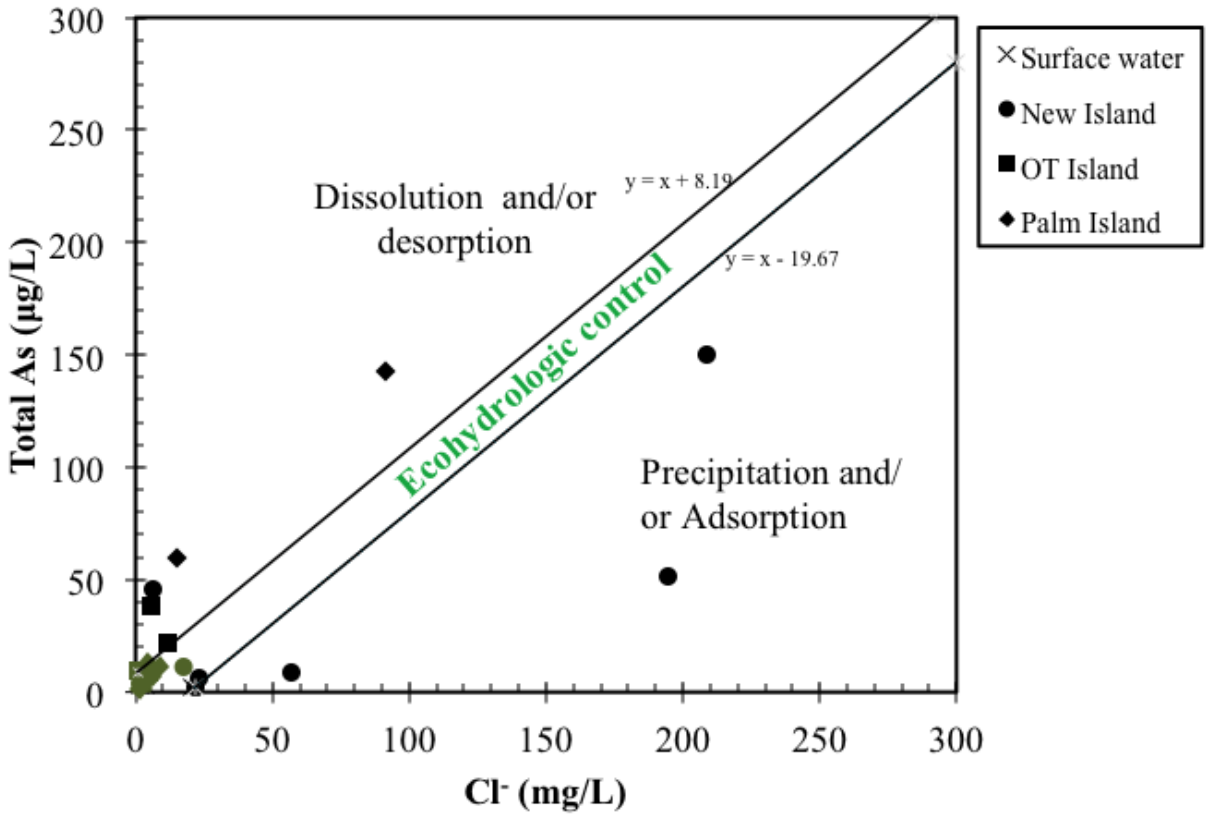

Figure 3-25. Concentrating effect of evapotranspiration. The upper limit of the evapoconcentration line is the highest As/Cl ratio and the lower limit is the lowest As/Cl ratio.

Below the evapoconcentration line (Figure 3-25) adsorption and/or precipitation of As (e.g. As-S precipitation) may be underway. Mladenov et al. (2013) found orpiment-like sediment or As solid species at New 11, which suggests precipitation of As with sulfide ions. In support of As-S mineral precipitation, microorganisms capable of sulfate reduction were present closer to the island center at New Island (New 5 and 12). Sulfate reduction results in the production of sulfide, which would be available for precipitation reactions.

At One Tusk Island, most of the groundwater samples' As/Cl ratio was plotted within the evapoconcentration line (Figure 3-25). This suggests that the high As at One Tusk Island was an

effect of evapotranspiration. Most of the wells at One Tusk Island had nearly neutral pH (up to 7.1) maintaining the assembly bond of sorbed As (V) in sediment surfaces (Welch and Lico, 1998). In addition, the species in Palm and One Tusk islands were mostly As (V), whereas at New Island and Camp Island As (III) species were more prevalent.

The high groundwater to surface water (GW:SW) ratio of Ca^{2+} at the low conductivity fringe zone compared to the ratio for Cl^- (Table 3-1) suggests evapotranspiration is not the only factor influencing Ca^{2+} in groundwater. Microbially-mediated silicate mineral weathering (e.g. weathering of Feldspar, $CaAl_2Si_2O_8$) presumably triggers calcite and dolomite formation (Roberts et al., 2004; Bennett et al., 2001), which could be an important mechanism in this zone. In a petroleum-contaminated and oligotrophic aquifer of Minnesota, metal-reducers and methanogens (i.e., dissimilatory iron reducing bacteria) were found to accelerate silicate weathering by destroying silicate mineral to access apatite (phosphate mineral) enclosed in the silicate mineral (Bennett et al., 2001). Phosphate is important in production of Adenosine Triphosphate (ATP) for cellular energy storage and metabolism. We propose that microbially induced silicate weathering could be happening in the islands' fringe zone. Silica in sediment was also found highest at the fringe zone and decreases towards the center of the island suggesting silicate weathering over time. If the oldest zones of this islands are at the center, as island growth theory would suggest (Ramberg and Wolski, 2006; McCarthy et al., 2011), then the low sediment Si in island centers is consistent with the idea of island centers having experienced most Si weathering over time.

The formation of carbonate minerals has been known to occur in the islands of Okavango (McCarthy et al., 2011; Bauer-Gottwein et al 2007; Ramberg and Wolski, 2006). However, microbial activity may be contributing and expediting the formation of carbonate minerals by

enrichment of Ca^{2+} and Mg^{2+} from silicate weathering. A laboratory experiment found methanogens to be important in dolomite formation (Roberts et al., 2004). In addition, sulfate-reducing bacteria also expedite carbonate mineral precipitation in seawater, which is supersaturated with respect to calcium carbonate (O'Braissant et al., 2007). The high SI values for New 7 and 12 groundwater samples show supersaturation with respect to dolomite in calcite and siderite (Table A-4) could be microbially mediated (i.e., methanogens and sulfate reducers). The findings were consistent with the laboratory study by Roberts et al. (2004) showing that the enrichment of Ca and Mg from silicate mineral (in Roberts et al. study basalt) weathering and methanogens consumption of dissolved CO_2 resulted in carbonate mineral precipitation. In this study, the high relative abundance of methanogens (Table 3-4) and high SI values indicate that the solution was supersaturated with respect to carbonate minerals, and methanogens could enhance carbonate mineral precipitation along with evapoconcentration. Further, the relative abundance at the family level of sulfate reducing bacteria was also found highest at the center zone at New Island (New 5, 7 and 12; Figure 3-21) These findings add new insights into the role of microorganisms on mineral precipitation in the islands of Okavango.

Microbial metabolism could also affect the stability of sorbed As. Production of HCO_3^- from microbial metabolism and weathering processes increases alkalinity in groundwater. Increasing alkalinity could disrupt the stability of As-S (e.g., orpiment) mineral and re-mobilize As. Arsenic is known to form thioarsenate complexes with sulfate, which are highly mobile As-S complexes, especially under alkaline pH and sulfidic conditions (Suess and Planer-Friedrich, 2012). At New Island and One Tusk Island, precipitation of orpiment-like minerals or surfaces on minerals could contribute to As sequestration. However, the moderate As and low S concentration in these islands compared to Camp 6 (6 m and 8.5 m depth), suggests that the

dissolution of As-S and its release into solution is not dominant. Instead, under anoxic conditions and alkaline pH, the kinetics of dissolved As re-sorption is faster (Seuss and Planer-Friedrich 2012). Some amount of re-sorption of dissolved As is likely to occur in the center of all the islands as a result of anoxic conditions and alkaline pH that accompany high groundwater EC in those zones.

Another desorption process mobilizing As into the groundwater is the competitive interaction of dissolved silica with dissolved As for sorption sites. In water, dissolved silica is mainly from soil and water interaction, chemical weathering and plant uptake and recycled back into the soil through plant litter (Derry et al., 2005). Analysis of dissolved Si is needed to better understand the importance of silica cycling for As mobilization.

3.5 Conclusion

In this chapter, the biogeochemical and ecohydrologic controls of As mobilization in the four islands (Camp Island, New Island, Palm Island and One Tusk Island) of the Okavango Delta were discussed. The concentrating effect of evapotranspiration was found to be important in solute and As accumulation in all four islands. Vegetation in the four islands could take up As in tree leaves and grasses inhabiting the islands. Our results showing vegetation uptake of As or other toxic metals, warrant further study of the influence of plant uptake on the fate of As in the Okavango Delta.

The microbial community composition results, examined for New Island and Camp Island, suggest that the fringe zone of these islands had more diverse microbial community composition than the high conductivity center zone. Microorganisms play an important role in As release to groundwater (i.e., release of As by microbial Fe-reductive dissolution and sequestration of As by forming As-S mineral, sulfide supplied by microbial sulfate reduction). In

addition, microorganisms may be also enhancing silicate weathering and expediting carbonate mineral precipitation.

Chapter 4 - Characterizing DOM to understand the biogeochemical processes in the islands of the Okavango Delta

4.1 Introduction

The Okavango Delta is a large wetland with an area of 25,000km^2 and punctuated with tens of thousands of islands. Most islands are characterized by fringe vegetation and barren center. The islands act as a sink for solute and because of the generally high infiltration rate (Ramberg et al., 2008) and the solute accumulates at the center zone influencing the barren, salt-crusted surface (McCarthy et al., 2010; Bauer-Gottwein et al., 2007). The islands also act as sink for dissolve organic matter (DOM) from the DOM-rich surface water (Mladenov et al., 2008). The high dissolved organic carbon (DOC) concentration in surface water (Mladenov et al., 2008) is an indicative of dissolved organic matter (DOM)-rich surface water. The high infiltration rate of surface water to the groundwater (Ramberg et al., 2006) supplies the groundwater with DOC. In groundwater, DOM plays an important role in controlling the speciation, solubility, mobility and bioavailability of trace metals (e.g., arsenic (As)) and other contaminants (Wang and Mulligan 2006). Fulvic acids, defined as moderate molecular weight acids that are soluble at all pH values, are known to be the dominant fraction of DOM in surface water (45-65%) and wetlands (80-90%) (Aiken et al., 1985; Thurman, 1985; McKnight et al., 2003). In groundwater, fulvic acids typically accounts for 10-30% of the DOM pool and mainly comprise microbially processed DOM (Thurman, 1985).

In the Okavango Delta, sorbed As on Fe-oxide minerals is believed to be mobilized via microbial Fe-reductive dissolution (Huntsman-Mapila et al., 2006). Microbial reductive dissolution of metal-(hydro) oxides, particularly iron Fe (III), result in the release and redox

transformation of arsenate, As (V), to a more toxic and more mobile arsenite, As (III) (Langner et al., 2011; Wang et al 2006; Mladenov et al., 2010). In environments with Fe (III) but low humic substances concentration, DOM can further enhance Fe (III) and As (V) reduction via the ability of humic substances to shuttle electrons (Mladenov et al 2010; Nevin and Lovley 2000). In DOM-rich soils (e.g., peat layers), As release to the water is governed by DOM through Fe-reductive dissolution (Langner et al., 2011), aqueous complexation (Guangliang et al., 2011) and competitive adsorption (Wang and Mulligan, 2006; Thanabalasingam and Pickering, 1986). Aqueous complexation and competitive adsorption could occur at higher pH, which enhance the ability of humic substances to sorb onto mineral surfaces and/or form aqueous complexes (Wang and Mulligan 2006; Mladenov et al., 2010).

The light absorbing characteristics of DOM enable environmental and aquatic scientists to characterize DOM using spectroscopic analyses (i.e., absorbance and fluorescence), a fast and relatively inexpensive alternative technique. Spectral properties, which are fast and simpler optical method to evaluate DOM quality, provide information on the aromaticity (specific UV-absorbance (SUVA)) and DOM source and molecular weight (spectral slopes and slope ratio (S_R)). Fluorescence, an advanced optical method to characterize DOM, occurs when a loosely held electron is excited over an excitation wavelength range to a higher energy level and the electron emits light over an emission wavelength range as the electron losses energy to go back to its original state. Organic compounds re-emitting light upon excitation are called fluorophores. Several studies have identified common fluorophores (i.e., protein-like and humic-like) and indices used to quantify DOM fluorescence properties (Coble 1996; McKnight et al., 2001; Ohno 2002; Wilson and Xenopolous, 2008: Cory and McKnight, 2005; Stedmon et al., 2003; Parlanti et al., 2000).

The spectral and fluorescence analyses are widely used to characterize DOM in many different water types, particularly marine samples, estuarine samples and DOM-rich terrestrial samples. However, there are still limited studies using spectral and fluorescence analyses to characterize DOM in groundwater samples. In subsurface environments, fluorescence of DOM acts as an indicator of groundwater quality for aquifers susceptible to contamination and can provide information on DOM source including total petroleum hydrocarbons (TPH), an anthropogenic carbon source (Lapworth et al., 2008). Further, the protein-like and fulvic acid fluorescence peaks are sensitive fingerprints for DOM quality in groundwater (Baker and Black, 2001). In the Okavango Delta, DOM variability in groundwater provides information on the degree of biogeochemical processing that occurs beneath the islands of delta (Mladenov et al., 2008).

In this study, the information from spectral and fluorescence analyses will provide complementary evidence to the analyses of microbial community composition, groundwater chemistry, and physical properties to better understand the biogeochemical processes controlling DOM transformation along flowpaths beneath the islands of the Okavango Delta. Previous studies on As mobilization in Camp Island and New Island indicated that microbial processing of DOM may be contributing to the mobilization of As in both Camp Island and New Island (Huntsman-Mapila et al., 2006; Mladenov et al., 2013). Based on these previous studies conducted on DOM in groundwater, I hypothesized that: *1)* in the island fringe zone, labile DOM is being consumed by microorganisms to reduce Fe-oxide minerals and release sorbed As from the sediments, *2)* the lateral flow of groundwater contributes to DOM transformation (i.e., DOM sorption to sediments and microbial processing), 3) high DOC and As in the center zone is mainly due to ecohydrologic controls (i.e., concentrating effects of evapotranspiration).

This paper aims to provide new insights into the behavior of DOM and its influence on the distribution of As in groundwater beneath the islands of Okavango. Four islands (i.e., Camp Island, New Island, Palm Island and One Tusk Island) were sampled in this study to build on the previous studies conducted in New Island (Mladenov et al., 2013) and Camp Island (Mladenov et al., 2007) and provide more extensive data on DOM spectroscopic characteristics and As mobilization. In addition, Palm and One Tusk Island, located in a seasonal floodplain, provide additional insights into the biogeochemical processes influencing As mobilization in islands.

4.2 Methods

4.2.1 Site Description

The annual discharge to Okavango delta range from 6.0 x 10^9 m3 to 1.64 x 10^{10} m^3 causing seasonal floods, which increases water level in the panhandle up to 2 m and inundates the seasonal floodplain (McCarthy, 2006). The major components of the delta are channels, wetlands and islands, which cover the area of almost 40,000 km^2 and about 150,000 islands ranging in size from small, irregular islands to large islands (Ramberg and Wolski, 2008; Gumbricht et al, 2004). Islands are made up of medium to fine-grained sandy soils and constitute about 5% of the permanent swamp and 25% of the seasonal swamp (Gumbricht et al 2004). The groundwater beneath the islands of the Okavango Delta has relatively high DOC concentration (Mladenov et al., 2008) due to the high infiltration rate driven by ecohydrologic controls (Ramberg et al., 2006). The groundwater follows a lateral and concentric flow direction (Figure 3-2) from surface water toward the island interior (Figure 4-1), which results in the accumulation of inorganic ions, As, and DOC in the center of the island (Ramberg and Wolski, 2008; Mladenov et al., 2013). Further, the concentric groundwater flow facilitates DOM transformation

controlled by biogeochemical processes (i.e., DOM sorption to sediments and microbial processing).

Figure 4-1. Surface water in the Okavango Delta. Left photo shows the dominant vegetation in the Boro River. Right photo shows the clear water and sandy bottom of the river.

4.2.2 Spectroscopic analyses

4.2.2.1 Sample preparation

At the ORI laboratory, samples were filtered through pre-combusted 0.7 µm glass-fiber filter (GFF) in a portable anaerobic glove bag filled with N_2 gas, and were crimp sealed to reduce oxygen exposure. At Kansas State University (KSU) Environmental Engineering laboratory, samples were transferred from the crimp-sealed bottles to 1cm quartz cuvettes in an anaerobic chamber. Samples were diluted with ultra-pure water at a 1:10 dilution factor under anaerobic conditions (Figure 4-2). Camp 6 (6m and 8m depth) were diluted 1:100, and New 11 (2m depth) was diluted 1:20. Camp Island samples from Camp FP1-FP4 and Camp 1-5 (Figure 4) were filtered through 0.7 µm GFF and acidified with HCl. Immediately after dilution; the samples were measured for fluorescence and UV-Visible (UV-Vis) absorbance.

Figure 4-2. Samples under anaerobic N_2 gas chamber for fluorescence and absorbance measurement.

4.2.2.2 UV-Vis absorbance

All Excitation and Emission Matrices (EEM) spectra and UV-Visible absorbance were collected using Aqualog Fluorometer (Jovin Yvon Horiba). Aqualog can simultaneously measure both absorbance spectra and fluorescence EEM or run UV-Vis absorbance alone. UV-Vis absorbance was acquired from 240 nm to 450 nm wavelength with 3 nm increments in a 1-cm path length quartz cuvette. To verify measurements obtained from the Aqualog, absorbance from 200 nm to 800 nm was measured on a subset of samples from Camp Island, New Island, Palm Island and One Tusk Island using Agilent Cary 60 UV absorbance spectrophotometer. The UV-Vis absorbance spectra was used to determine the spectral slope and slope ratios, the ratio of the shorter wavelength region, 275 nm to 295 nm ($S_{275\text{-}295}$), to that of the longer wavelength, 350 nm to 400 nm ($S_{350\text{-}400}$) (Helms et al., 2008). The spectral slope and slope ratio provides information on the biogeochemical processes (e.g., photo bleaching and microbial degradation of DOM) that could be explained by the change in UV-Vis absorbance. Absorption, spectral slopes and spectral

ratio can provide information on the chemical composition, sources and diagenesis of DOM (Helms et al., 2008). Spectral slopes and spectral slope ratio (S_R) can also provide information on the effects of salinity, photodegradation and microbial processing on the DOM characteristics (Helms et al., 2008). Spectral regions 275-295 nm ($S_{275-295}$) and 350-400nm ($S_{350-400}$) can distinguish between terrestrial or marine samples. For example, $S_{275-295} > S_{350-400}$ mainly occurs for marine samples whereas the opposite occurs for terrestrial samples ($S_{275-295} < S_{350-400}$). Helms et al. (2008) found that long-term irradiation of aquatic samples caused significant increases in S_R values from terrestrial (S_R=~0.71) to estuarine or coastal samples (S_R~1.1). A decreased in S_R value from 1.02 to 0.94 over a timescale of 2 weeks indicated processing of DOM by microorganism (Helms et al., 2008).

To calculate spectral slopes and slope ratio, absorbance units were converted to absorption coefficient using:

$$a=2.303\ A/l \quad \frac{\mathbf{A}}{\mathbf{l\ (m)}}$$

where *a =absorption, A=absorbance, and l= path length (m)*

In addition, specific UV-Absorbance (SUVA) can provide information on the aromaticity or humification of DOM (Weishaar et al., 2003). The SUVA value of the sample was also calculated using the ratio of UV-Vis absorbance at an excitation wavelength of 254 nm to that of the DOC concentration ($mg \cdot L^{-1}$) and path length (m).

$$\mathbf{SUVA} = \frac{\mathbf{A_{254\ nm}}}{\mathbf{DOC}\left(\frac{\mathbf{mg}}{\mathbf{L}}\right) * \mathbf{l\ (m)}}$$

The specific UV-Vis absorbance (SUVA) is indicative of aromaticity where a higher value up to 5 $L \cdot mg^{-1} \cdot m^{-1}$ indicates highly aromatic DOM (Weishaar et al., 2003). Weishaar et al. (2003) reported a range of SUVA values from 0.6 to 3.2 $L \cdot mg^{-1} \cdot m^{-1}$ for coastal samples and fulvic acid

isolates, respectively. The concentration of dissolved Fe in samples should be taken into consideration because the UV absorbance of Fe adds to the SUVA values, which could result in SUVA values greater than 5 $L \cdot mg^{-1} \cdot m^{-1}$ (Weishaar et al., 2003).

4.2.2.3 Fluorescence spectroscopy

The Emission Excitation Matrix (EEM) spectra were collected at an increment of 3 nm excitation wavelength over 250 to 400 nm range and increment of 10 nm emission wavelength over 350 to 600nm. EEMs for most samples were scanned using a 1.5 second integration time and four samples (Camp 6 (6m), Camp 6 (8.5m) and New 13), which were scanned using 1.0 second integration. To correct for instrument specific biases and to compare results to other environments, spectra were collected with signal to reference (*S:R*) mode. EEMs were corrected for the inner filter effect using the equation in Lakowicz (1999). Intensities were normalized to the daily area under the Raman curve (at an excitation=~397nm). Ultra-pure water blank EEMs were subtracted from each sample EEM. EEMs were corrected using modified Matlab correction function for Aqualog fluorometer. Peaks intensities (A, B,C, M, T), fluorescence indices (FI, $\beta:\alpha$ and HIX) and UV 254 were calculated from the Matlab correction code.

Fluorescence spectroscopy provides reliable information about the source, redox state, and biological reactivity of fluorescing DOM (Coble, 1996; McKnight et al., 2003; Fellman et al., 2010). The EEM spectra is a three-dimensional representation of the fluorescence intensities over a range of excitation wavelength and emission wavelength. In an EEM spectrum, the location of peaks (Figure 15) may be indicative of various DOM sources. Coble (1996) identified five peaks associated with the following: Peak **A** (*Ex 275 nm and Em 310nm*) and **C** (*Ex 350 nm and Em 420 – 480nm*) are humic-like DOM, Peak **M** (Ex 312 nm and 380-420 nm) is marine-

humic like DOM and Peak **B** (*Ex 275 nm and Em 310 nm*) and **T** (*Ex 275 nm and Em 340 nm*) are protein-like DOM (Figure 4-3).

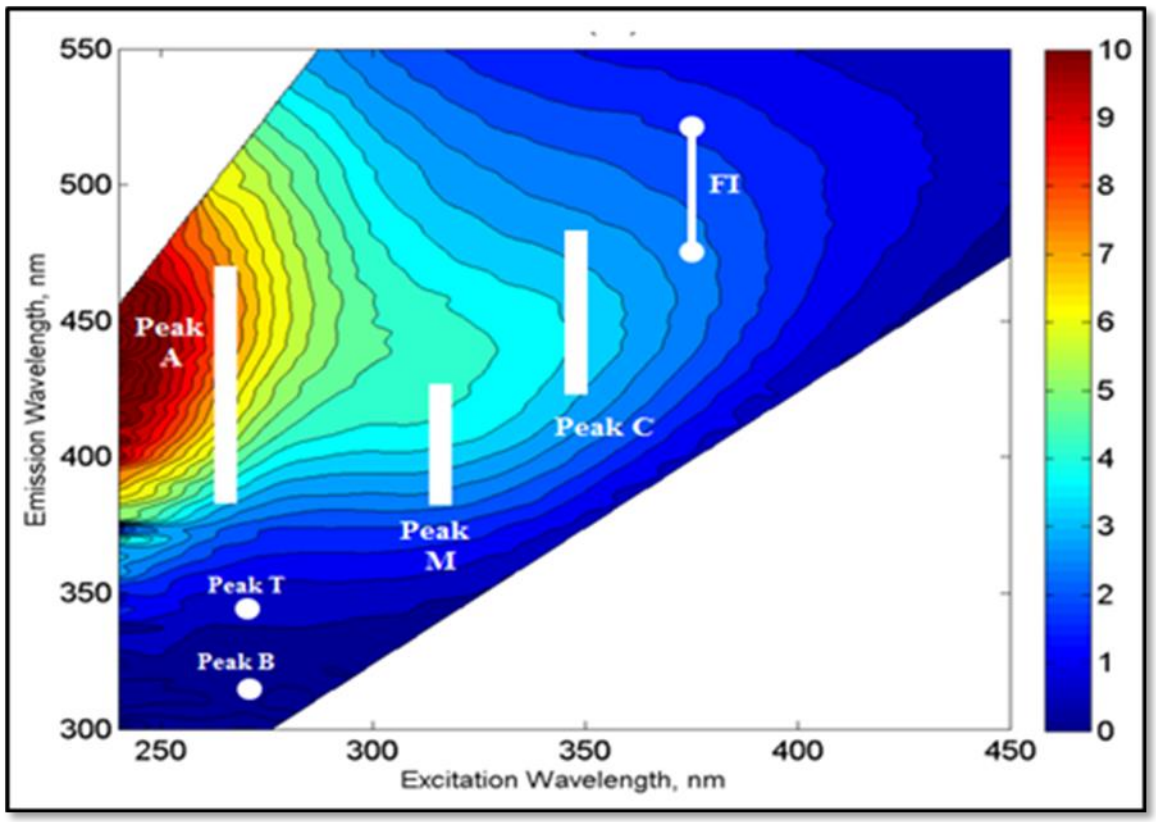

Figure 4-3. Example of groundwater DOM EEM showing the position of the five primary peaks (Coble 1996; Cory and McKnight, 2010)

Fluorescence indices were calculated to quantify variation in the DOM fluorescence properties. The calculations used to determine the values for FI, $\beta{:}\alpha$ and HIX are summarized in Table 4-1. The two-dimensional fluorescence index (FI) is widely used to identify the source of DOM (McKnight et al., 2003; Cory and McKnight, 2006). To estimate biological activity and stage of biological production, the β peak /α peak ratio intensity (also termed as the freshness index) is useful in identifying freshly transformed DOM and more decomposed DOM (Parlanti et al., 2000). The humification index (HIX) is an indicator of humicity or degree of DOM degradation (Zsolnay et al., 1999).

Table 4-1. Summary of fluorescence indices, excitation wavelength, calculation and description. Ex is excitation wavelength and Em is Emission wavelength.

Indices	Ex (nm)	Calculated: Intensities at given Em	Description
FI	370	Ratio: $\frac{470\text{nm}}{520\text{ nm}}$	High FI 1.8 derived from extracellular release and leachate from bacteria Low FI 1.2, terrestrial plant and soil organic matter (Cory and McKnight, 2006)
$\beta{:}\alpha$	310	Ratio: $\frac{380\text{nm}}{\max 420-435\text{nm}}$	High β:α 0.95 more recently derived DOM Low β:α 0.5 more decomposed DOM (Parlanti et al., 2000)
HIX	254	Ratio: $\frac{\text{Area under } 435-480\text{nm}}{\text{Area under } 300-445\text{nm}}$	Higher HIX values indicate increasing degree of humification (Wilson and Xenopolous, 2008)

4.3 Results

4.3.1 DOM in surface water

The DOC concentration was found to be high in floodplain surface water (adjacent to New Island and Palm Island) with a concentration ranging from 8.4 $mg{\cdot}L^{-1}$ to 32 $mg{\cdot}L^{-1}$, the highest found in the sample of Palm Island floodplain water. The DOC in the Boro Channel was found to be fairly constant in the samples collected, with an average concentration of 8.4 $mg{\cdot}L^{-1}$. The FI of floodplain water was slightly lower compared to FI values of samples from the Boro Channel (Table 4-2). The aromaticity, indicated by the SUVA values, was found to be highest in the Boro Channel adjacent to Camp Island with SUVA value of 4.36. There were no significant difference between the SUVA values in the Boro Channel adjacent to New Island and floodplain surface water with values ranging from 2.58 to 2.63 L $mg^{-1}{\cdot}m^{-1}$ (Table 4-2).

Table 4-2. Summary of DOM characteristics using Fluorescence Indices

Sample ID	DOC ($mg \cdot L^{-1}$)	FI	FrI	HIX	SUVA 254nm
Boro Channel near Camp Isld	8.01	1.40	0.54	17.67	4.39
Palm Isld Floodplain SW	32.5	1.34	0.51	17.86	2.58
Boro near New	8.86	1.36	0.54	17.68	2.81
New Isld Floodplain SW	12.7	1.31	0.54	14.26	2.63

The slope ratio (S_R) in Boro Channel was higher in the Boro Channel near Camp Island (S_R=0.92) than in the Boro Side Channel (S_R=1.04) adjacent to New Island. The increase in SR was a result of greater change higher wavelength slope ($S_{350-400}$) value. The SR in the floodplain surface water was similar for both New Island and Palm Island (Table 4-3).

Table 4-3. Summary of Spectral Slope for Boro River and Floodplain surface water (SW)

Sample ID	$S_{275-295}$	$S_{350-400}$	Spectral Slope (S_R)
Boro Channel near Camp Isld	0.0156	0.0165	0.918
Palm Isld Floodplain SW	0.0175	0.0215	0.804
Boro near New	0.0148	0.0141	1.04
New Isld Floodplain SW	0.0127	0.0146	0.870

4.3.2 DOM in groundwater

4.3.2.1 Camp island

The DOC concentrations along the west to east transect gradually increased and reached a maximum of 223 $mg \cdot L^{-1}$ in Camp 6 (Table 4-4). The increasing trend of DOC also followed the trend for As, which increased from 2 $\mu g \cdot L^{-1}$ (fringe zone) to 4050 $\mu g \cdot L^{-1}$ (center zone). In the floodplain groundwater samples, the DOC concentration was in the range of 8 to 25 $mg \cdot L^{-1}$. The SUVA value of groundwater at Camp 6 was found to be 3.01 L $mg^{-1} \bullet m^{-1}$, which was lower than the SUVA value in adjacent surface water. The decreased in SUVA value was due to the significant increase of UV 254nm (6.62). The FI value was similar in the groundwater sampled from the floodplain and surface water, which range from 1.42 to 1.47 (Table 4-4;Figure 4-4).

The β:α slightly increased from the surface water (0.65) to the Camp Island floodplain groundwater (0.75 at Camp FP 4; Table 4-4).

Table 4-4. Summary of DOC concentration, UV 254nm, specific UV-Vis absorbance (SUVA), fluorescence index (FI), freshness (β:α), humification index (HIX), absorption spectral slope and spectral slope ratio (S_R) and EEM peak intensities of groundwater samples from Camp Island.

							Fluorescence peak intensities					Absorption Spectral Slope		
Sample ID	**DOC (mg/L)**	**UV 254**	**SUVA ($Lm^{-1}m^{-1}$)**	**FI**	**B:α**	**HIX**	**Peak A/UV_{254}**	**Peak B/UV_{254}**	**Peak T/UV_{254}**	**Peak C/UV_{254}**	**Peak M/UV_{254}**	**$S_{275-296}$**	**$S_{350-400}$**	**(S_R)**
Boro Ch. Near camp FP	8.05	0.1578	1.96	1.47	0.65	0.15	0.461	0.244	0.472	0.575	0.494	0.0175	0.0147	1.19
Camp FP 1	10.42	0.3824	3.67	1.42	0.69	1.88	2.187	1.414	2.567	3.155	2.740	0.0113	0.0071	1.58
Camp FP2	14.17	0.3962	2.8	1.47	0.7	2.98	2.860	2.125	3.694	4.513	3.923	0.0158	0.0107	1.47
Camp FP3	14.21	0.3228	2.27	1.46	0.75	1.71	2.899	2.160	2.746	3.373	3.031	0.0154	0.0067	2.29
Camp FP 4	24.67	-	-0.25	1.5	0.63	4.08	-	-	-	-	-	0.0197	0.0041	-
Camp1	23.33	-	-0.36	1.62	0.69	3.74	-	-	-	-	-	0.0116	0.0061	-
Camp 2	46.27	4.0258	8.7	1.37	0.57	33.3	1.476	1.396	4.127	4.966	4.002	0.0146	0.0123	1.19
Camp 3	47.24	2.6604	5.63	1.39	0.57	40.9	1.329	1.952	7.711	9.286	7.595	0.0149	0.0197	0.76
Camp 4	82.06	4.3347	5.28	1.43	0.58	71.9	0.577	1.352	7.888	9.973	8.233	0.0158	0.0206	0.77
Camp 5	230.7	11.5073	4.99	1.35	0.6	60.1	0.071	0.406	2.264	2.857	2.411	0.0159	0.0227	0.70
Camp 6 (6m)	220	6.62	3.01	1.2	0.48	47.7	1104	0.00	50.35	431.76	552.58	0.0135	0.0192	0.71
Camp 6 (8.5m)	223	6.60	2.6	1.2	0.5	38.4	1288	0.00	58.05	468.96	587.12	0.0132	0.0161	0.82

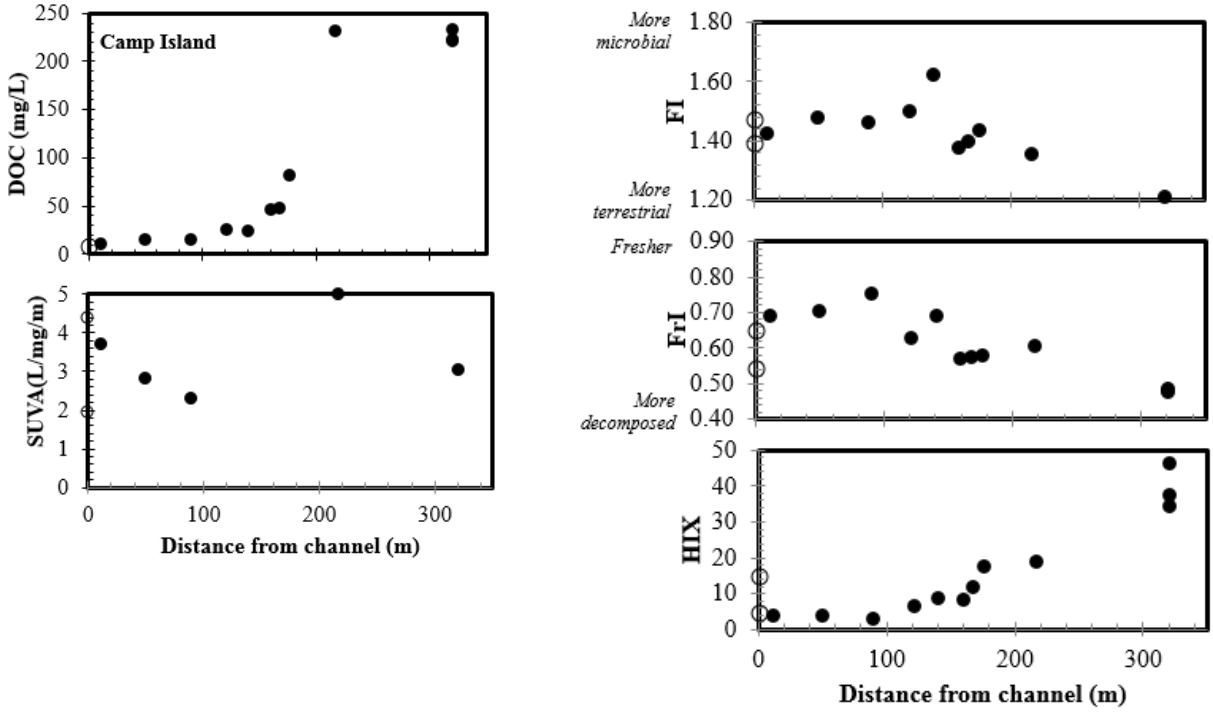

Figure 4-4. Camp Island: changes in groundwater DOM characteristics (DOC, SUVA, FI, FrI and HIX). Surface water (unfilled triangle) is also included in this figure.

4.3.2.2 New Island

In the island fringe zone, piezometers New 3 and New1, 2, 5 and 7 (Table 4-5) had DOC concentrations ranging from 19.16-23.47 mg·L^{-1} (Table 4-5). Further, the quality of DOM was slightly different from surface water. FI values indicate mixed terrestrial and microbially derived DOM (range between 1.48 and1.62), and $\beta:\alpha$ values (0.54-0.65) showed more decomposed DOM than in surface water. A highest intensity was found at peaks A, C and M (humic-like) groundwater samples from this zone, and low intensity at peaks B and T (protein-like) region (Table 4-5). The DOC concentration in New 11 was measured at 45 mg·L^{-1}. The DOM characteristics in the high conductivity center zone, which includes piezometer New 7, 9, 11 and 12, were also changing. The FI values from New 7 to New 11 decreased from 1.60 to 1.4 (Figure 4-6) and $\beta:\alpha$ values followed the same trend as FI. The HIX trend in the high conductivity zone was found to be have reached the maximum values along the west to east transect for this study. The values for HIX were in the range of 20 to 30 from New 7 to New 11 (Figure 4-6). There was also a positive correlation (R^2=0.4792) between total As concentration and HIX (Figure 4-5)

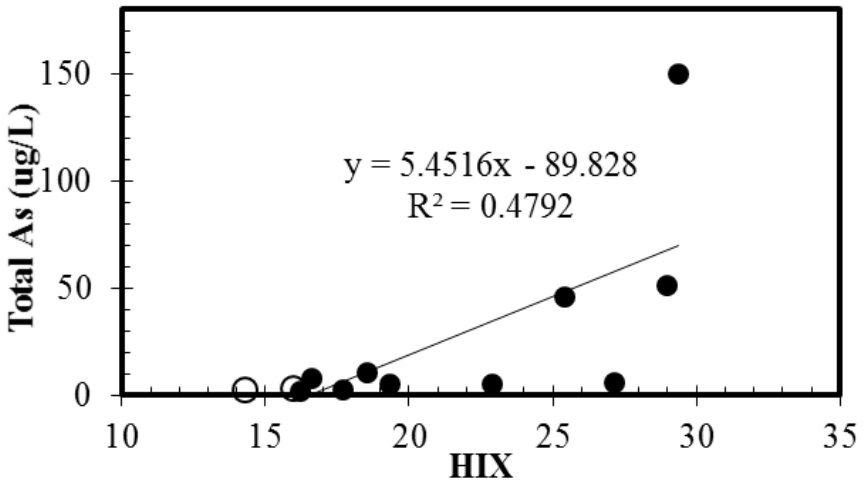

Figure 4-5. Correlation plot of total As and humification index (HIX) for samples from New Island.

The S_R from Boro Channel to New 2 decreased from 1.04 to 0.8 (Figure **4-11**) and then again increased to 1.04 at New 3 and decreased at ~0.8 at New 7. Starting at new 7, the S_R increased to ~1.0 with increasing ionic strength from 0.01 to 0.05 molal (Figure **4-11**).

Table 4-5. Summary of DOC concentration, UV 254nm, specific UV-Vis absorbance (SUVA), fluorescence index (FI), freshness (β:α), humification index (HIX), absorption spectral slope and spectral slope ratio (S_R) and EEM peak intensities of groundwater samples from New Island.

							Fluorescence peak intensities					Absorption Spectral Slope		
Sample ID	**DOC (mg/L)**	**UV 254**	**SUVA ($Lm^{-1}m^{-1}$)**	**FI**	**B:α**	**HIX**	**Peak A/UV_{254}**	**Peak B/UV_{254}**	**Peak T/UV_{254}**	**Peak C/UV_{254}**	**Peak M/UV_{254}**	**$S_{275-296}$**	**$S_{350-400}$**	**(S_R)**
Boro channel near New	8.862	0.24891	2.81	1.36	0.54	17.7	24.14	1.482	2.91	9.85	12.28	0.0148	0.0141	1.04
New 1	19.16	0.53591	2.8	1.55	0.57	27.1	27.10	60.76	0.7725	4.05	26.64	0.0127	0.0146	0.87
New 2	21.25	0.57576	2.71	1.59	0.62	16.0	15.96	41.62	1.773	3.86	19.27	0.0095	0.0133	0.71
New 3	166	1.57734	0.95	1.48	0.54	18.53	18.53	163.2	15.58	16.01	69.27	0.0148	0.0142	1.04
New 5	19.99	0.91424	4.57	1.56	0.65	16.2	16.20	56.06	1.56	6.29	24.68	0.0151	0.0162	0.93
New 7	23.47	0.4500	1.9	1.62	0.63	21.08	19.32	56.99	1.640	5.331	25.03	0.0177	0.0268	0.66
New 9	32.5	0.73772	2.27	1.52	0.57	28.96	28.96	76.16	0.000	4.839	32.25	0.0169	0.0214	0.79
New 11	45.13	0.6541	1.45	1.43	0.52	29.37	29.37	122.8	3.302	7.633	51.63	0.0183	0.0212	0.86
New12	21.9	0.28417	1.3	1.56	0.6451	16.6	16.60	41.60	1.431	4.372	18.57	0.0224	0.0091	2.45
New 13	25.86	0.66988	2.59	1.44	0.52	25.4	25.40	174.7	1.710	13.063	71.65	0.0134	0.0129	1.03
New TM	-	1.78711	-	1.57	0.63	7.21	7.21	121.2	16.18	18.11	53.86	0.0098	0.0049	1.99
Palm 5	29.78	0.4288	1.44	1.48	0.56	35.6	35.62	81.75	0.0000	4.399	34.70	0.0222	0.0723	0.19
Palm 6	23.94	0.4451	1.86	1.53	0.57	34.79	34.79	68.81	0.0000	4.027	29.65	0.0168	0.0135	1.25

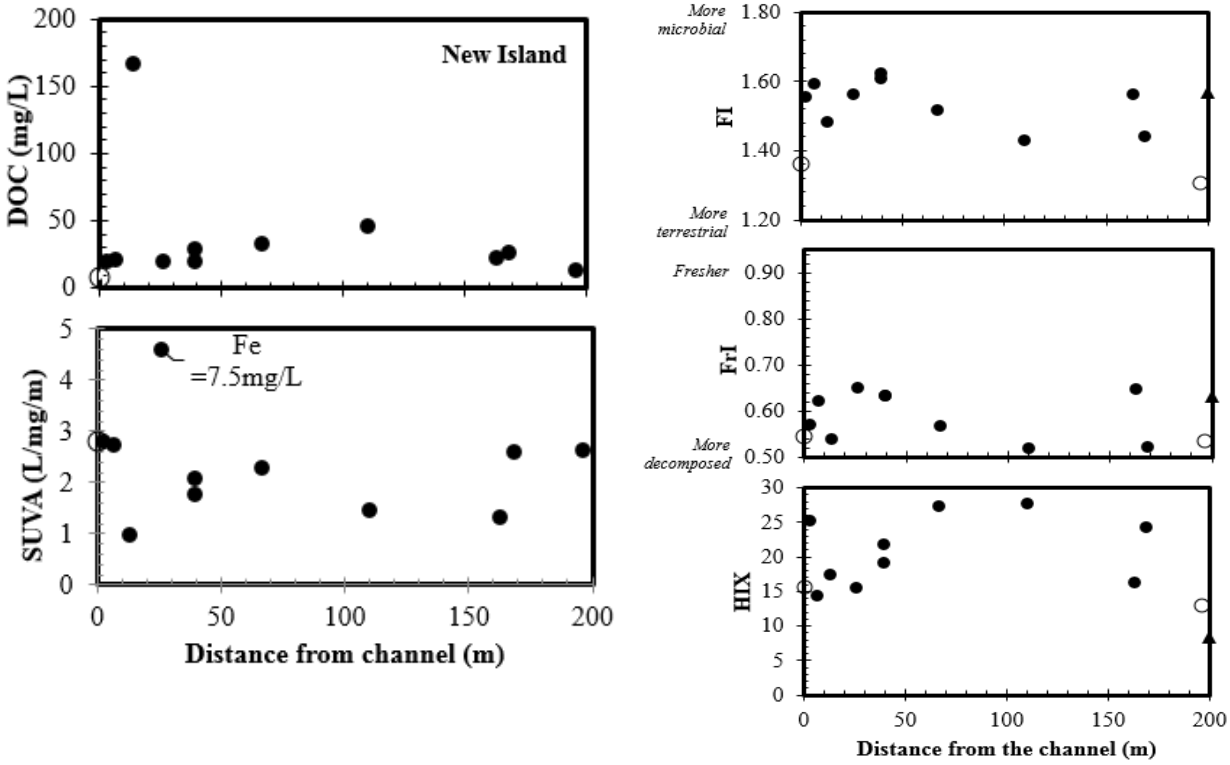

Figure 4-6. New island: changes in groundwater DOM characteristics (DOC, SUVA, FI, FrI and HIX). Boro channel and floodplain surface water (unfilled circle) are included in this figure.

4.3.2.3 Palm Island

The DOC concentration in the low conductivity fringe zone was found to range between 24.5-30.3 mg•L^{-1} (Table 4-6). The DOC concentrations at Palm 5 and 6 were 29 mg•L^{-1} and 24 mg•L^{-1}, respectively. The FI values and β:α ratios along the southwest-northeast transect of Palm Island were constant (Figure 4-8). In the fringe zone, the FI values ranged from 1.4 to 1.48 and *β:α* ratio was between 0.50 and 0.60. The SUVA values ranged from 1.7 L·mg^{-1}·m^{-1} to 2.7 L·mg^{-1}·m^{-1} and HIX values were between 7.77 and 28.7 in the fringe zone (Figure 4-8). The highest intensity at each piezometer was at peak C and M (Palm 1-4), and the intensity at peak T was highest at Palm 2 (Peak T intensity = 0.1063, Table 4-6). Palm 5 had a mid-range FI (1.5), low *β:α* ratio (0.56), high HIX (35.6), and low SUVA=(1.44). There was also a positive correlation (R^2=0.551) between total As concentration and HIX (Figure 4-7). The intensity of fluorescent peaks for Palm 5 was highest at Peak M (at 0.5028 RU), indicating more marine humic-like DOM. The S_R values remained constant in the southwest-northeast transect, which was found in the range of 0 to 0.8 in the island's fringe and increased to 1.3 at Palm 5 (Table 4-6), which also had high ionic strength 0.45 molal (Table A-8).

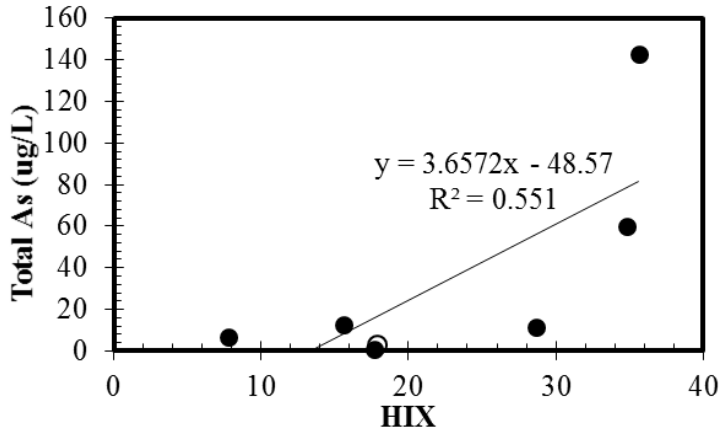

Figure 4-7. Correlation plot of total As and humification index (HIX) for samples from Palm Island.

Table 4-6. Summary of DOC concentration, UV 254nm, specific UV-Vis absorbance (SUVA), fluorescence index (FI), freshness (β:α), humification index (HIX), absorption spectral slope and spectral slope ratio (S_R) and EEM peak intensities of groundwater samples from Palm Island.

							Fluorescence peak intensities					Absorption Spectral Slope		
Sample ID	**DOC (mg/L)**	**UV 254**	**SUVA ($Lm^{-1}m^{-1}$)**	**FI**	**B:α**	**HIX**	**Peak A/UV_{254}**	**Peak B/UV_{254}**	**Peak T/UV_{254}**	**Peak C/UV_{254}**	**Peak M/UV_{254}**	**$S_{275-296}$**	**$S_{350-400}$**	**(S_R)**
Palm FP SW	32.53	0.83809	2.58	1.34	0.51	17.9	17.86	71.20	0.8331	6.890	28.21	0.0173	0.0215	0.80
Palm 1	24.57	0.6612	2.69	1.42	0.54	17.7	17.67	38.90	0.9616	3.612	18.26	0.0168	0.0218	0.77
Palm 2	30.23	0.4925	1.63	1.47	0.61	7.77	7.77	37.81	8.566	8.521	16.25	0.0177	0.0251	0.71
Palm 3	24.79	0.3362	1.36	1.48	0.6	15.6	15.58	59.10	2.6640	6.057	25.45	-	-	-0.08
Palm 4	30.3	0.5000	1.70	1.40	0.50	28.7	28.68	96.85	0.2915	6.029	40.85	0.0189	0.0243	0.78
Palm 5	29.78	0.4288	1.44	1.48	0.56	35.6	35.62	81.75	0.0000	4.399	34.70	0.0222	0.0723	0.19
Palm 6	23.94	0.4451	1.86	1.53	0.57	34.79	34.79	68.81	0.0000	4.027	29.65	0.0168	0.0135	1.25

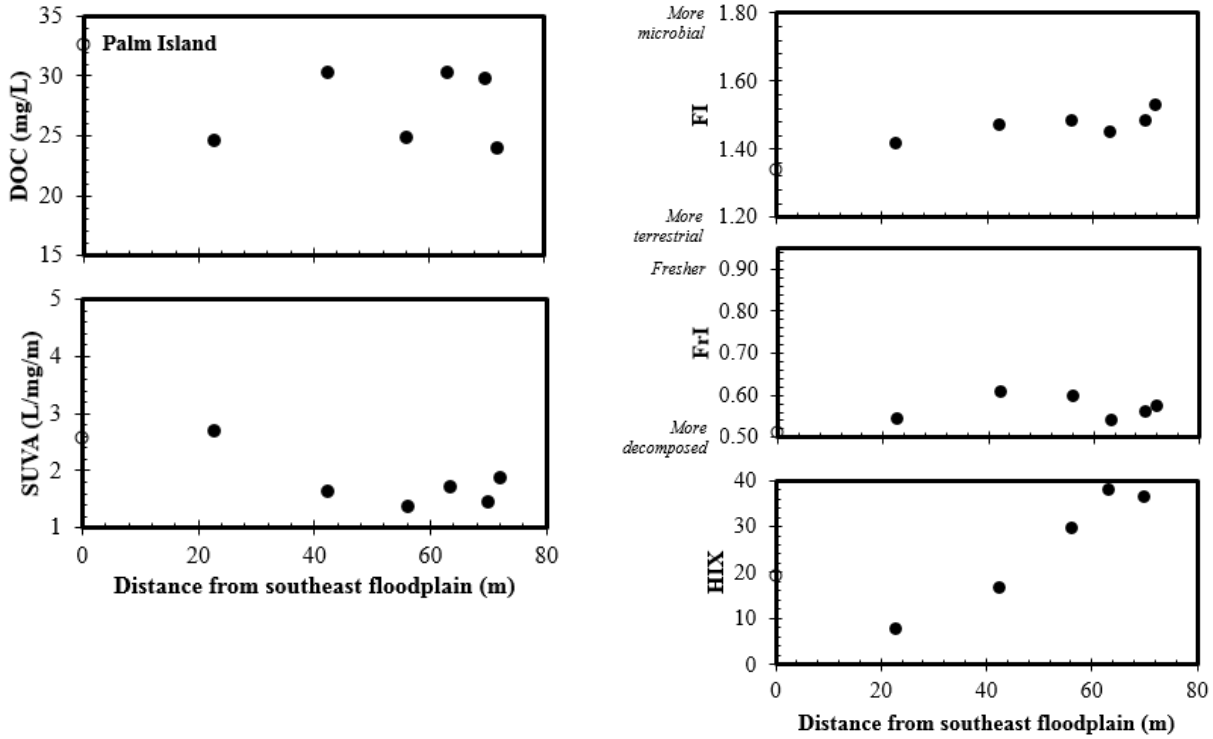

Figure 4-8. Palm Island: changes in groundwater DOM characteristics (DOC, SUVA, FI, FrI and HIX). Floodplain surface water sample is depicted by the open diamond on the 0m distance.

4.3.2.4 One Tusk (OT) Island

Similar to Palm Island, the fluorescence properties only changed slightly along the east to west transect. The DOM quality in the fringe zone indicates mixed microbially and terrestrially derived DOM (FI values between 1.55 and 1.66; Table 4-7), with fairly low $\beta:\alpha$ ratios (between 0.59 and 0.64; Table 4-7) and less aromatic DOM (SUVA values between 1.77 and 2.48) than in the center zone. Piezometers OT 2 and 3 are within the high conductivity center zone. There is a more noticeable decrease in DOC concentration from OT 1 to OT 6 (Figure 4-10). The DOM characteristics at OT 2 and 3 reflect a mixture of terrestrial and microbially derived DOM (FI values from 1.61 to 1.62) and decomposed DOM ($\beta:\alpha$ values from 0.64 to 0.66). The HIX was found highest at the west floodplain piezometer with a value of 30. In relation to As concentration, negative correlation (R^2=0.5232;) in total As concentration and HIX was found (Figure 4-9). There was a noticeable increase in spectral slope at OT 3 (S_R= 1.6) and OT 4 (S_R=1.5) corresponding to the increase in ionic strength (I=0.21 molal). The S_R at OT 1, 2, 5 and 6 were at 1.0 (Figure 4-11).

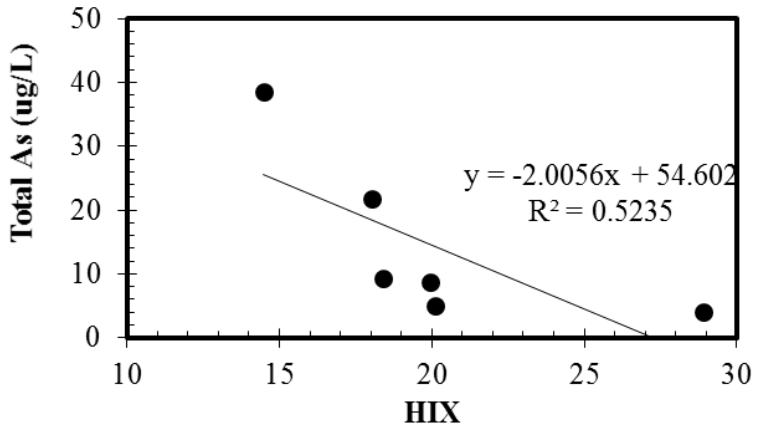

Figure 4-9. Correlation plot of total As and humification index (HIX) for samples from One Tusk Island.

Table 4-7. Summary of DOC concentration, UV 254nm, specific UV-Vis absorbance (SUVA), fluorescence index (FI), freshness (β:α), humification index (HIX), absorption spectral slope and spectral slope ratio (S_R) and EEM peak intensities of groundwater samples from One Tusk Island.

							Fluorescence peak intensities					Absorption Spectral Slope		
Sample ID	**DOC (mg/L)**	**UV 254**	**SUVA ($Lm^{-1}m^{-1}$)**	**FI**	**B:α**	**HIX**	**Peak A/UV_{254}**	**Peak B/UV_{254}**	**Peak T/UV_{254}**	**Peak C/UV_{254}**	**Peak M/UV_{254}**	**$S_{275-296}$**	**$S_{350-400}$**	**(S_R)**
OT 1	25.2	0.4996	1.98	1.55	0.59	18.4	18.40	55.35	1.011	5.155	23.25	0.0158	0.0156	1.01
OT 2	22.36	0.5697	2.55	1.62	0.64	14.5	14.48	69.12	2.611	8.619	30.93	0.0167	0.0168	1.00
OT 3	20.52	0.4024	1.96	1.61	0.66	18.04	18.04	62.01	2.136	6.464	27.84	0.0134	0.0080	1.67
OT 4	12.28	0.2178	1.77	1.61	0.64	19.9	19.95	40.42	1.346	3.683	17.87	0.0201	0.0139	1.44
OT 5	13.13	0.2835	2.16	1.60	0.61	20.1	20.12	29.54	1.378	3.888	13.31	0.0161	0.0156	1.03
OT 6	11.45	0.2840	2.48	1.56	0.61	28.9	28.89	21.50	0.000	1.396	9.73	0.0115	0.0103	1.12

Table 4-8. Table Summary of Minimum, average and maximum values for fluorescence indices, peak intensities spectral slope and slope ratio.

Sample ID	Camp Island			New Island			One Tusk Island			Palm Island		
	Min	***Ave***	***Max***	***Min***	***Ave***	***Max***	***Min***	***Ave***	***Max***	***Min***	***Ave***	***Max***
FI	1.18	1.39	1.62	1.31	1.51	1.62	1.55	1.59	1.62	1.34	1.45	1.53
FrI	0.48	0.60	0.75	0.52	0.58	0.65	0.59	0.62	0.66	0.51	0.56	0.61
HIX	2.8	16	46	8.3	19	28	14	21	34	7.6	24	38
Max Emission at Excitation 370nm	453	459	470	449	455	460	447	455	459	456	459	462
Peak A	1.48	280	1300	3.9	12	28	3.4	7.4	11	6.0	10	15
Peak B	0	1.26	5.7	0.0	0.58	2.6	0	0.19	0.54	0.0	0.37	1.4
Peak T	0.24	14	59	0.37	1.1	2.9	0.16	0.74	1.4	0.59	0.94	1.4
Peak C	0.72	106	479	1.57	5.1	11	1.56	3.28	4.9	2.6	4.4	6.5
Peak M	0.87	133	598	1.97	6.1	14	1.84	3.94	6.0	3.3	5.3	7.8
$S_{275-296}$	0.011	0.0149	0.020	0.009	0.015	0.0	0.012	0.016	0.020	0.017	0.018	0.022
$S_{350-401}$	0.004	0.0141	0.023	0.005	0.016	0.0	0.008	0.013	0.017	0.013	0.030	0.072
Spectral Slope Ratio (S_R)	0.000	0.46	2.3	0.66	1.1	2.5	1.0	1.2	1.7	0	0.631	1.3

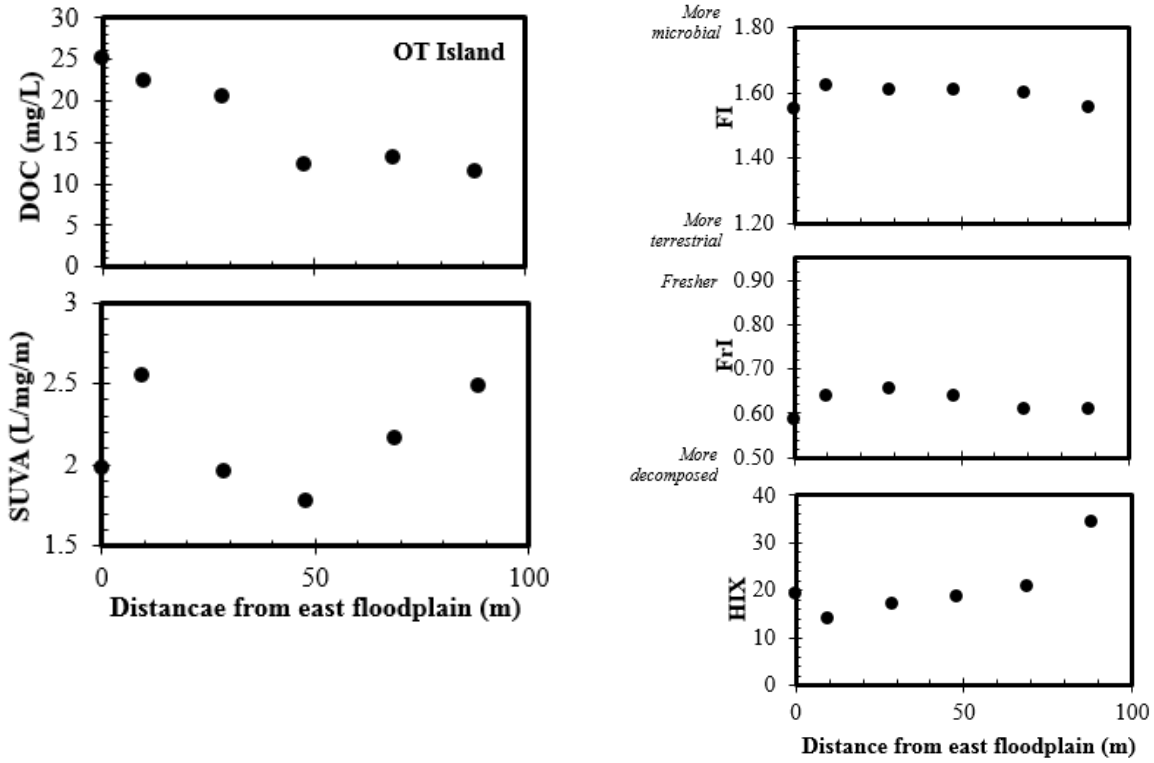

Figure 4-10. One Tusk Island: changes in groundwater DOM characteristics (DOC, SUVA, FI, FrI and HIX). Floodplain surface water sample is depicted by the open diamond on the 0m distance.

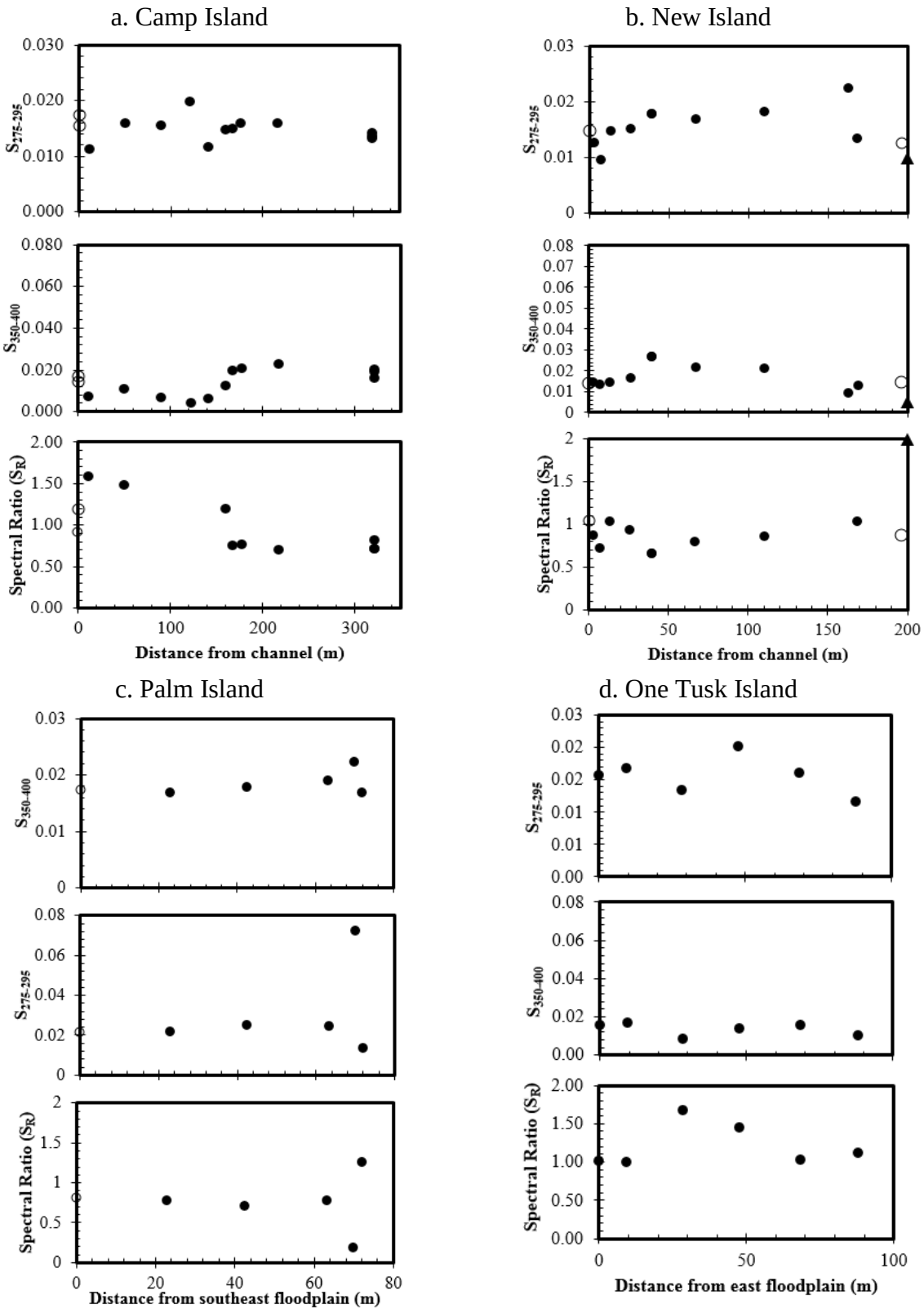

Figure 4-11. Spectral slope and slope ratio for Camp Island (a), New Island (b), Palm Island (c) and One Tusk Island (d). One Tusk Island

4.3.3 Microbial community

The microbial community was investigated using high-throughput DNA sequencing i.e., pyrosequencing for 8 sediments samples from New Island (New 1, 3, 5, 7, 11, 12 and termite mound, TM) and 2 samples from Camp Island (Camp 2 and 5). Pyrosequencing generated up to between 758 (Camp 5) and 1922 (New 3) bacterial sequence counts and between 1347 (New 1) and 14261 (New 3) archaeal sequences counts (Table 3-4). There was a negative correlation (R^2 =0.2358) between the β:α and number of sequences generated in each sediment sample (Figure 4-12). At the family level, the relative abundance of microorganisms capable of reducing NO_3^- was highest at New 1 (23%) and lowest at New 11 (4.2% relative abundance). Microorganisms capable of sulfate reduction were highest at New TM with 8% relative abundance. Methane-producing archaea were highest at New 7 (~24% relative abundance) and New 12 (~25% relative abundance), and lowest at New 11 (~7% relative abundance). There was a positive correlation (R^2=0.5895) between the relative abundance of methanogens at the order level and the relative abundance of microorganisms capable of sulfate reduction (R^2=0.7088; Figure 4-12) and the β:α index.

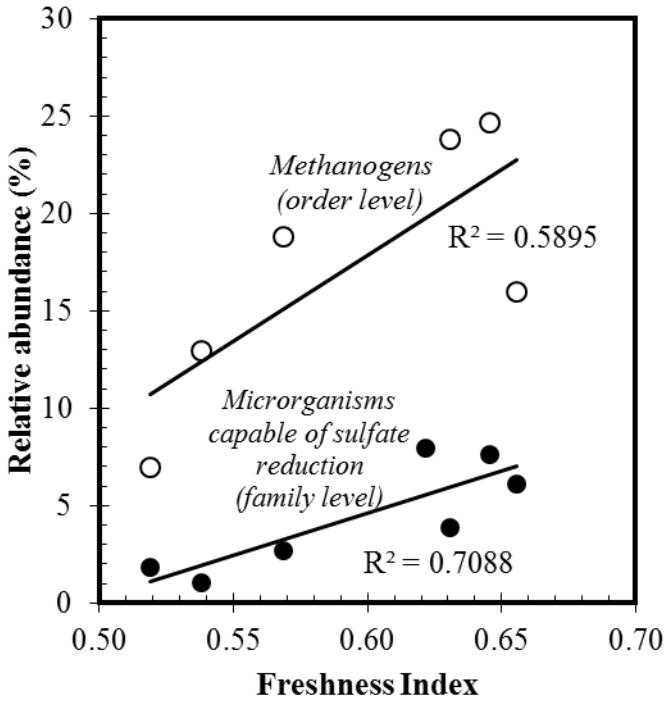

Figure 4-12. Correlation plot of Methanogens (*Methanococcales*, *Methanocellales*, *Methanobacteriales*, *Methanomicrobiales*, *Methanosarcinales*) at order level and Freshness Index (FrI)

4.4 Discussion

4.4.1 DOM characteristics in surface waters

In the Okavango delta, there is an apparent spatial variability of DOC concentration and DOM characteristics in surface water supplied by leaching of vegetation (Mladenov et al 2005; 2007). Our findings are in agreement with Mladenov et al. (2005) showing higher DOC concentrations in the floodplain surface water than in the river. The spectroscopic characteristics of the river and floodplain were similar with the exception of higher SUVA in Boro River near Camp Island than in the floodplain. The higher DOC concentration in the floodplain surface water could be an effect of accumulation through hydrological processes and plant leaching being higher in the floodplain.

The variability of DOM characteristic in the surface water could be derived from a numerous biogeochemical processes acting upon DOM, including photobleaching and microbial degradation. Mladenov et al. (2005) attributed the shift in SUVA in the surface water to the effect of photobleaching. From our spectral slope analysis, the shift of the spectral slope ratio (S_R) from terrestrial DOM (S_R = 0.92) to a more estuarine or coastal (S_R=1.04) suggests photo degradation of DOM in the river (Table 4-3). Photobleaching could enhance the lability of DOM for microbial processing (Moran and Zepp, 1997; Mladenov et al., 2005).

A two-week microbial incubation study identified a shift on SR from S_R=1.02 to S_R=0.94 was due to microbial processing and over a timescale of days to weeks could be statistically significant (Helms et al., 2008). In our study, the S_R (ranging from 0.80 to 0.87) in the floodplain surface water was lower (Table 4-3) compared to that of river S_R (ranging from 0.918 to 1.04) suggesting microbially processed DOM may be accumulating in the floodplain surface water. However, more surface water samples should be examined, as in previous studies, to definitively provide interpretations regarding the quality of surface water DOM.

4.4.2 Biogeochemical controls on the variability of DOM characteristics

In groundwater, DOC concentration is generally considered to be lower than DOC in surface waters (Thurman, 1986). The high DOC in groundwater beneath the island of Okavango (up to ~220 $mg{\cdot}L^{-1}$) reflects the influx of plant-derived DOM from surface water infiltration and subsequent evaporative concentration of DOM. Removal mechanism of DOM along the lateral flow path in groundwater include: sorption and microbial processing (Mladenov et al., 2008) and potentially chemical oxidation under certain circumstances (cite). Abundance of labile DOM leads to reducing conditions in groundwater, as O_2 and other electron-acceptors are depleted during microbial degradation of DOM (Mladenov et al., 2013). Therefore high DOC

concentrations in groundwater of each island reflect reduced groundwater. The mechanism of DOM transformation is explained for each island in the following sections.

4.4.2.1 Islands adjacent to a river

Camp Island and New Island are both adjacent to river channels, the Boro River and Boro Side Channel, respectively. At Camp 6 and New 11 (located at the center zone), the groundwater to surface water (GW: SW) ratio for DOC concentration was lower than that of Cl^- concentration (Table 3-1) for both wells. This suggests removal of DOC along the flow path. At New Island, a high SUVA value at New 5 (4.57) may reflect preferential consumption of labile, less aromatic DOM along the lateral flow path, leaving more aromatic high SUVA DOM in solution. In addition, the also a relatively high amount of total dissolved Fe at New 3 and 5, which may also contribute to the high SUVA value in those samples (Weishaar et al., 2003).

In surface water systems, spectral slopes and S_R has been widely used (Helms et al., 2008). Helms et al. (2008) hypothesized that a shift in S_R from higher to lower is due to microbial processing and/or selective preservation of long-wavelength –absorbing DOM. Less is known about how spectral slopes change along groundwater flow paths. At New Island, the shift in S_R between New 3 and New 7 (Figure 4-11) is consistent with the findings of Helms et al. (2008) noted above and may, therefore, be attributed in part to microbial processes. Sorption of humic and fulvic acids with increasing ionic strength (Mladenov et al., 2008) could also influence the shift in the S_R if longer wavelength absorbing compounds are preferentially removed. In piezometers New 3, 5and 7, pH and ionic strength were constant, suggesting the S_R shift was mainly due to microbial processing. With regards to mobilization of As, the variability of DOM characteristics in the fringe zone supports the hypothesized microbial Fe-reductive dissolution mechanism in As release (Huntsman-Mapila 2006; 2011; Mladenov et al., 2013).

In the high conductivity center zone, the concentrating effect of evapotranspiration is also evident in the increase of DOC. There was also a major effect of evapoconcentration on DOM characteristics. The spectral slope ratio increased from New 7(0.66) to New 11 (0.86), which could be due to increasing salinity (Helms et al., 2008). Along the groundwater flow path, there was an increasing trend in intensity for peak A, C and M, which corresponds to humic-like DOM peaks. In the presence of humic substances, particularly humic acids (HA), the rate and amount of As sorption in soil surfaces tends to decrease (Wang and Mulligan, 2005). At New Island, the positive correlation (R^2=0.4792;Figure 4-5) between As and HIX may signify that both As and humic DOM are becoming more concentrated due to evapotranspirative enrichment. If there had been competitive interaction between humic substances and As for sorption sites, we would expect to see a negative relationship.

The effect of increasing pH is also an integral factor in the increase in HIX and As along the groundwater flow path. Precipitation of As with sulfide may explain why the As/Cl ratio is below the evapoconcentration line (Figure 3-25). At New 11, the GW:SW ratio of SO_4^{2-} (9.5) was lower than the GW:SW of Cl (63), which suggests removal of sulfate from groundwater (i.e., microbial sulfate reduction). Mladenov et al. (2013) used x-ray near edge structure spectroscopy techniques to speciate As and found 76% of As in the solid phase was present as orpiment (As_2S_3) and that 24% is present as As (III) oxide. From our microbial analysis, the highest relative abundance of sequences grouping capable of SO_4^{2-} reduction were found in New 7 and New 12. Because of the concentric flow of groundwater, the sulfide produced by SO_4^{2-} reducers from New 7 and New 12 zones could be transporting sulfide to New 11 (Total S=2.55mg$\cdot L^{-1}$), which then may enhance precipitation of As-S mineral.

At Camp 5, the GW:SW ratio of SO_4^{2-} (1036) was much higher than the GW:SW ratio of Cl^- (94), which suggest addition of SO_4^{2-} to groundwater. From microbial analysis, the relative abundance of sequences grouping at the genus level capable sulfur oxidation under oxidizing conditions (*Genus: Thiobacillus*; Figure **3-23**) was found to be highest at Camp 5. Sulfur or sulfide oxidation could be contributing to the release of As by oxidizing sulfide from As-S mineral precipitation. At New 11, the relative abundance of sequences grouping as thiorhodovibrio (genus level) was found to be highest. *Genus Thiorhodovibrio* is known photoautotrophs (uses light as energy source) under anaerobic condition (Overmann et al., 1992). The absence of light at New 11 may suggest that these organisms do not require light to oxidize sulfide. The relative abundance of sequences grouping in families capable of sulfate reduction was found to be in greater abundance at New Island compared to Camp Island (Figure **3-21**), which could be responsible for the precipitation of As-S minerals at New Island and not at Camp Island. However, the presence of As-S minerals at Camp Island has not yet been investigated.

4.4.2.2 Islands surrounded by seasonal floodplain

The DOM characteristics of groundwater at Palm Island and One Tusk Island provide new insights into the biogeochemical processes influencing As mobility in islands surrounded by seasonal floodplains, which is different from the channel influence on New Island and Camp Island. In Palm Island's fringe zone (from floodplain surface water to Palm 4), the DOM had an FI of 1.5, which reflects a mixture of plant derived and microbially derived DOM. Between surface water and Palm 6, there was an increasing HIX trend, which was highly correlated with pH (Figure 4-9). This may be due to microbial processing of DOM along the flow path, which produces more HCO_3^- (increased alkalinity) as a result of microorganism consuming labile DOM and leaving behind more humic DOM. In addition, the increase in $S_{275-295}$ at Palm Island is

indicative of the influence of increasing salinity on DOM chemical character (Helms et al., 2008).

At One Tusk Island, the fringe zone (OT 1, 4-6) DOC was relatively lower than the DOC in the high conductivity center zone. DOM characteristics were similar to Palm Island, with plant derived and decomposed DOM along the island transect and no apparent change in S_R. The FI values and $\beta{:}\alpha$ were also marginally constant at Palm Island (Figure 4-8) and One Tusk Island (Figure 4-10). The variation of HIX and S_R values along the groundwater flowpath could be an effect of increasing pH and solute concentration at the center zone (Palm 5 and OT 3).

At Palm Island, the As/Cl ratio for Palm 5 and 6 were plotted above the evapoconcentration line (Figure 3-25), which means that the As in these two wells were accumulating more than Cl^-. This high As concentration compared to Cl suggests that desorption of sorbed As may have occurred (Welch and Lico, 1998). The adsorption of As (V) in clay minerals is pH dependent leading to desorption of As (V) with increasing pH (Welch et al 2000). Moreover, the competitive interactions between As and humic DOM for sorption sites, driven by increasing pH (up to 8.01), may also contribute to the desorption of As from sediments.

4.5 Conclusion

The non-conservative behavior of DOM suggests transformation of DOM along the lateral flow path of in groundwater include, which include sorption and microbial processing. Our findings show that DOM transformation along the groundwater flowpath could be due to microbial processing. By supplying electron donors to microorganisms and stimulating reductive dissolution, As mobility is indirectly linked to DOM quality in groundwater of the Okavango Delta. For islands adjacent to river channels (i.e., New Island and Camp Island), the DOM spectroscopic characteristics had more variability in the groundwater, suggesting more

biogeochemical processes transforming DOM, which may be influencing As mobility. Islands surrounded by seasonal floodplain (i.e., Palm Island and One Tusk Island) had marginal variation of DOM in groundwater, which suggest ecohydrologic controls may be dominant process on As mobility (i.e., desorption of As from sediments) in groundwater of these islands.

Chapter 5 - Summary and Conclusions

5.1 Relevant findings from this study

This study reveals that biogeochemical and ecohydrologic mechanisms play an important role in As cycling in the islands of the Okavango Delta. The following recounts the relevant findings in this study:

1) In the fringe zone of New Island and Camp Island, the microbial community composition was more diverse compared to the microbial community composition in the high conductivity center zone;
2) Ecohydrologic control (i.e., concentrating effect of evapotranspiration) was important mechanism in As accumulation in all four islands;
3) Microorganisms play an important role in As release to groundwater (i.e., release of As by microbial Fe-reductive dissolution and sequestration of As by forming As-S mineral, sulfide supplied by microbial sulfate reduction);
4) Microorganisms may be also enhancing silicate weathering and expediting carbonate mineral precipitation;
5) Vegetation in the four islands could take up As in tree leaves and grasses inhabiting the islands;
6) Islands adjacent to river channel (i.e., New Island and Camp Island), the groundwater DOM spectroscopic characteristics were more variable than in islands surrounded by floodplains, suggesting more biogeochemical processes transforming DOM, which may indirectly influence As mobility;

Camp Island and New Island have been previously studied, but the extensive DOM spectroscopic characteristics and microbial community composition performed in this study

provides new information to support the hypotheses posed by previous studies (Huntsman-Mapila et al., 2006; Mladenov et al., 2013). Our spectroscopic analyses of groundwater DOM and chemical analyses of groundwater showed that in the fringe zone, less humic DOM (lower HIX) may fuel microbial processes that release As from sediments, and in the center zone, As accumulation was controlled by ecohydrologic (i.e., evapotranspiration). In addition, our findings from characterization of the microbial community composition of New Island and Camp Island provided further support for the microbial processes that may mobilize or sequester arsenic (i.e., Fe-reductive dissolution of As-Fe mineral and As-S mineral precipitation driven by sulfate reducing bacteria) in groundwater of these islands. In addition, microorganisms may also be contributing to the growth and formation of the islands in the Okavango Delta.

Our microbial analysis (for New Island and Camp Island) also provided information regarding the microbial processes influencing carbonate mineral precipitation. Microbial silicate weathering (by Fe-reducing bacteria) may be contributing to the influx of Ca^{2+} to the groundwater. Concurrently, sulfate-reducing bacteria (O'Braissant et al., 2007) and methanogens (Roberts et al., 2004) may be expediting carbonate precipitation by enrichment of Ca^{2+} and Mg^{2+} in the water. In addition, microbial consumption of labile DOM produces HCO_3^-, which precipitates carbonate minerals. With evapoconcentration, HCO_3^- accumulates in groundwater, affecting the affinity of As for sediments and ultimately affecting the mobility of As in the solution.

The findings from Palm Island and One Tusk Island provided new insights into As mobilization in the islands of the Okavango Delta. Our findings suggest that the variation of DOM chemical characteristics were mainly driven by ecohydrologic controls. Another mechanism transforming DOM along the groundwater flow path of the islands surrounded by

seasonal floodplain (i.e., Palm Island and One Tusk Islands) may be preferential sorption of reactive DOM (i.e., fulvic acids), which could be competing with As for sorption sites. In addition, the proposed mechanisms for As release at Palm Island and One Tusk Island (i.e., desorption of As from sediments with increasing pH) are similar to the mechanisms releasing As.

5.2 Recommendations for future work

This study provides new information on As mobilization from four different islands of the Okavango Delta. However, there are still uncertainties with respect to the overall mechanisms driving As release in all islands of Okavango, which include: 1) the influence of DOM chemical characteristics (e.g., lability of DOM) on the microbial metabolism affecting As release beneath the islands; and 2) the varying role of roots and different plant species As uptake from sediments and groundwater; 3) the influence of salinity and pH on speciation and mobility of As in groundwater in this semi-arid environment.

These uncertainties warrant further investigation to provide more consistent information about the probable remediation methods for As contamination not only in groundwater of Okavango but also in other semi-arid environments and reducing aquifers. Our preliminary measurements of As uptake by vegetation signified that it may be important in the fate and transport of As in groundwater beneath the islands of Okavango Delta. In addition, further investigation of the role of sulfate-reducing bacteria in sulfide generation and subsequent precipitation of As-sulfides has important implications for mitigating arsenic contamination in groundwater. Future work on these topics will inform more efficient and sustainable design of constructed wetlands or other in-situ systems for remediating metal contaminants.

References

Anonymous (1988) Arsenic in Ground Water of the Western United States. Ground Water 26, 333-347.

Ahmed K. M., Bhattacharya P., Hasan M. A., Akhter S. H., Alam S. M. M., Bhuyian M. A. H., Imam M. B., Khan A. A. and Sracek O. (2004) Arsenic enrichment in groundwater of the alluvial aquifers in Bangladesh: an overview. Appl. Geochem. 19, 181-200.

Bauer-Gottwein P., Langer T., Prommer H., Wolski P. and Kinzelbach W. (2007) Okavango Delta Islands: Interaction between density-driven flow and geochemical reactions under evapo-concentration. J. Hydrol. 335, 389-405.

Bennett P., Rogers J. and Choi W. (2001) Silicates, silicate weathering, and microbial ecology. Geomicrobiol. J. 18, 3-19.

Borrelli N., Osterrieth M., Romanelli A., Alvarez M. F., Cionchi J. L. and Massone H. (2012) Biogenic silica in wetlands and their relationship with soil and groundwater biogeochemistry in the Southeastern of Buenos Aires Province, Argentina. Environ. Earth Sci. 65, 469-480.

Brandstetter A., Sletten R., Mentler A. and Wenzel W. (1996) Estimating dissolved organic carbon in natural waters by UV absorbance (254 nm). Z. Pflanzen. Bodenk. 159, 605-607.

Burton E. D., Johnston S. G. and Bush R. T. (2011) Microbial sulfidogenesis in ferrihydrite-rich environments: Effects on iron mineralogy and arsenic mobility. Geochim. Cosmochim. Acta 75, 3072-3087.

Cawley K. M., Wolski P., Mladenov N. and Jaffe R. (2012) Dissolved Organic Matter Biogeochemistry Along a Transect of the Okavango Delta, Botswana. Wetlands 32, 475-486.

Champ D. R., Gulens J. and Jackson R. E. (1979) Oxidation-Reduction Sequences in Ground-Water Flow Systems. Canadian Journal of Earth Sciences 16, 12-23.

Chapelle F. H. and Lovley D. R. (1992) Competitive Exclusion of Sulfate Reduction by Fe (lll)-Reducing Bacteria: A Mechanism for Producing Discrete Zones of High-Iron Ground Water. Ground Water 30, 29-36.

Chin Y. P. (1998) Abundance and properties of dissolved organic matter in pore waters of a freshwater wetland. Limnol. Oceanogr. 43, 1287.

Coble P. (1996) Characterization of marine and terrestrial DOM in seawater using excitation emission matrix spectroscopy. Mar. Chem. 51, 325-346.

Cory R. M. and McKnight D. M. (2005) Fluorescence spectroscopy reveals ubiquitous presence of oxidized and reduced quinones in dissolved organic matter. Environ. Sci. Technol. 39, 8142-8149.

Cory R. M., Boyer E. W. and McKnight D. M. (2011) Spectral Methods to Advance Understanding of Dissolved Organic Carbon Dynamics in Forested Catchments. In Forest Hydrology and Biogeochemistry (Anonymous). Springer Netherlands, pp. 117-135.

Cory R. M., Miller M. P., McKnight D. M., Guerard J. J. and Miller P. L. (2010) Effect of instrument-specific response on the analysis of fulvic acid fluorescence spectra. Limnol. Oceanogr. Meth. 8, 67-78.

Cronberg G., Gieske A., Martins E., Nengu J. P. and Stenstrom I. -. (1996) Major ion chemistry, plankton, and bacterial assemblages of the Jao/Boro River, Okavango Delta, Botswana: The swamps and flood plains. Archiv fuer Hydrobiologie Supplement 107, 335-407.

Dixit S. and Hering J. G. (2003) Comparison of arsenic (V) and arsenic (III) sorption onto iron oxide minerals: Implications for arsenic mobility. Environ. Sci. Technol. 37, 4182-4189.

Dowling C., Poreda R., Basu A., Peters S. and Aggarwal P. (2002) Geochemical study of arsenic release mechanisms in the Bengal Basin groundwater. Water Resour. Res. 38, 1173.

Essington M. (2004) Soil and Water Chemistry: An Integrative Approach. CRC Press LLC, Boca Raton, Florida.

Frost R. and Griffin R. (1977) Effect of Ph on Adsorption of Arsenic and Selenium from Landfill Leachate by Clay-Minerals. Soil Sci. Soc. Am. J. 41, 53-57.

Gao S., Fujii R., Chalmers A. T. and Tanji K. K. (2004) Evaluation of adsorbed arsenic and potential contribution to shallow groundwater in Tulare Lake bed area, Tulare Basin, california. Soil Sci. Soc. Am. J. 68, 89-95.

Grafe M., Eick M. J. and Grossl P. R. (2001) Adsorption of arsenate (V) and arsenite (III) on goethite in the presence and absence of dissolved organic carbon. Soil Sci. Soc. Am. J. 65, 1680-1687.

Harte P. T., Ayotte J. D., Hoffman A., Revesz K. M., Belaval M., Lamb S. and Boehlke J. K. (2012) Heterogeneous redox conditions, arsenic mobility, and groundwater flow in a fractured-rock aquifer near a waste repository site in New Hampshire, USA. Hydrogeol. J. 20, 1189-1201.

Harvey C. F., Ashfaque K. N., Yu W., Badruzzaman A. B. M., Ali M. A., Oates P. M., Michael H. A., Neumann R. B., Beckie R., Islam S. and Ahmed M. F. (2006) Groundwater dynamics and arsenic contamination in Bangladesh. Chem. Geol. 228, 112-136.

Helms J. R., Stubbins A., Ritchie J. D., Minor E. C., Kieber D. J. and Mopper K. (2009) Absorption spectral slopes and slope ratios as indicators of molecular weight, source, and photobleaching of chromophoric dissolved organic matter (vol 53, pg 955, 2008). Limnol. Oceanogr. 54, 1023-1023.

Hudson N., Baker A. and Reynolds D. (2007) Fluorescence analysis of dissolved organic matter in natural, waste and polluted waters - A review. River Res. Appl. 23, 631-649.

Huntsman-Mapila P., Nsengimana H. and Torto, N. and S. Diskin. (2011) Arsenic distribution and geochemistry in groundwater of a recharge wetland in NW Botswana" . In Sustaining Groundwater Resources, Internation Year of Planet Earth (eds. J. Jones and Anthony A.). SpringerLink, pp. 55-67.

Huntsman-Mapila P., Ringrose S., Jellema A., Matheson W. and and Kemosedile T. (December 4-8, 2002) Environmental response to drying in the Okavango Delta , Environmental Monitoring of Tropical and Sutropical Wetlands: proceedings of a conference edited by Ted Bernard, Keta Mosepele and Lars Ramberg in Maun, Botswana: HOORC, 2003. 97-112.

Huntsman-Mapila P., Mapila T., Letshwenyo M., Wolski P. and Hemond C. (2006) Characterization of arsenic occurrence in the water and sediments of the Okavango Delta, NW Botswana. Appl. Geochem. 21, 1376-1391.

Jakobsen R. and Postma D. (1999) Redox zoning, rates of sulfate reduction and interactions with Fe-reduction and methanogenesis in a shallow sandy aquifer, Romo, Denmark. Geochim. Cosmochim. Acta 63, 137-151.

Juhasz A. L., Smith E., Weber J., Rees M., Rofe A., Kuchel T., Sansom L. and Naidu R. (2006) In vivo assessment of arsenic bioavailability in rice and its significance for human health risk assessment. Environ. Health Perspect. 114, 1826-1831.

Kaiser K. and Zech W. (1999) Release of natural organic matter sorbed to oxides and a subsoil. Soil Sci. Soc. Am. J. 63, 1157-1166.

Kalbitz K. and Wennrich R. (1998) Mobilization of heavy metals and arsenic in polluted wetland soils and its dependence on dissolved organic matter. Sci. Total Environ. 209, 27-39.

Kappler A., Benz M., Schink B. and Brune A. (2004) Electron shuttling via humic acids in microbial iron(III) reduction in a freshwater sediment. FEMS Microbiol. Ecol. 47, 85-92.

Kirk M. F., Holm T. R., Park J., Jin Q. S., Sanford R. A., Fouke B. W. and Bethke C. M. (2004) Bacterial sulfate reduction limits natural arsenic contamination in groundwater. Geology 32, 953-956.

Langner P., Mikutta C. and Kretzschmar R. (2012) Arsenic sequestration by organic sulphur in peat. Nature Geoscience 5, 66-73.

Leenheer J. A. (2009) Systematic approaches to comprehensive analyses of natural organic matter. Annals of Environmental Science 3, 1-130.

Legg T. M., Zheng Y., Simone B., Radloff K. A., Mladenov N., Gonzalez A., Knights D., Siu H. C., Rahman M. M., Ahmed K. M., McKnight D. M. and Nemergut D. R. (2012) Carbon, metals, and grain size correlate with bacterial community structure in sediments of a high arsenic aquifer. Frontiers in Microbiology 3, 82-Article 82.

Lengke M. F. and Tempel R. N. (2005) Geochemical modeling of arsenic sulfide oxidation kinetics in a mining environment. Geochim. Cosmochim. Acta 69, 341-356.

Li R. Y., Stroud J. L., Ma J. F., McGrath S. P. and Zhao F. J. (2009) Mitigation of Arsenic Accumulation in Rice with Water Management and Silicon Fertilization. Environ. Sci. Technol. 43, 3778-3783.

Liu F., De Cristofaro A. and Violante A. (2001) Effect of pH, phosphate and oxalate on the adsorption/desorption of arsenate on/from goethite. Soil Sci. 166, 197-208.

Liu G. and Cai Y. (2013) Studying arsenite-humic acid complexation using size exclusion chromatography-inductively coupled plasma mass spectrometry. J. Hazard. Mater. 262, 1223-1229.

Masscheleyn P. H., Delaune R. D. and Patrick W. H. (1991) Effect of Redox Potential and Ph on Arsenic Speciation and Solubility in a Contaminated Soil. Environ. Sci. Technol. 25, 1414-1419.

McArthur J. M., Banerjee D. M., Hudson-Edwards K. A., Mishra R., Purohit R., Ravenscroft P., Cronin A., Howarth R. J., Chatterjee A., Talukder T., Lowry D., Houghton S. and Chadha D. K. (2004) Natural organic matter in sedimentary basins and its relation to arsenic in anoxic ground water: the example of West Bengal and its worldwide implications. Appl. Geochem. 19, 1255-1293.

McKnight D., Boyer E., Westerhoff P., Doran P., Kulbe T. and Andersen D. (2001) Spectrofluorometric characterization of dissolved organic matter for indication of precursor organic material and aromaticity. Limnol. Oceanogr. 46, 38-48.

Milzow C., Kgotlhang L., Bauer-Gottwein P., Meier P. and Kinzelbach W. (2009) Regional review: the hydrology of the Okavango Delta, Botswana-processes, data and modelling. Hydrogeol. J. 17, 1297-1328.

Mladenov, Natalie McKnight, Diane Macko, Stephan Norris, Marnie Cory,Rose Ramberg, Lars (2007) Chemical characterization of DOM in channels of a seasonal wetland. Aquat. Sci. 69, 456-471.

Mladenov N., Gardner J. R., Flores N. E., Mbaiwa J. E., Mmopelwa G. and Strzepek K. M. (2007) The value of wildlife-viewing tourism as an incentive for conservation of biodiversity in the Okavango Delta, Botswana. Development Southern Africa 24, 409-423.

Mladenov N., McKnight D. M., Wolski P. and Murray-Hudson M. (2007) Simulation of DOM fluxes in a seasonal floodplain of the Okavango Delta, Botswana. Ecol. Model. 205, 181-195.

Mladenov N., McKnight D. M., Wolski P. and Ramberg L. (2005) Effects of annual flooding on dissolved organic carbon dynamics within a pristine wetland, the Okavango Delta, Botswana. Wetlands 25, 622-638.

Mladenov N., Huntsman-Mapila P., Wolski P., Masarnba W. R. L. and McKnight D. M. (2008) Dissolved organic matter accumulation, reactivity, and redox state in ground water of a recharge wetland. Wetlands 28, 747-759.

Mladenov N., McKnight D. M., Macko S. A., Norris M., Cory R. M. and Ramberg L. (2007) Chemical characterization of DOM in channels of a seasonal wetland. Aquat. Sci. 69, 456-471.

Mohapatra D., Mishra D., Rout M. and Chaudhury G. R. (2007) Adsorption kinetics of natural dissolved organic matter and its impact on arsenic(V) leachability from arsenic-loaded ferrihydrite and Al-ferrihydrite. J. Environ. Sci. Health Part A-Toxic/Hazard. Subst. Environ. Eng. 42, 81-88.

Moran M. A. and Zepp R. G. (1997) Role of photoreactions in the formation of biologically labile compounds from dissolved organic matter. Limnol. Oceanogr. 42, 1307-1316.

Mulholland P. and Hill W. (1997) Seasonal patterns in streamwater nutrient and dissolved organic carbon concentrations: Separating catchment flow path and in-stream effects. Water Resour. Res. 33, 1297-1306.

Neumann R. B., Ashfaque K. N., Badruzzaman A. B. M., Ali M. A., Shoemaker J. K. and Harvey C. F. (2010) Anthropogenic influences on groundwater arsenic concentrations in Bangladesh. Nat. Geosci. 3, 46-52.

Nevin K. P. and Lovley D. R. (2000) Lack of production of electron-shuttling compounds or solubilization of Fe(III) during reduction of insoluble Fe(III) oxide by Geobacter metallireducens. Appl. Environ. Microbiol. 66, 2248-2251.

Newman D. K., Ahmann D. and Morel F. M. M. (1998) A brief review of microbial arsenate respiration. Geomicrobiol. J. 15, 255-268.

Newman D. K., Beveridge T. J. and Morel F. M. M. (1997) Precipitation of arsenic trisulfide by Desulfotomaculum auripigmentum. Appl. Environ. Microbiol. 63, 2022-2028.

Nordstrom D. K., Alpers C. N., Ptacek C. J. and Blowes D. W. (2000) Negative pH and extremely acidic mine waters from Iron Mountain, California. Environ. Sci. Technol. 34, 254-258.

Nordstrom D. (2002) Public health - Worldwide occurrences of arsenic in ground water. Science 296, 2143-2145.

O. Braissanta A. W., Decho C., Dupraz C., Glunk K. M. and Prezokopandp. T. Visscher. (2007) Exopolymeric substances of sulfate-reducing bacteria:Interactions with calcium at alkaline pH and implication forformation of carbonate minerals. Geobiology 5, 401-411.

Ohno T. (2002) Fluorescence inner-filtering correction for determining the humification index of dissolved organic matter. Environ. Sci. Technol. 36, 742-746.

O'Reilly J., Watts M. J., Shaw R. A., Marcilla A. L. and Ward N. I. (2010) Arsenic contamination of natural waters in San Juan and La Pampa, Argentina. Environ. Geochem. Health 32, 491-515.

OTTE M., KEARNS C. and DOYLE M. (1995) Accumulation of Arsenic and Zinc in the Rhizosphere of Wetland Plants. Bull. Environ. Contam. Toxicol. 55, 154-161.

Overmann J, Fischer U, Pfennig N. A New Purple Sulfur Bacterium from Saline Littoral Sediments, Thiorhodovibrio-Winogradskyi Gen-Nov and Sp-Nov. Arch Microbiol 1992;157:329-35.

Parlanti E., Worz K., Geoffroy L. and Lamotte M. (2000) Dissolved organic matter fluorescence spectroscopy as a tool to estimate biological activity in a coastal zone submitted to anthropogenic inputs. Org. Geochem. 31, 1765-1781.

Persson T. and Wedborg M. (2001) Multivariate evaluation of the fluorescence of aquatic organic matter. Anal. Chim. Acta 434, 179-192.

Pester M., Knorr K. H., Friedrich M. W., Wagner M. and Loy A. (2012) Sulfate-reducing microorganisms in wetlands - fameless actors in carbon cycling and climate change. Frontiers in Microbiology 3, 72-Article 72.

Pierce M. L. and Moore C. B. (1982) Adsorption of arsenite and arsenate on amorphous iron hydroxide. Water Res. 16, 1247-1253.

Qian Y., Gallagher F. J., Feng H. and Wu M. (2012) A geochemical study of toxic metal translocation in an urban brownfield wetland. Environ. Pollut. 166, 23-30.

Ramberg L. and Wolski P. (2008) Growing islands and sinking solutes: processes maintaining the endorheic Okavango Delta as a freshwater system. Plant Ecol. 196, 215-231.

Raven K. P., Jain A. and Loeppert R. H. (1998) Arsenite and arsenate adsorption on ferrihydrite: Kinetics, equilibrium, and adsorption envelopes. Environ. Sci. Technol. 32, 344-349.

Ravenscroft P., Brammer H. and Richards K. (2009; 2009) Introduction. In Arsenic Pollution (Anonymous). Wiley-Blackwell, pp. 1-24.

SENESI N., MIANO T., PROVENZANO M. and BRUNETTI G. (1991) Characterization, Differentiation, and Classification of Humic Substances by Fluorescence Spectroscopy. Soil Sci. 152, 259-271.

Smedley P. L. and Kinniburgh D. G. (2002) A review of the source, behaviour and distribution of arsenic in natural waters. Appl. Geochem. 17, 517-568.

Smedley P., Nicolli H., Macdonald D., Barros A. and Tullio J. (2002) Hydrogeochemistry of arsenic and other inorganic constituents in groundwaters from La Pampa, Argentina. Appl. Geochem. 17, 259-284.

Stute M., Zheng Y., Schlosser P., Horneman A., Dhar R. K., Datta S., Hoque M. A., Seddique A. A., Shamsudduha M., Ahmed K. M. and van Geen A. (2007) Hydrological control of As concentrations in Bangladesh groundwater. Water Resour. Res. 43, W09417.

Suess E. and Planer-Friedrich B. (2012) Thioarsenate formation upon dissolution of orpiment and arsenopyrite. Chemosphere 89, 1390-1398.

Swedlund P. J. and Webster J. G. (1999) Adsorption and polymerisation of silicic acid on ferrihydrite, and its effect on arsenic adsorption. Water Res. 33, 3413-3422.

Thanabalasingam P. and Pickering W. F. (1986) Arsenic Sorption by Humic Acids. Environmental Pollution Series B-Chemical and Physical 12, 233-246.

Thurman E. M. and Malcolm R. L. (1981) Preparative Isolation of Aquatic Humic Substances. Environ. Sci. Technol. 15, 463-466.

Van Beek, C.G.E.M and van der Kooij, D. (May-June 1982) Sulfate Reducing Bacteria in Groundwater from Clogging and Nonclogging Shallow Wells in the Netherlands River Region. Groundwater 20,

Vinson D. S., McIntosh J. C., Dwyer G. S. and Vengosh A. (2011) Arsenic and other oxyanion-forming trace elements in an alluvial basin aquifer: Evaluating sources and mobilization by isotopic tracers (Sr, B, S, O, H, Ra). Appl. Geochem. 26, 1364-1376.

Violante A. and Pigna M. (2002) Competitive sorption of arsenate and phosphate on different clay minerals and soils. Soil Sci. Soc. Am. J. 66, 1788-1796.

Wang S. and Mulligan C. N. (2006) Effect of natural organic matter on arsenic release from soils and sediments into groundwater. Environ. Geochem. Health 28, 197-214.

Xu H., Allard B. and Grimvall A. (1991) Effects of Acidification and Natural Organic Materials on the Mobility of Arsenic in the Environment. Water Air and Soil Pollution 57-8, 269-278.

Xu H., Allard B. and Grimvall A. (1988) Influence of pH and Organic-Substance on the Adsorption of As (V) on Geologic Materials. Water Air Soil Pollution. 40, 293-305.

Appendix A - Tables

Table A-1. Extractable Aluminum and Silica and Amorphous Iron in sediments.

Sample ID	Extractable Al conc. (mg/L)	Extractable Si conc. (mg/L)	Amp. Fe conc. (mg/L)
Camp FP 1	24.00	9.53	1.85
Camp FP 2	49.29	16.64	4.22
Camp FP 3	14.51	3.91	1.44
Camp FP 4	29.99	23.44	6.83
Camp New 1	175.47	155.19	63.35
Camp New 2	386.34	157.68	44.93
Camp 1	67.09	41.96	23.98
Camp 2	279.29	127.78	27.30
Camp 3	260.01	164.68	28.94
Camp 4	363.19	161.90	20.41
Camp 5	371.78	136.68	21.53
Camp TM	301.95	263.35	199.51
New 1	149.78	54.48	27.55
New 2	97.95	55.01	36.28
New 5	100.33	56.78	43.80
New 7	93.93	49.48	36.08
New 7			
New 9	102.96	38.70	19.83
New 12	220.71	86.81	51.13
New 13	202.12	129.96	64.01
New TM	292.94	123.75	25.93
New TM WC	374.99	203.70	36.20
OT 1	155.75	96.85	24.45
OT 2	352.25	163.05	35.92
OT 3	230.06	124.76	112.89
OT 4	555.32	187.06	34.58
OT 5	289.80	133.32	28.63
OT 6	148.65	90.30	18.26
Palm 1	5.14	3.54	< D. L.
Palm 2	24.08	16.48	8.38
Palm 3	332.24	182.85	54.63
Palm 4	384.84	215.53	30.48
Palm 5	587.43	487.51	37.12
Palm 6	318.47	333.00	29.30

Table A-2. Arsenic concentration in Vegetation collected from near wells

Plant Sample ID	As conc. (µg/kg)
New 1 - Grass	130
New 2	180
New 2 - Grass	75
New 2 - Grass	52
New 3	1192
New 3 - Grass	71
New 3 Rain Tree Leaves	595
New 5	117
New 5 - Grass	69
New 7	184
New 7 - Herbs	8
New 7 - Leaves	58
New 9	101
New 9 - Grass	102
New 11	150
New 11 Spiky Grass	121
New 12	466
New 12 - Grass	1767
New 13	676
New 13 - Grass	1560
Termite mound	630
New TM Grass	764
Camp 1 Grass	< D. L.
Camp 1 Tree Leaves	150
Camp 2 Grass	112
Camp 3 Grass	41
Camp 3 Leaves	362
Camp 4 Grass	< D. L.
Camp 6 Grass	405
Camp FP Grass	24
Palm 1 Grass	34
Palm 3 Grass	100
Palm 3 Leaves	413
Palm 4 Grass	78
Palm 5 Grass	43
Palm 6 Grass	170
One Tusk 1 Grass	408
One Tusk 2 Grass	60
One Tusk Rain Tree Leaves	1665
One Tusk 3 Grass	155
One Tusk 4 Grass	29
One Tusk 5 Grass	28
One Tusk 6 Grass	332

Table A-3. Complete sediment chemistry sampled from 2m depth. New 3 and New 11 (**) were samples from January 2011 (Mladenov et al 2013).

Sample ID	Approx. Location (m)	Al (mg·kg^{-1})	Si (mg·kg^{-1})	S (mg·kg^{-1})	Mn (mg·kg^{-1})	Fe (mg·kg^{-1})	As (µg·kg^{-1})	As conc. Surface soil (µg·kg^{-1})	Total N %	TOC %	Total C %	TIC %
Camp FP 1	11.6	409	214	11.8	< D.L.	189	115	-	0.05	0.19	0.19	0.00
Camp FP2	50.3	2106	16	12.6	0.5	1029.3	184.7	-	0.05	0.20	0.20	0.01
Camp FP3	90	619	184	13	0.89	326	156	-	0.06	0.16	0.18	0.02
Camp FP 4	122	934	157	12	2.94	656	41	-	0.06	0.28	0.42	0.13
Camp 1	-	8211	66	15	34	5122	308	-	0.05	0.19	0.20	0.01
Camp 2	-	9799	76	55	112	7202	989	-	0.06	0.19	0.39	0.20
Camp 1	141	2940	143	10	15	2028	149	431	0.04	0.19	0.19	0.00
Camp 2	160	7377	106	50	211	4899	910	444	0.07	0.21	0.50	0.29
Camp 3	168	11769	118	45	205	7155	859	685	0.06	0.23	0.54	0.31
Camp 4	177	6145	88	102	432	3982	1695	625	0.06	1.24	2.61	1.37
Camp 5	217	8582	94	148	147	5082	1180	389	0.07	0.19	0.43	0.24
Camp TM	160	9628	157	28	50	6449	421	-	0.07	0.29	0.29	0.00
New 1	3.0	3333	147	20	88	2409	272	864	0.04	0.23	0.34	0.11
New 2	7.1	2492	112	18	9.4	2394	269	983	0.07	0.21	0.21	0.01
****New 3**	14	2424	9.4	25	22	3111	772	1290	0.015 99	0.1486	0.1616	0.013
New 5	26	2602	122	26	32	4110	1381	801	0.05	0.20	0.24	0.04
New 7	40	13771	127	21	35	3762	703	845	0.05	0.20	0.20	0.00
New 9	67	1206	130	41	81	6370	2236	684	0.05	0.16	0.20	0.03
****New 11**	110	3418	36	19	78	3842	1598	451	0.015	0.280	0.137	0.143
New12	163	4839	89	24	183	5320	1562	843	0.05	0.20	0.56	0.36
New 13	169	6747	95	17	50	4789	436	665	0.06	0.20	0.23	0.03
New TM	200	8437	130	121	190	4381	1489	773	0.08	0.30	0.77	0.46
New TM WC	-	8586	64	227	248	4642	1730	-	0.08	0.58	1.43	0.85
OT 1	0	5523	91	12	36	3139	599	506	0.05	0.22	0.22	-0.01
OT 2	9.6	7561	77	30	59	6399	1740	657	0.06	0.22	0.29	0.07
OT 3	29	4900	102	20	140	13046	2997	735	0.07	0.23	0.24	0.01
OT 4	48	10335	144	35	357	6975	1561	892	0.07	0.28	1.28	1.00
OT 5	69	9999	79	21	104	8397	1646	532	0.06	0.19	0.24	0.05
OT 6	88	8092	97	14	64	4902	338	625	0.04	0.21	0.25	0.04
Palm 1	23	606	163	15	0.92	322	100	746	0.06	0.24	0.22	-0.02
Palm 2	42	1678	182	12	10	981	137	543	0.07	0.23	0.24	0.01
Palm 3	56	9190	157	33	202	5494	525	620	0.07	0.23	0.68	0.46
Palm 4	63	10363	93	32	250	6300	750	614	0.07	0.24	0.91	0.67
Palm 5	70	10974	123	41	198	6849	1093	512	0.07	0.30	0.79	0.49
Palm 6	72	6756	138	45	141	4733	734	496	0.07	0.26	0.82	0.55

Table A-4. Saturation Indices with respect to Calcite. Dolomite and Siderite. Groundwater samples from Camp Island, New Island, Palm Island and One Tusk Island. (*Calculated using Geochemist Workbench 10.0*)

Sample ID	SI: Calcite*	SI: Dolomite*	SI: Siderite*
Boro Channel	0.0148	0.08602	-
Camp FP SW	-	-	-
Camp FP 1	-	-	-
Camp FP2	-	-	-
Camp FP3	-	-	-
Camp FP 4	-	-	-
Camp 1	-	-	-
Camp 2	-	-	-
Camp 3	-	-	-
Camp 4	-	-	-
Camp 5	-	-	-
Camp 6 (6m)	-	106.1	-
Camp 6 (8.5m)	-	120.4	-
Boro Side Channel	0.08443		0.3443
New 1	0.8289	0.8633	1.94
New 2	0.2805	0.2345	0.1928
New 3	8.491	177.9	61.73
New 5	0.4785	0.9299	0.2385
New 7	1.83	17.25	1.81
New 9	4.251	243	4.873
New 11 (2m)	11.89	4247	71.19
New12	2.521	7.123	0.5417
New 13	0.3994	0.09971	1.1
NEW FP SW	0.00517	1.289E-05	0.027
New TM	-	-	-
OT 1	3.76	91.08	1.595
OT 2	2.5	12.5	1.485
OT 3	3.679	42.03	1.517
OT 4	2.923	33.11	0.3259
OT 5	2.866	12.73	0.8176
OT 6	1.572	3.468	0.3505
Palm FP SW	0.01294		0.05671
Palm 1	0.02883	0.000417	0.04054
Palm 2	0.2096	0.1635	0.4066
Palm 3	1.195	6.772	0.2898
Palm 4	-	-	-
Palm 5	3.552	812.6	4.71
Palm 6	3.862	502.1	11.12

Table A-5. Bivariate correlation. (R^2 value, number of samples in parentheses) and significance (p-value <0.05) for chemical characteristics in Camp, New, Palm and One Tusk Islands.

	pH	EC	Alk	B	Na	Mg	S	K	Ca	Total Fe	F^-	Cl^-	NO_2^-	Br^-	NO_3^-	PO_4^{3-}	SO_4^{2-}	Total As
pH		.8096 (28) p=.000	.7730 (26) p=.000	.6876 (27) p=.000	.7020 (27) p=.000		.6020 (27) p=.001	.7450 (27) p=.000				.4555 (27) p=.017	-.5967 (27) p=.001		.7310 (27) p=.000	.4059 (27) p=.036	.4174 (27) p=.030	.7185 (27) p=.000
EC	.8096 (28) p=.000		.9805 (26) p=.000	.7195 (27) p=.000	.7160 (27) p=.000	.5263 (27) p=.005	.8072 (27) p=.000	.8641 (27) p=.000				.6686 (27) p=.000	-.7208 (27) p=.000		.8654 (27) p=.000	.4094 (27) p=.034	.6870 (27) p=.000	.8852 (27) p=.000
Alk	.7730 (26) p=.000	.9805 (26) p=.000		.7395 (25) p=.000	.6620 (25) p=.000		.8397 (25) p=.000	.8806 (25) p=.000				.6820 (25) p=.000	-.6308 (25) p=.001		.8621 (25) p=.000	.4471 (25) p=.025	.6529 (25) p=.000	.8606 (25) p=.000
B	.6876 (27) p=.000	.7195 (27) p=.000	.7395 (25) p=.000		.5386 (28) p=.003		.6498 (28) p=.000	.8851 (28) p=.000					-.4475 (28) p=.017		.7334 (28) p=.000		.3951 (28) p=.037	.6639 (28) p=.000
Na	.7020 (27) p=.000	.7160 (27) p=.000	.6620 (25) p=.000	.5386 (28) p=.003			.4561 (28) p=.015	.5148 (28) p=.005				.4158 (28) p=.028		.4137 (28) p=.029	.3976 (28) p=.036			.5032 (28) p=.006
Mg		.5263(27) p=.005						.4700 (28) p=.012	.5576 (28) p=.002				-.4487 (28) p=.017				.3948 (28) p=.038	.3918 (28) p=.039
S	.6020 (27) p=.001	.8072 (27) p=.000	.8397 (25) p=.000	.6498 (28) p=.000	.4561 (28) p=.015			.7298 (28) p=.000				.5887 (28) p=.001	-.5817 (28) p=.001		.6914 (28) p=.000		.8270 (28) p=.000	.6989 (28) p=.000
K	.7450 (27) p=.000	.8641 (27) p=.000	.8806 (25) p=.000	.8851 (28) p=.000	.5148 (28) p=.005	.4700 (28) p=.012	.7298 (28) p=.000						-.7035 (28) p=.000		.8262 (28) p=.000		.5532 (28) p=.002	.8127 (28) p=.000
Ca						.5576 (28) p=.002									-.4092 (28) p=.031			
Total Fe																		
F																		
Cl	.4555 (27) p=.017	.6686 (27) p=.000	.6820 (25) p=.000		.4158 (28) p=.028		.5887 (28) p=.001							.4755 (28) p=.011	.5568 (28) p=.002	.5283 (28) p=.004	.6146 (28) p=.001	.5108 (28) p=.005
NO_2^-	-.5967 (27) p=.001	-.7208 (27) p=.000	-.6308 (25) p=.001	-.4475 (28) p=.017		-.4487 (28) p=.017	-.5817 (28) p=.001	-.7035 (28) p=.000							-.6167 (28) p=.000		-.4796 (28)p=.010	-.7364 (28) p=.000
Br^-					.4137 (28) p=.029							.4755 (28) p=.011						
NO_3^-	.7310 (27) p=.000	.8654 (27) p=.000	.8621 (25) p=.000	.7334 (28) p=.000	.3976 (28) p=.036		.6914 (28) p=.000	.8262 (28) p=.000	-.4092 (28) p=.031			.5568 (28) p=.002	-.6167 (28) p=.000			.3906 (28) p=.040	.5535 (28) p=.002	.8668 (28) p=.000
PO_4^{3-}	.4059 (27) p=.036	.4094 (27) p=.034	.4471(25) p=.025									.5283 (28) p=.004			.3906 (28) p=.040			.4244 (28) p=.024
SO_4^{2-}	.4174 (27) p=.030	.6870 (27) p=.000	.6529 (25) p=.000	.3951 (28) p=.037		.3948 (28) p=.038	.8270 (28) p=.000	.5532 (28) p=.002				.6146 (28) p=.001	-.4796 (28) p=.010		.5535 (28) p=.002			.5954 (28) p=.001
Total As.	.7185 (27) p=.000	.8852 (27) p=.000	.8606 (25) p=.000	.6639 (28) p=.000	.5032 (28) p=.006	.3918 (28) p=.039	.6989 (28) p=.000	.8127 (28) p=.000				.5108 (28) p=.005	-.7364 (28) p=.000		.8668 (28) p=.000	.4244 (28) p=.024	.5954 (28) p=.001	
DOC											.9509 (28) p=.000							
TN							.5036 (28) p=.006			.4361 (28) p=.020		.6127 (28) p=.001		.5316 (28) p=.004			.5771 (28) p=.001	

Table A-6. Physical and chemical characteristics of Camp Island groundwater and adjacent surface water. A complete set of data was not employed for samples Camp FP1-FP4, 1-5 for anions. The absorbance and fluorescences indices were measured using a filtered acidified samples.

Sample ID	Boro Channel	Camp FP SW	Camp FP 1	Camp FP2	Camp FP3	Camp FP 4	Camp 1	Camp 2	Camp 3	Camp 4	Camp 5	Camp 6	Camp 6
GPS coordinates Lat Long			-19.5474 23.1748	-19.5471 23.17488	-19.546 23.1752	-19.5464 23.1754	-19.5463 23.1755	-19.5462 23.1756	-19.5462 23.1757	-19.5461 23.1757	-19.5459 23.1760	-19.5453 23.1767	-19.5453 23.1767
Depth of Piezometer (m)	0	0	1	1	1	1	2	2	2	2	2	6	8.5
Distance (m)	0	0	11.6	50.3	90.1	121.9	141.1	160.1	168.1	177.0	217.3	320.8	320.8
Conductivity (uS/cm)	77	-	196	269	230	475	316	1430	2750	2390	-	30740	30930.0
pH	6.76	-	6.3	6.12	6.65	6.43	-	8.66	8.41	8.18	-	8.8	8.9
$\delta^{18}O$	-3.3	-	-	-	-	-	-	-	-	-	-	-2.2	-1.6
δ D	-28	-	-	-	-	-	-	-	-	-	-	-22	-19.6
Eh (V) (As^{5+} /As^{3+})*	-	-	0.0889	-	0.0573	0.0876	-	-0.1825	-0.1335	-	--	-0.2265	
Ionic strength (molal)*	1.07E-03	8.40E-04	-	-	-	-	-	-	-	-	-	0.2977	0.2
Alkalinity ($mg \cdot L^{-1}$ CaCO3)	65.9	-	-	-	-	-	-	-	-	-	-	20835.8	21348
B ($mg \cdot L^{-1}$)	0.76	1.47	1.95	2.55	3.07	0.94	0.84	0.94	0.75	0.79	1.27	0.88	0.77
Na ($mg \cdot L^{-1}$)	36	57	98	160	173	13	40	540	786	1808	10534	10182	10473
Mg ($mg \cdot L^{-1}$)	9	11	17	35	38	7.4	8.22	< D. L.	< D. L.	0.27	< D. L.	< D. L.	< D. L.
S ($mg \cdot L^{-1}$)	< D. L.	< D. L.	< D. L.	< D. L.	< D. L.	< D. L.	< D. L.	23	20	73	557	450	527
K ($mg \cdot L^{-1}$)	31	30	33	68	136	11	8.1	10	30	54	555	52	41
Ca ($mg \cdot L^{-1}$)	53	60	128	238	211	50	55	4.1	1.88	4.8	0.58	< D. L.	< D. L.
Total Fe ($mg \cdot L^{-1}$)	0.00	0.00	0.00	0.00	0.00	0.00	0.57	1.08	0.00	0.00	0.00	0.00	0.0
Fe(II) ($mg \cdot L^{-1}$)	0.48	-	-	-	-	-	-	-	-	-	-	5.94	2.78
Fluoride ($mg \cdot L^{-1}$)	21	-	-	-	-	-	-	-	-	-	-	1938	2690
Chloride ($mg \cdot L^{-1}$)	1.09	-	-	-	-	-	-	-	-	-	-	< D.L.	< D.L.
Nitrite ($mg \cdot L^{-1}$)	< D.L.	-	-	-	-	-	-	-	-	-	-	< D.L.	< D.L.
Bromide ($mg \cdot L^{-1}$)	0.95	-	-	-	-	-	-	-	-	-	-	< D.L.	51
Nitrate ($mg \cdot L^{-1}$)	< D.L.	-	-	-	-	-	-	-	-	-	-	< D.L.	10
Phosphate ($mg \cdot L^{-1}$)	< D.L.	-	-	-	-	-	-	-	-	-	-	1507	1947
Sulfate ($mg \cdot L^{-1}$)	1.46	-	-	-	-	-	-	-	-	-	-	5.94	2.78
Total As Conc. ($\mu g \cdot L^{-1}$)	2	1	4	3	4	7	9	155	655	675	4806	4050	5499
As(+3) conc. ($\mu g \cdot L^{-1}$)	0	3	1	0	1	1	7	77	108	864	3981	3018	3804
As(+5) conc. ($\mu g \cdot L^{-1}$)	2.16	-2.05	2.27	3	3	6	2	77	546	-189	825	1032	1695
DOC ($mg \cdot L^{-1}$)	8.014	8.05	10.42	14.17	14.21	24.67	23.33	46.27	47.24	82.06	230.7	220	223
TN ($mg \cdot L^{-1}$)	0.2962	0.3266	0.5504	0.8041	1.279	1.814	1.407	2.844	2.911	4.648	24.28	11.18	8.2
UV 254	0.35201	0.1578	0.3824	0.3962	0.3228			4.0258	2.6604	4.3347	11.5073	6.62	6.6
SUVA (L/mg-m)	4.39	1.96	3.67	2.80	2.27	-0.25	-0.36	8.70	5.63	5.28	4.99	3.01	2.6
FI	1.40	1.47	1.42	1.47	1.46	1.50	1.62	1.37	1.39	1.43	1.35	1.20	1.2
Max Em at 370 nm Ex	463	454	453	453	453	456	455	459	458	458	463	470	462
FrI	0.54	0.65	0.69	0.70	0.75	0.63	0.69	0.57	0.57	0.58	0.60	0.48	0.5
HIX	14.93	4.61	3.66	3.71	2.82	6.16	8.64	8.17	11.39	17.14	18.90	46.24	34.14

Table A-7. Physical and chemical characteristics of New Island groundwater and adjacent surface water. Ionic strength, SI, Eh (As^{5+} /As^{3+}) and Eh (NO_3^-/NO_2^-) were calculated using Geochemist Workbench 10.0.

Sample ID	Boro Side Channel	New 1	New 2	New 3	New 5	New 7	New 9	New 11 (2m)	New12	New 13	NEW FP SW	New TM
GPS coordinates Lat Long		-19.6872 23.2242	-19.6872 23.2242	-19.6872 23.2243	-19.6872 23.2244	-19.6873 23.2245	-19.6874 23.2247	-19.6874 23.2248	-19.6874 23.2249	-19.68749 23.2249		-19.6873 23.2249
Depth of Piezometer (m)		2	2	2	2		2	2	2	2		
Distance (m)	0	3	7.08	13.6	26.21	39.64	67.12	110.24	163.26	168.91	196.10	200
Conductivity (uS/cm)	114	840	416	1303	569	1328.00	2981	4950	822	779	95	-
pH	7.32	6.65	6.50	7.4	6.58	7.16	7.52	8.03	6.88	7.10	6.04	-
$\delta^{18}O$	-2.4	-0.4	0.3	2.0	3.3	2.55	1.9	2.2		2.7	-2.5	-
δ D	-20	-11	-7	4	10	6.83	3	2		4	-26	-
Eh (V) (As^{5+} /As^{3+})*	-0.0554			-0.0119		-0.01	-0.0335	-0.1249	0.0123			-
Eh (V) (NO3-/NO2-)*	0.3803	0.4208	0.4319	0.3837	0.4242		0.3959		0.4024	0.3953	0.4531	-
Ionic strength (molal)*	0.001458	0.01138	0.006861	0.01747	0.009248	0.01	0.03035	0.05058	0.0145	0.008216	0.001561	-
Alkalinity (mg•L^{-1} CaCO3)	1.75	1.30	1.51	1.03	0.78	0.70	0.68	0.72	0.51	0.51	0.79	-
B (mg•L^{-1})	54.08	95.13	164.19	139.71	17.61	222.02	657.45	916.13	52.16	159.73	65.35	-
Na (mg•L^{-1})	12.82	5	112.07	7.59	11.02	3.25	12.74	17.80	0.86	0.49	15.36	-
Mg (mg•L^{-1})	< D. L.	< D. L.	< D. L.	< D. L.	< D. L.	< D. L.	< D. L.	< D. L.	< D. L.	< D. L.	< D. L.	-
S (mg•L^{-1})	40.84	7	112.93	83.19	6.44	17.53	74.95	268.06	11.6	5.98	40.73	-
K (mg•L^{-1})	6.98	32.87	440.46	67.89	43.05	9.73	70.05	14	76.93	11.07	82.50	-
Ca (mg•L^{-1})	< D. L.	0.75	10.02	6.59	4.2	< D. L.	< D. L.	< D. L.	< D. L.	0.04	0.05	-
Total Fe (mg•L^{-1})	1.75	1.30	1.51	1.03	0.78	0.70	0.68	0.72	0.51	0.51	0.79	-
Fe(II) (mg•L^{-1})	0.43	2.37	0.52	11.63	0.49	0.54	0.41	1.81	0.36	0.51	0.71	0.3648
Fluoride (mg•L^{-1})	0.34	0.42	0.44	9.44	0.53	1.80	1.12	1.57	0.43	1.21	0.27	0.92
Chloride (mg•L^{-1})	3.34	2.79	1.85	18	22	23	194	208	57	6.30	3.47	22.55
Nitrite (mg•L^{-1})	0.99	1.13	0.86	0.77	1.34	0.86	0.99	< D.L.	1.55	1.42	1.28	0.95
Bromide (mg•L^{-1})	< D.L.	< D.L.	0.95	0.85	1.49	0.88	2.00	< D.L.	1.69	0.80	< D.L.	1.00
Nitrate (mg•L^{-1})	0.86	1.06	0.96	1.27	1.19	< D.L.	7.31	10.67	1.00	1.44	0.89	6.96
Phosphate (mg•L^{-1})	1.09	< D.L.	< D.L.	< D.L.	< D.L.	< D.L.	1.67	1.81	< D.L.	1.10	< D.L.	1.25
Sulfate (mg•L^{-1})	1.39	3.56	1.54	1.66	10.38	2.61	2.77	13.18	1.41	1.59	1.71	9.84
Total As Conc. (µg•L^{-1})	3	7	4	11	2	5.87	51	150	9	46	3	-
As(+3) conc. (µg•L^{-1})	3	0	0	1	0	1.17	7	95	5	0	0	-
As(+5) conc. (µg•L^{-1})	0.38	6.59	3.62	10.41	2.11	4.70	44.43	55.19	3.64	45.97	2.73	-
DOC (mg•L^{-1})	8.862	19.16	21.25	166	19.99	23.47	32.5	45.13	21.9	25.86	12.69	-
TN (mg•L^{-1})	0.5519	1.298	1.192	3.239	1.723	1.07	2.022	2.865	0.8169	1.228	0.6086	-
UV 254	0.24891	0.53591	0.57576	1.57734	0.91424	0.45	0.73772	0.6541	0.28417	0.66988	0.33369	1.78711
SUVA (L/mg-m)	2.81	2.80	2.71	0.95	4.57	1.90	2.27	1.45	1.30	2.59	2.63	
FI	1.36	1.55	1.59	1.48	1.56	1.62	1.52	1.43	1.562353	1.44	1.31	1.57
Max Em at 370 nm Ex	456	452	452	458	458	453	452	460	454	457	457	449
FrI	0.54	0.57	0.62	0.54	0.65	0.63	0.57	0.52	0.645092	0.52	0.54	0.63
HIX	15.73	25.11	14.36	17.41	15.43	19.00	27.31	27.65	16.25	24.14	13.09	8.29

Table A-8. Physical and chemical characteristics of Palm Island groundwater and adjacent surface water. Ionic strength, SI, Eh (As^{5+} /As^{3+}) and Eh (NO_3^-/NO_2^-) were calculated using Geochemist Workbench 10.0.

Sample ID	Palm FP SW	Palm 1	Palm 2	Palm 3	Palm 4	Palm 5	Palm 6
GPS coordinates Lat Long		-19.5472 23.1915	-19.5471 23.1913	-19.5469 23.1913	-19.54693 23.1912	-19.5469 23.1912	-19.5469 23.1912
Depth of Piezometer (m)							
Distance (m)	0	22.83	42.44	56.17	63.38	69.99	72.07
Conductivity (uS/cm)	102	140	470	1071	1865.00	3976	3580
pH	6.55	6.43	6.38	6.57	6.74	7.62	8.01
$\delta^{18}O$	-5.7	2.9	1.8	0.6	-0.3	-0.3	-0.5
δ D	-43	15	5	0	-8.6	-7	-9
Eh (V) (As^{5+} /As^{3+})*			0.0722	0.0422		-0.0625	-0.0965
Eh (V) (NO3-/NO2-)*	0.4286	0.4364	0.4412				0.3716
Ionic strength (molal)*	0.001467	0.002123	0.007733	0.01647	0.0	0.04494	0.03367
Alkalinity (mg•L^{-1} CaCO3)	77.7	108.1	332.4	742.1	1784.4	3593.1	2640.2
B (mg•L^{-1})	0.78	0.64	4.5	2.5	1.9	2.0	1.9
Na (mg•L^{-1})	84	80	25	36	296	629	568
Mg (mg•L^{-1})	11	20	6.4	28	36	40	7.3
S (mg•L^{-1})	< D. L.	< D. L.	< D. L.	< D. L.	< D. L.	< D. L.	< D. L.
K (mg•L^{-1})	50	34	18	116	127	555	535
Ca (mg•L^{-1})	58	131	29	83	53	10.3	5.6
Total Fe (mg•L^{-1})	< D. L	< D. L	< D. L	< D. L	< D. L	< D. L	< D. L
Fe(II) (mg•L^{-1})	0.45	0.32	1.51	0.40	0.4	0.26	0.33
Fluoride (mg•L^{-1})	0.32	0.29	0.91	0.75	1.31	1.37	1.94
Chloride (mg•L^{-1})	1.94	1.48	6.11	4.65	8.98	91.53	15.06
Nitrite (mg•L^{-1})	1.03	1.13	0.97	0.91	0.89	< D.L.	0.83
Bromide (mg•L^{-1})	< D.L.	< D.L.	< D.L.	< D.L.	0.93	0.85	0.85
Nitrate (mg•L^{-1})	1.11	1.29	1.28	< D.L.	< D.L.	8.20	8.78
Phosphate (mg•L^{-1})	< D.L.	< D.L.	0.84	< D.L.	< D.L.	< D.L.	< D.L.
Sulfate (mg•L^{-1})	1.45	1.42	3.62	3.23	2.10	8.45	7.11
Total As Conc. (µg•L^{-1})	3	1	7	13	11.4	143	60
As(+3) conc. (µg•L^{-1})	11	0	3	8	5.4	51	12
As(+5) conc. (µg•L^{-1})	0	1.08	3.81	4.75	6.0	92.04	47.29
DOC (mg•L^{-1})	32.53	24.57	30.23	24.79	30.3	29.78	23.94
TN (mg•L^{-1})	1.465	1.154	0.9974	1.131	1.5	1.415	1.35
UV 254	0.83809	0.6612	0.49249	0.33617	0.5	0.42878	0.44511
SUVA (L/mg-m)	2.58	2.69	1.63	1.36	1.7	1.44	1.86
FI	1.34	1.42	1.47	1.48	1.4	1.481002	1.53
FrI	0.51	0.54	0.61	0.60	0.5	0.56	0.57
Max Em at 370 nm Ex	460	458	456	462	461	456	460
HIX	18.70	19.16	7.64	16.52	29.60	37.75	36.37
Water type*	Na-HCO3	Ca-HCO3	Ca-HCO3	Ca-HCO3	H-HCO3	K-HCO3	K-HCO3

Table A-9. Physical and chemical characteristics of One Tusk Island groundwater. Ionic strength, SI, Eh (As^{5+} /As^{3+}) and Eh (NO_3^-/NO_2^-) were calculated using Geochemist Workbench 10.0.

Sample ID	OT 1	OT 2	OT 3	OT 4	OT 5	OT 6
GPS coordinates Lat Long	 -19.5414 23.1872	 -19.5414 23.1873	 -19.5415 23.1875	 -19.5416 23.1876	 -19.5416 23.1878	 -19.5417 23.1879
Depth of Piezometer (m)	2	2	2	2	2	2
Distance (m)	0	9.58	28.53	47.89	68.65	88.08
Conductivity (uS/cm)	1061	990	1656	1137	793	630
pH	7.1	6.96	6.85	6.71	7.05	6.77
$\delta^{18}O$	0.8	2.2	3.5	2.8	-1.3	0.4
δ D	-3	2	6	1	-17	-6
Eh (V) (As^{5+} /As^{3+})*		-0.0122	0.0203			
Eh (V) (NO3-/NO2-)*	0.4053	0.4017		0.418	0.3991	0.4165
Ionic strength (molal)*	0.01705	0.01395	0.02116	0.01985	0.01213	0.01107
Alkalinity (mg•L^{-1} CaCO3)	860.6	715.4	1185.2	808.7	564.3	471
B (mg•L^{-1})	3.3	2.2	1.7	1.3	1.1	1.4
Na (mg•L^{-1})	80	121	231	21	32	97
Mg (mg•L^{-1})	32	4	18	41	2	121
S (mg•L^{-1})	< D. L.	< D. L.	< D. L.	< D. L.	< D. L.	< D. L.
K (mg•L^{-1})	52	22	44	19	38	101
Ca (mg•L^{-1})	71	69	104	164	75	106
Total Fe (mg•L^{-1})	0.03	0.94	0.11	< D. L.	< D. L.	0.10
Fe(II) (mg•L^{-1})	0.59	0.84	0.80	0.32	0.45	0.42
Fluoride (mg•L^{-1})	0.10	0.78	0.55	0.55	0.70	0.48
Chloride (mg•L^{-1})	0.8	5.8	12.1	4.9	2.7	2.2
Nitrite (mg•L^{-1})	0.92	0.89	0.98	1.08	0.93	0.80
Bromide (mg•L^{-1})	< D.L.	< D.L.	0.90	< D.L.	< D.L.	< D.L.
Nitrate (mg•L^{-1})	2.05	0.79	< D.L.	1.08	1.02	0.94
Phosphate (mg•L^{-1})	< D.L.	< D.L.	1.43	0.92	< D.L.	< D.L.
Sulfate (mg•L^{-1})	1.5	1.6	1.6	2.0	2.3	1.6
Total As Conc. (µg•L^{-1})	9	39	22	9	5	4
As(+3) conc. (µg•L^{-1})	0	32	10	0	0	5
As(+5) conc. (µg•L^{-1})	8.84	6.78	11.23	8.75	4.93	-1.35
DOC (mg•L^{-1})	25.2	22.36	20.52	12.28	13.13	11.45
TN (mg•L^{-1})	1.27	1.33	0.78	0.58	0.49	0.45
UV 254	0.4996	0.5697	0.4024	0.2178	0.2835	0.2840
SUVA (L/mg-m)	1.98	2.55	1.96	1.77	2.16	2.48
FI	1.55	1.62	1.61	1.61	1.60	1.56
Max Em at 370 nm Ex	453	447	456	459	456	456
FrI	0.59	0.64	0.66	0.64	0.61	0.61
HIX	19.22	14.10	17.03	18.64	20.77	34.35
Water type*	Ca-HCO3	Na-HCO3	Ca-HCO3	Ca-HCO3	Ca-HCO3	Ca-HCO3

Appendix B - Figures

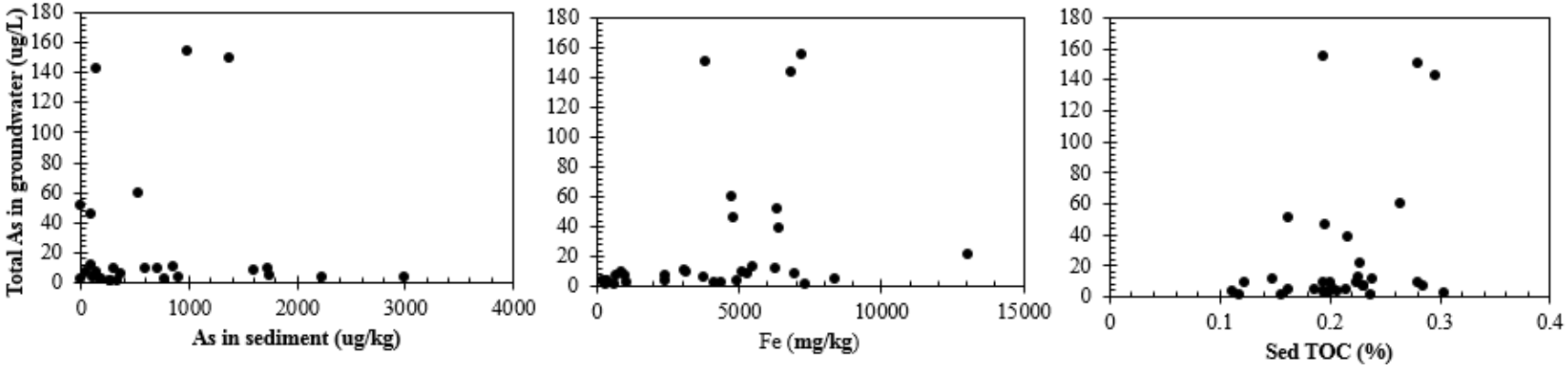

Figure B.1. Soil chemistry. Regression plot of Arsenic, Fe and TOC (b) content in sediment versus total arsenic in groundwater.

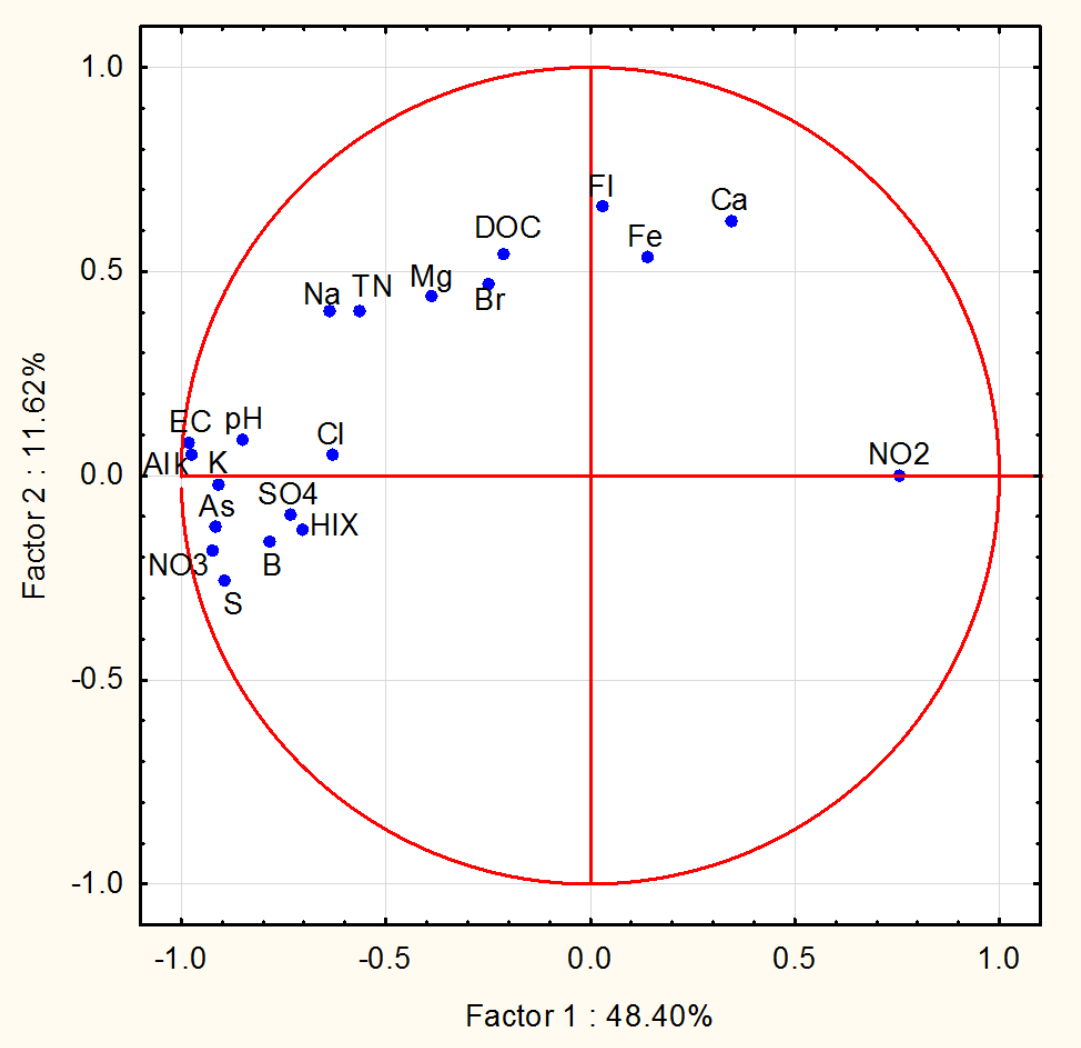

Figure B.2. PCA plot of Factor 1 and Factor 2 using 27 groundwater samples from New, Palm and One Tusk Islands. (*Analyzed with STATISCA*)

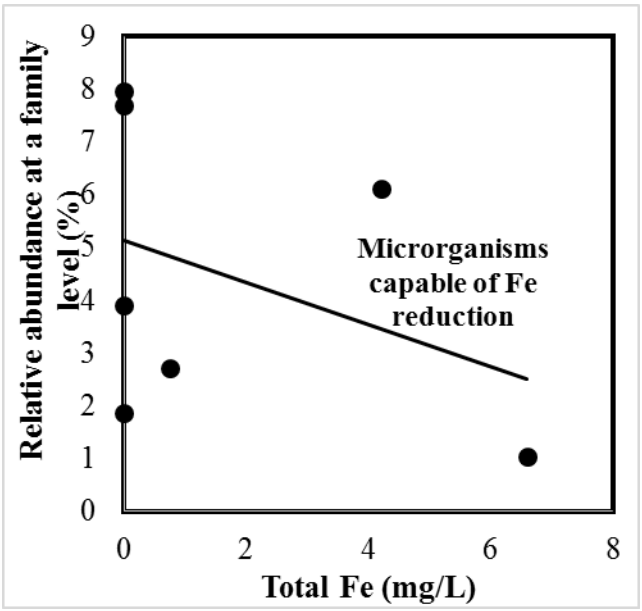

Figure B.3. Correlation plot of Methanogens at a order level and freshness index (B:α).

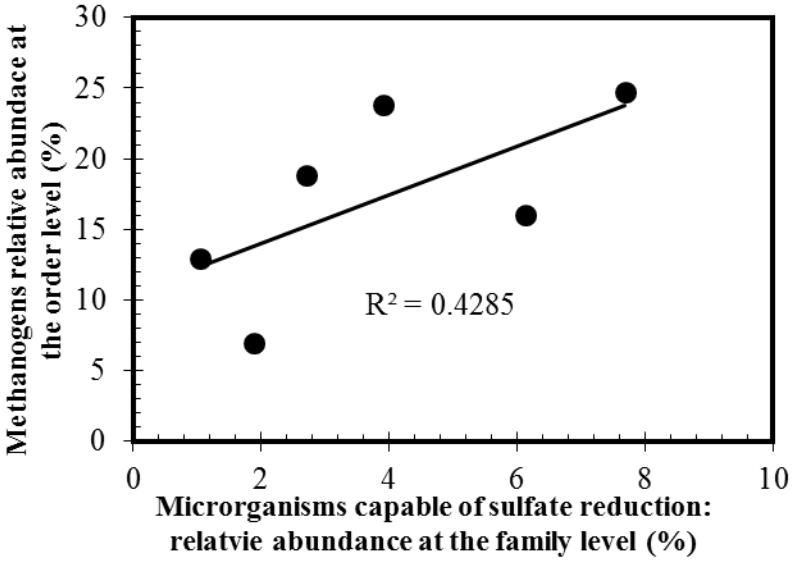

Figure B.4. Correlation plot of Methanogens at order level and microorganisms capable of sulfate reduction at family level (Desulfobacteraceae, Desulfobulbaceae, Desulfovibrionaceae Syntrophaceae Syntrophobacteraceae, Thermodesulfovibrionaceae, Desulfuromonadaceae).

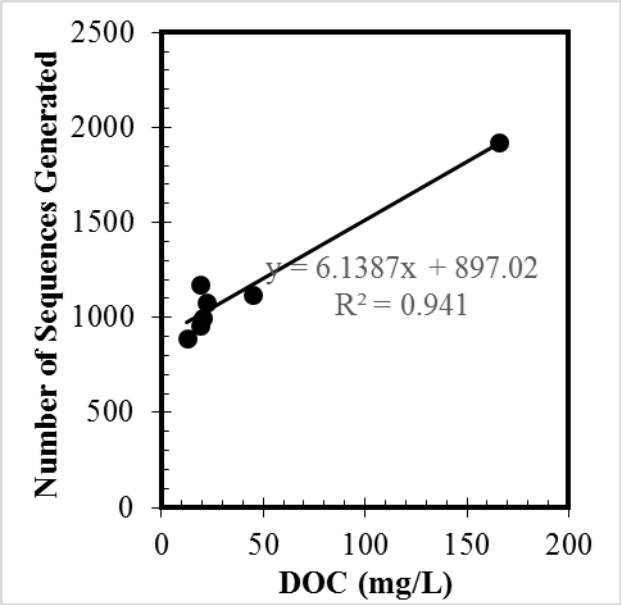

Figure B.5. Correlation plot of total number of sequences generated and DOC concentration.

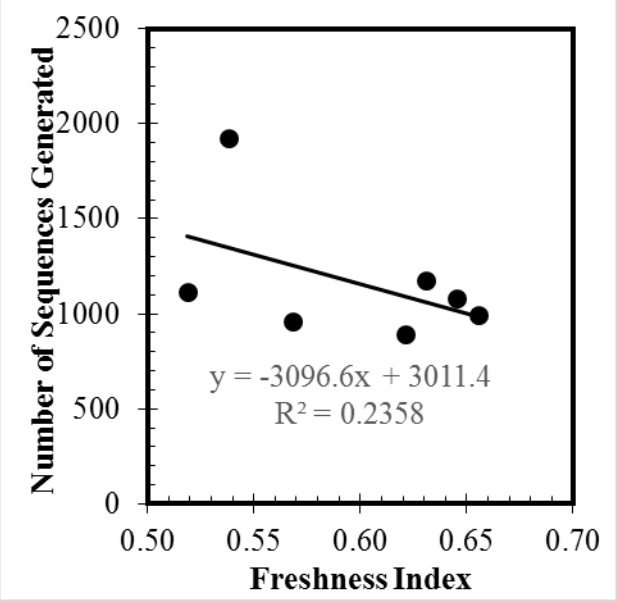

Figure B.6. Correlation plot of total number of sequences generated and B:α.

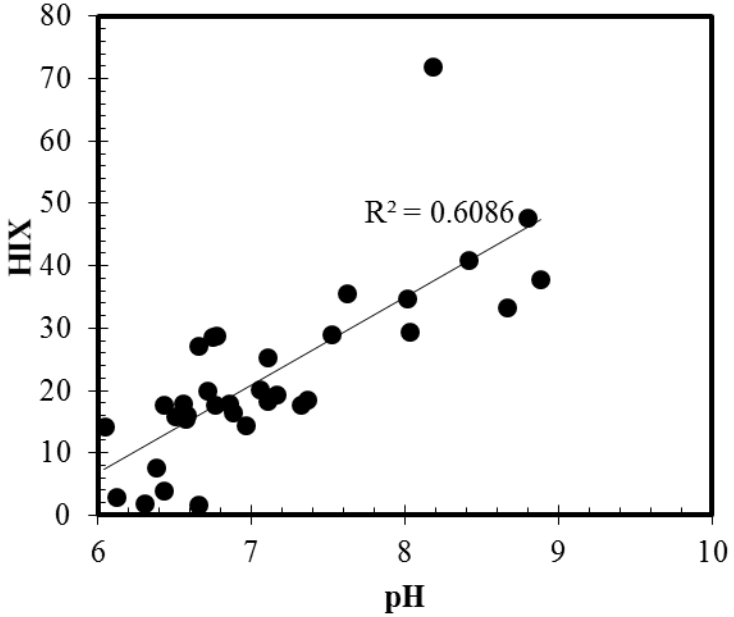

Figure B.7. Correlation plot of pH and humification index (HIX) for all four islands.

Appendix C - Fluorescence Excitation-Emission Matrix (EEM) 3-D Spectra

Camp Island

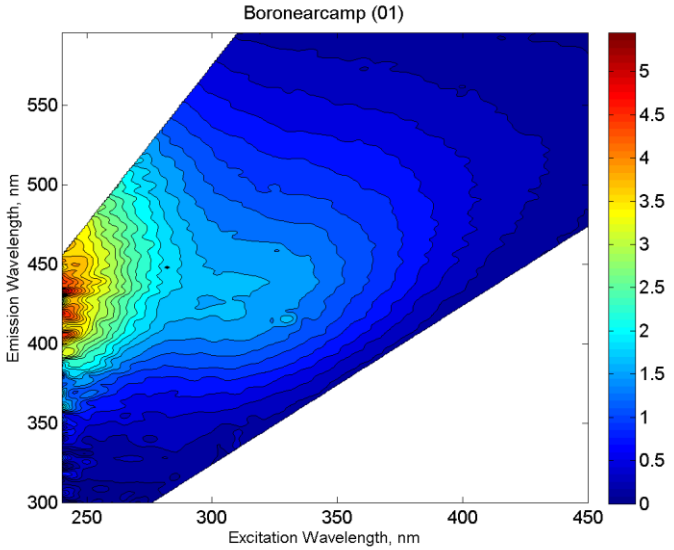

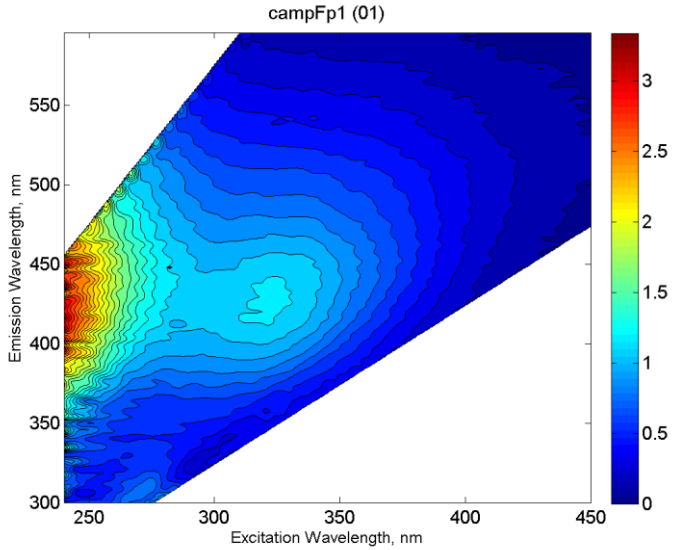

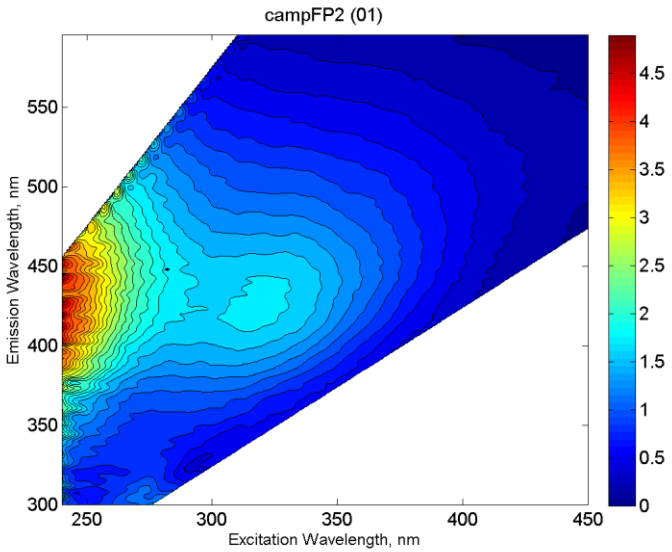
campFP2 (01)
Emission Wavelength, nm
Excitation Wavelength, nm
300
350
400
450
500
550
250
300
350
400
450
0
0.5
1
1.5
2
2.5
3
3.5
4
4.5

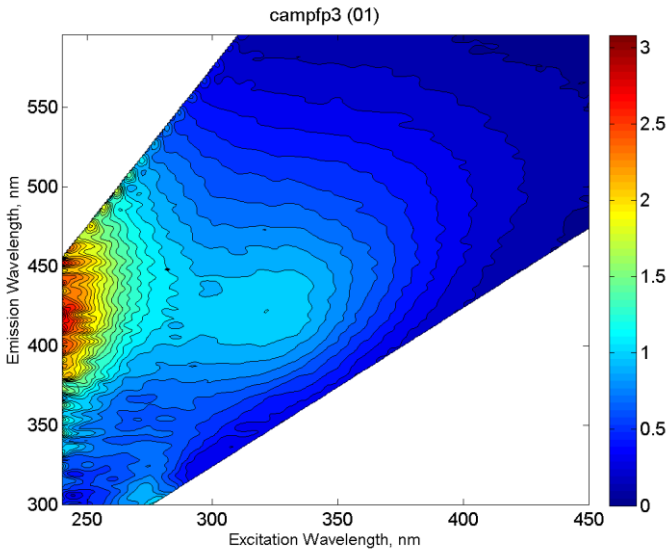
campfp3 (01)
Emission Wavelength, nm
Excitation Wavelength, nm
300
350
400
450
500
550
250
300
350
400
450
0
0.5
1
1.5
2
2.5
3

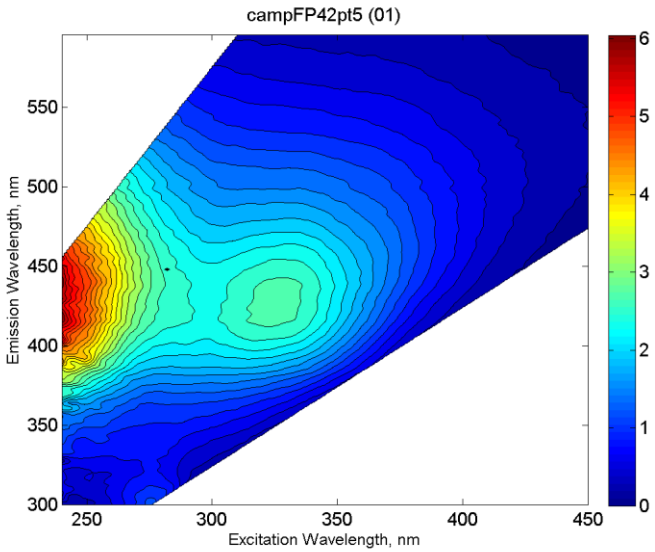
campFP42pt5 (01)
Emission Wavelength, nm
Excitation Wavelength, nm
300
350
400
450
500
550
250
300
350
400
450
0
1
2
3
4
5
6

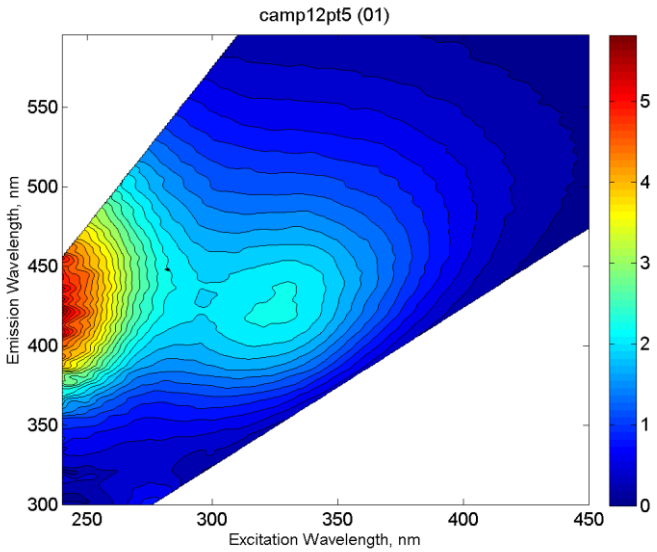
camp12pt5 (01)
Emission Wavelength, nm
Excitation Wavelength, nm
300
350
400
450
500
550
250
300
350
400
450
0
1
2
3
4
5

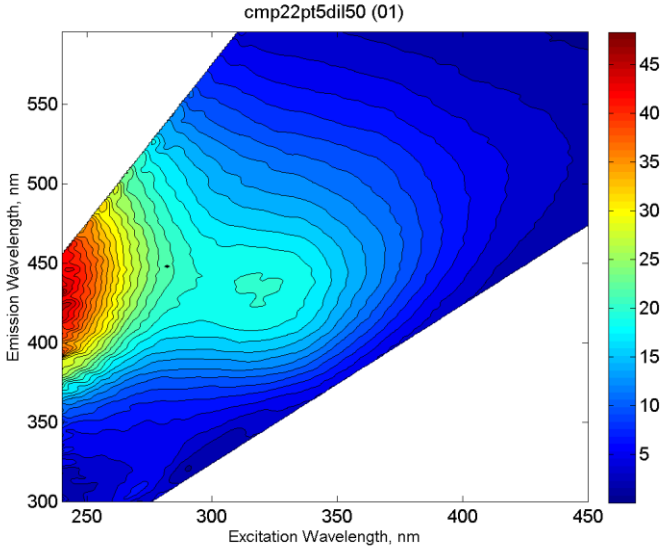
cmp22pt5dil50 (01)
Emission Wavelength, nm
Excitation Wavelength, nm
300
350
400
450
500
550
250
300
350
400
450
5
10
15
20
25
30
35
40
45

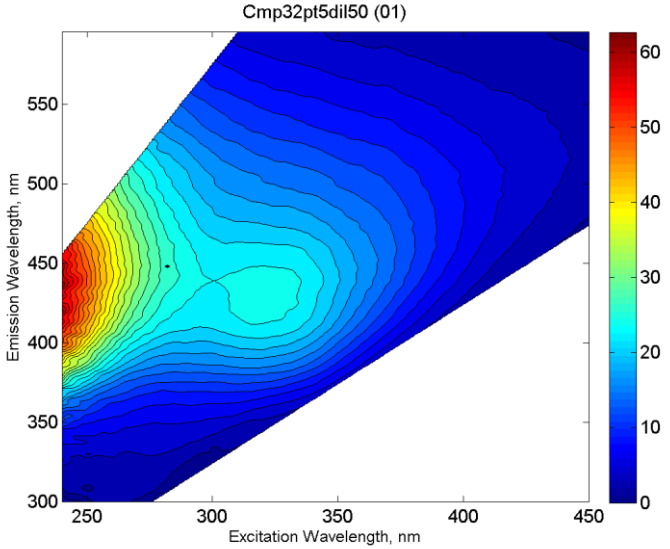
Cmp32pt5dil50 (01)
Emission Wavelength, nm
Excitation Wavelength, nm
300
350
400
450
500
550
250
300
350
400
450
0
10
20
30
40
50
60

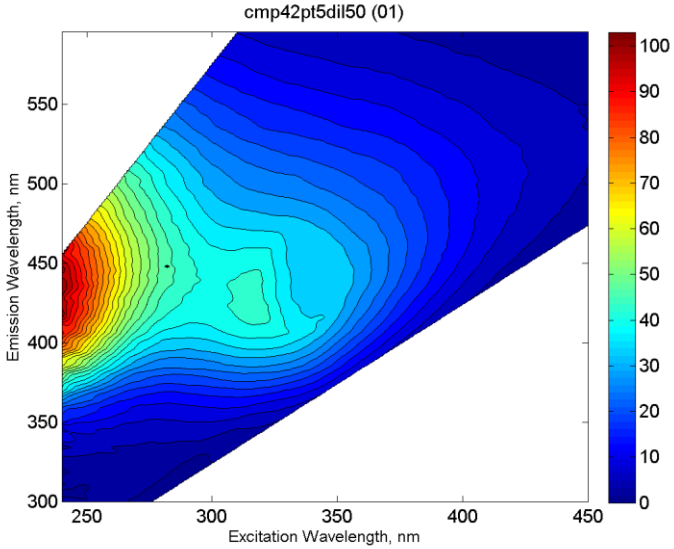
cmp42pt5dil50 (01)
Emission Wavelength, nm
Excitation Wavelength, nm
300
350
400
450
500
550
250
300
350
400
450
0
10
20
30
40
50
60
70
80
90
100

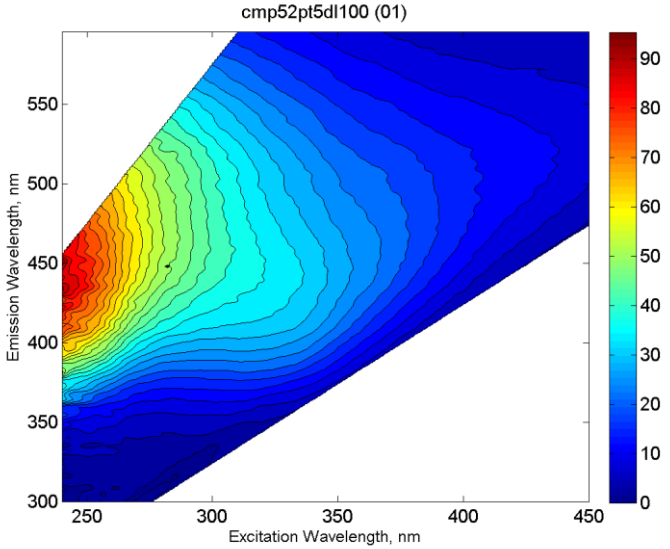
cmp52pt5dl100 (01)
Emission Wavelength, nm
Excitation Wavelength, nm
300
350
400
450
500
550
250
300
350
400
450
0
10
20
30
40
50
60
70
80
90

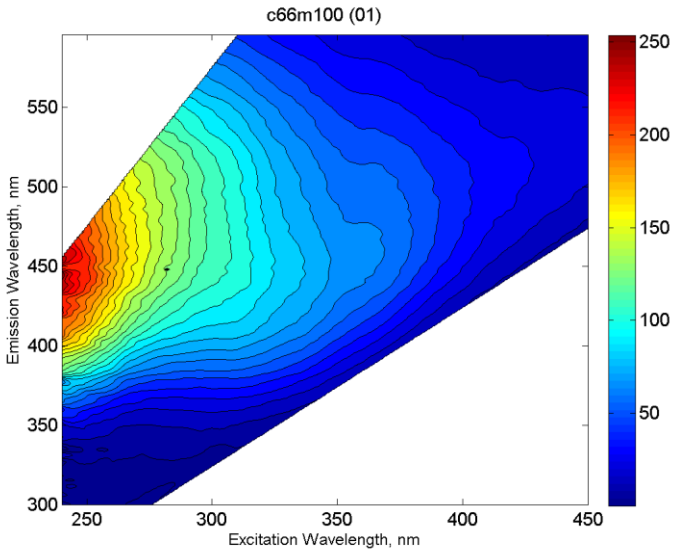
c66m100 (01)
Emission Wavelength, nm
Excitation Wavelength, nm
250
300
350
400
450
500
550
50
100
150
200
250

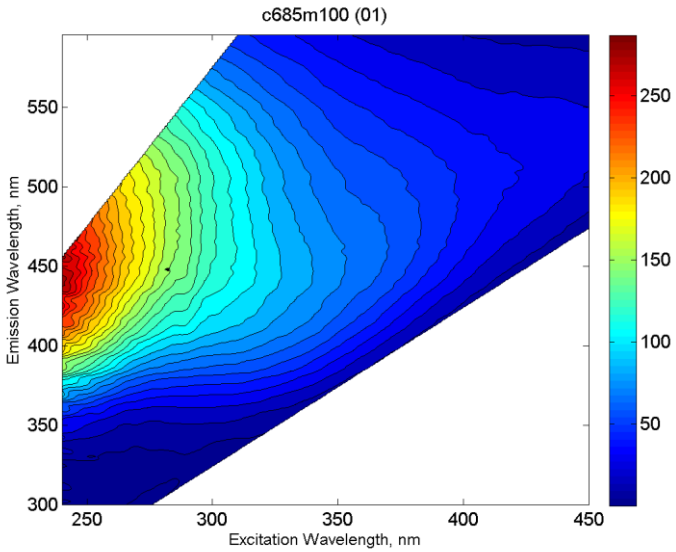
c685m100 (01)
Emission Wavelength, nm
Excitation Wavelength, nm
250
300
350
400
450
500
550
50
100
150
200
250

New Island

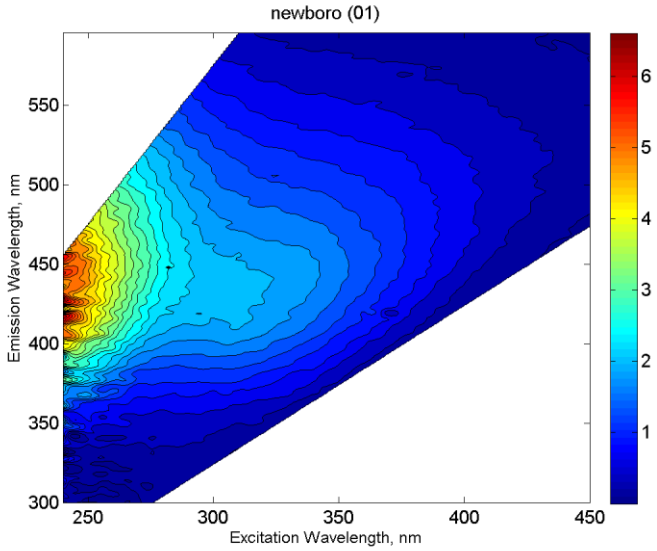
newboro (01)
Emission Wavelength, nm
Excitation Wavelength, nm
300
350
400
450
500
550
250
300
350
400
450
1
2
3
4
5
6

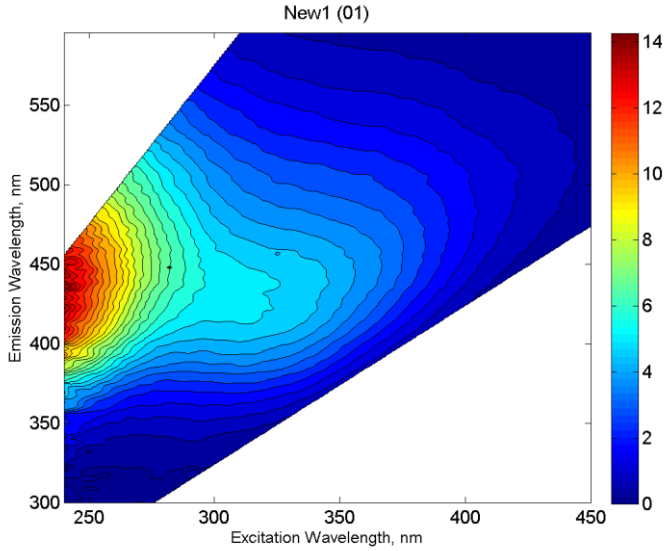
New1 (01)
Emission Wavelength, nm
Excitation Wavelength, nm
300
350
400
450
500
550
250
300
350
400
450
0
2
4
6
8
10
12
14

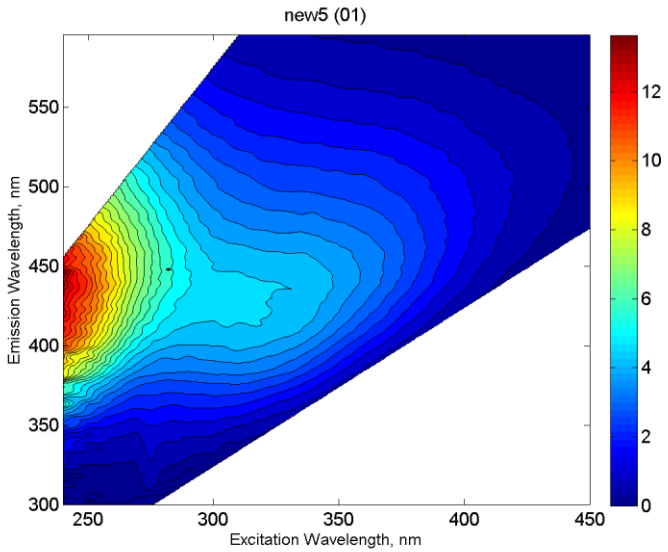
new5 (01)
Emission Wavelength, nm
Excitation Wavelength, nm
300
350
400
450
500
550
250
300
350
400
450
0
2
4
6
8
10
12

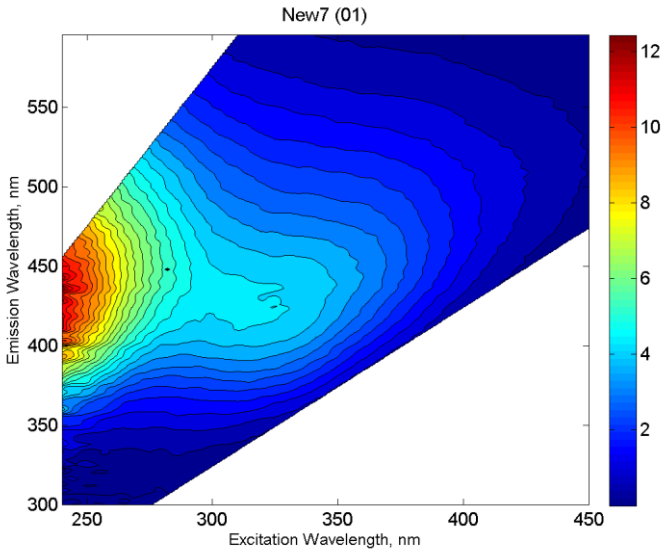
New7 (01)
Emission Wavelength, nm
Excitation Wavelength, nm
300
350
400
450
500
550
250
300
350
400
450
2
4
6
8
10
12

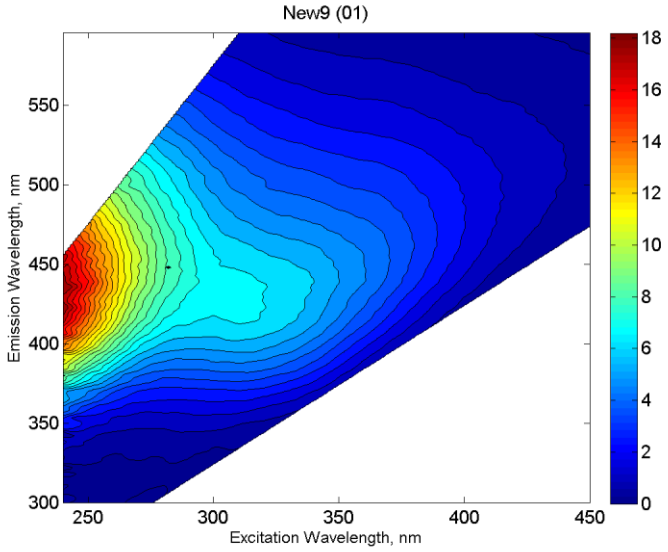
New9 (01)
Emission Wavelength, nm
Excitation Wavelength, nm
300
350
400
450
500
550
250
300
350
400
450
0
2
4
6
8
10
12
14
16
18

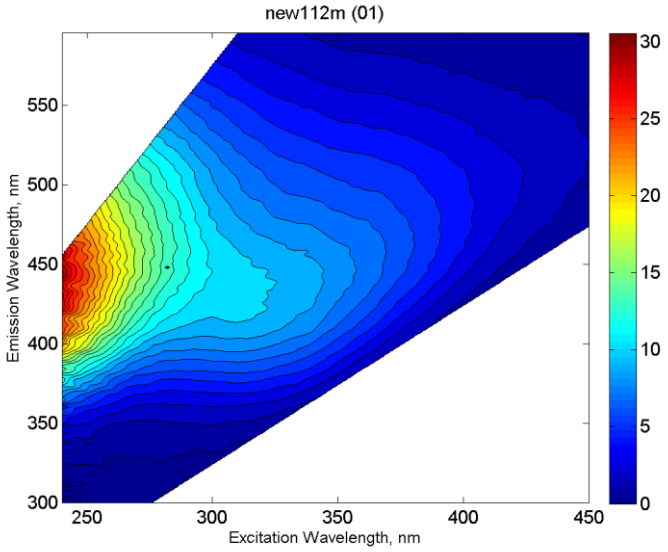
new112m (01)
Emission Wavelength, nm
Excitation Wavelength, nm
300
350
400
450
500
550
250
300
350
400
450
0
5
10
15
20
25
30

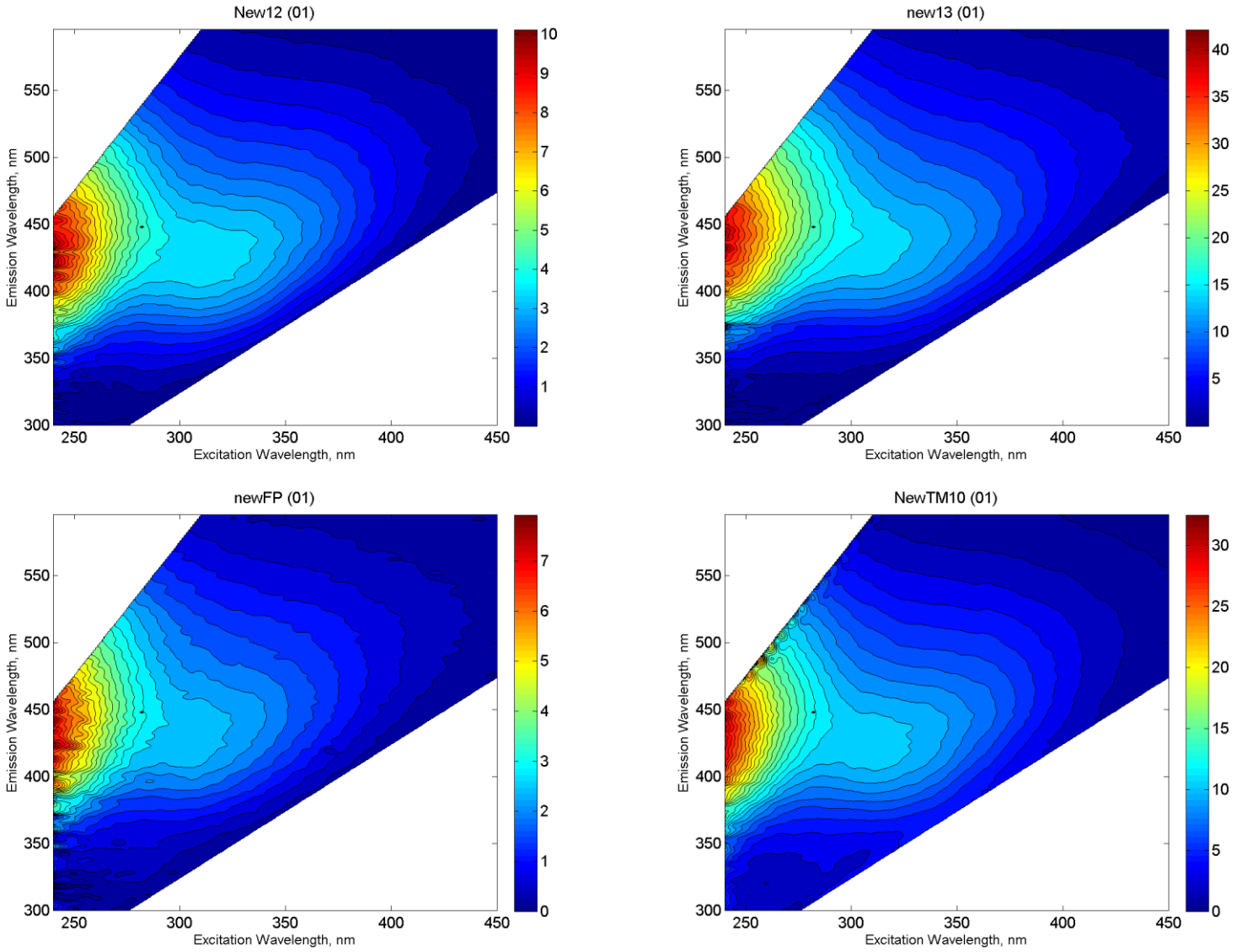
New12 (01)
new13 (01)
newFP (01)
NewTM10 (01)
Emission Wavelength, nm
Excitation Wavelength, nm
300
350
400
450
500
550
250
300
350
400
450
1
2
3
4
5
6
7
8
9
10
5
10
15
20
25
30
35
40
0
1
2
3
4
5
6
7
0
5
10
15
20
25
30

Palm Island

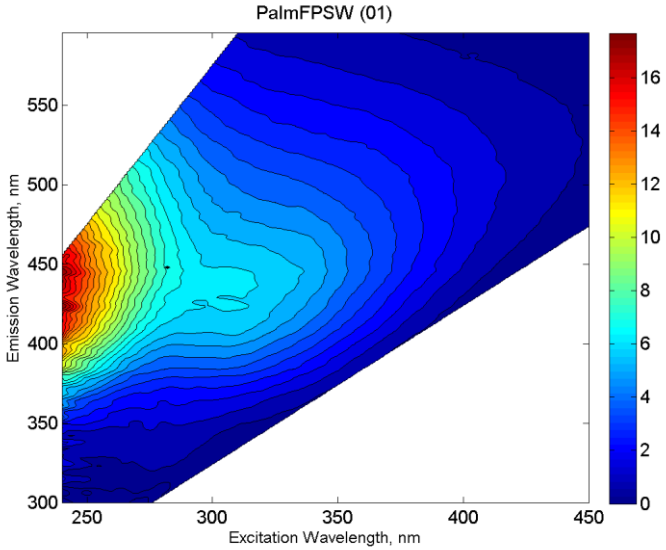
PalmFPSW (01)
Emission Wavelength, nm
Excitation Wavelength, nm
300
350
400
450
500
550
250
300
350
400
450
0
2
4
6
8
10
12
14
16

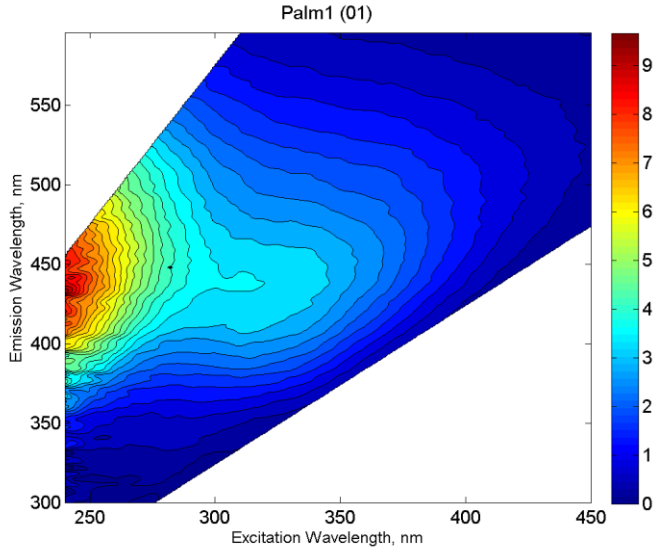
Palm1 (01)
Emission Wavelength, nm
Excitation Wavelength, nm
300
350
400
450
500
550
250
300
350
400
450
0
1
2
3
4
5
6
7
8
9

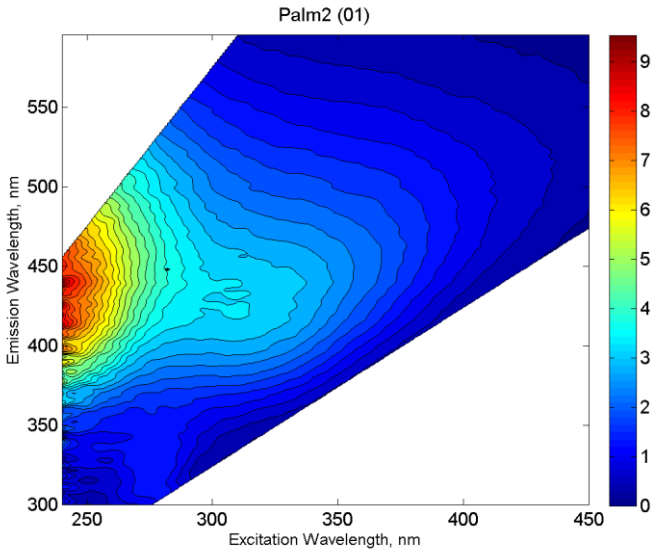
Palm2 (01)
Emission Wavelength, nm
Excitation Wavelength, nm
300
350
400
450
500
550
250
300
350
400
450
0
1
2
3
4
5
6
7
8
9

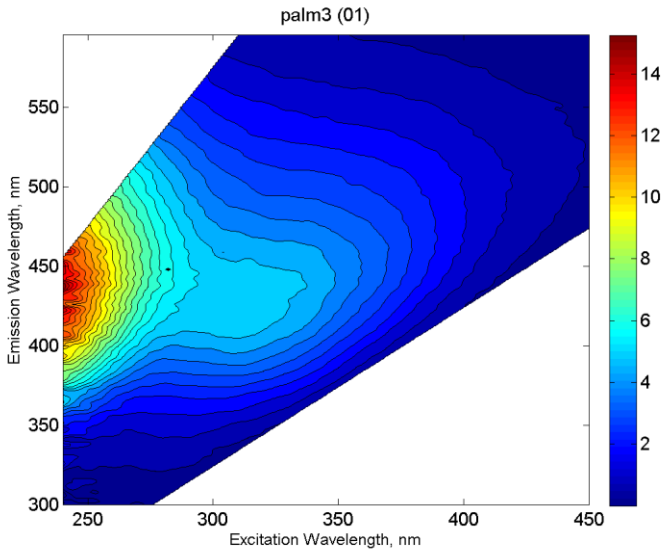
palm3 (01)
Emission Wavelength, nm
Excitation Wavelength, nm
300
350
400
450
500
550
250
300
350
400
450
2
4
6
8
10
12
14

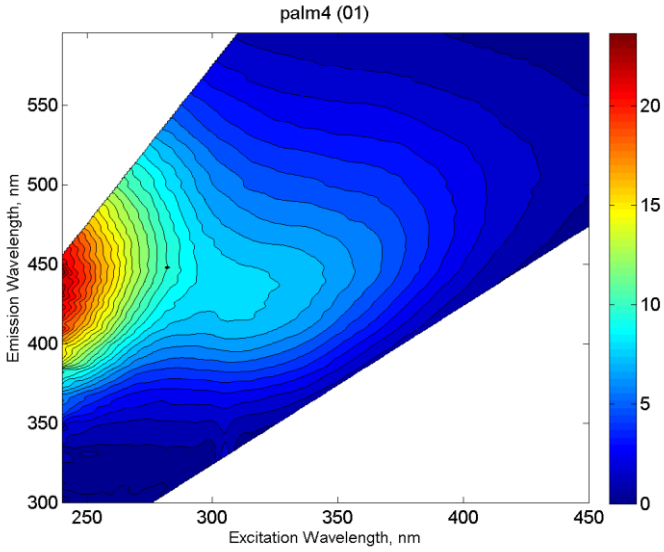
palm4 (01)
Emission Wavelength, nm
Excitation Wavelength, nm
300
350
400
450
500
550
250
300
350
400
450
0
5
10
15
20

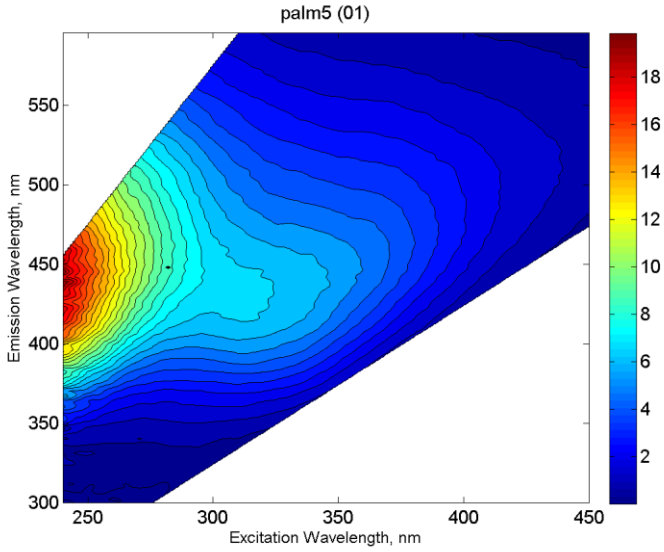
palm5 (01)
Emission Wavelength, nm
Excitation Wavelength, nm
300
350
400
450
500
550
250
300
350
400
450
2
4
6
8
10
12
14
16
18

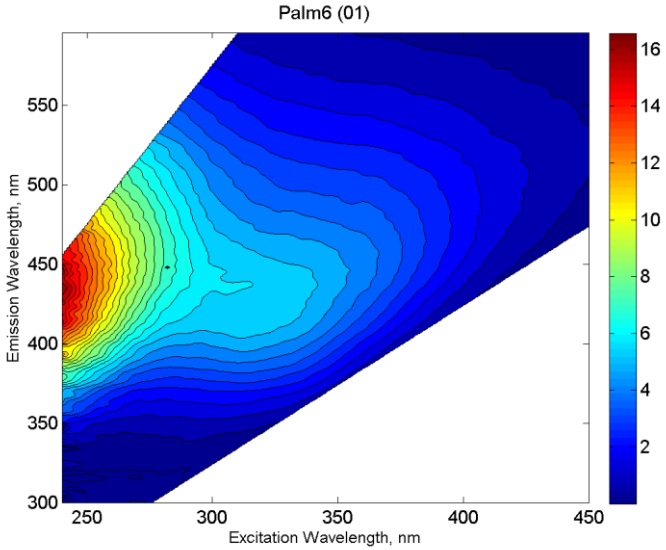
Palm6 (01)
Emission Wavelength, nm
Excitation Wavelength, nm
300
350
400
450
500
550
250
300
350
400
450
2
4
6
8
10
12
14
16

One Tusk Island

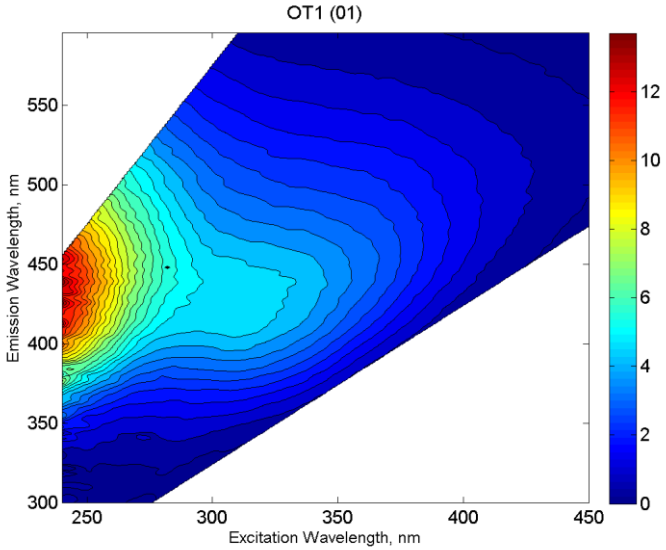

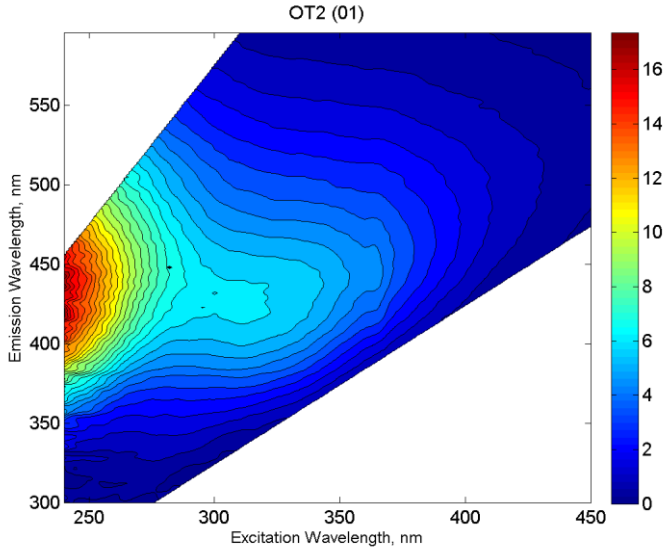

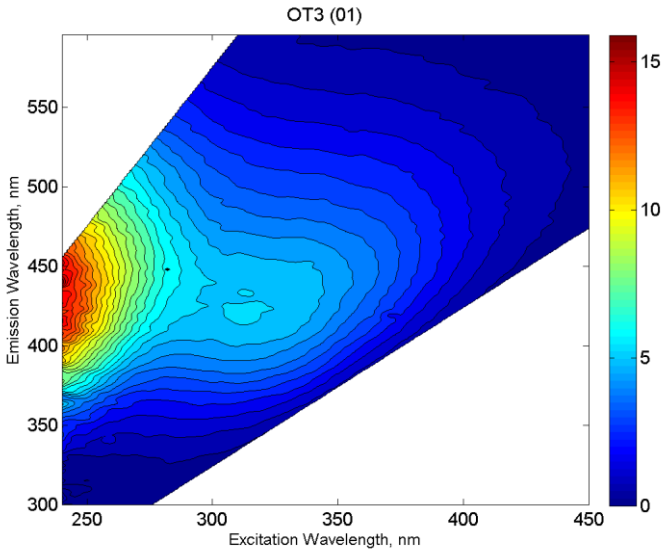
OT3 (01)
Emission Wavelength, nm
Excitation Wavelength, nm
300
350
400
450
500
550
250
300
350
400
450
0
5
10
15

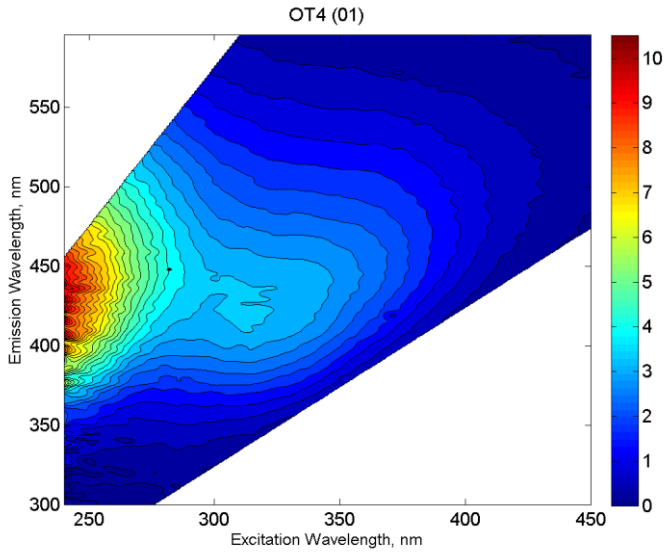
OT4 (01)
Emission Wavelength, nm
Excitation Wavelength, nm
300
350
400
450
500
550
250
300
350
400
450
0
1
2
3
4
5
6
7
8
9
10

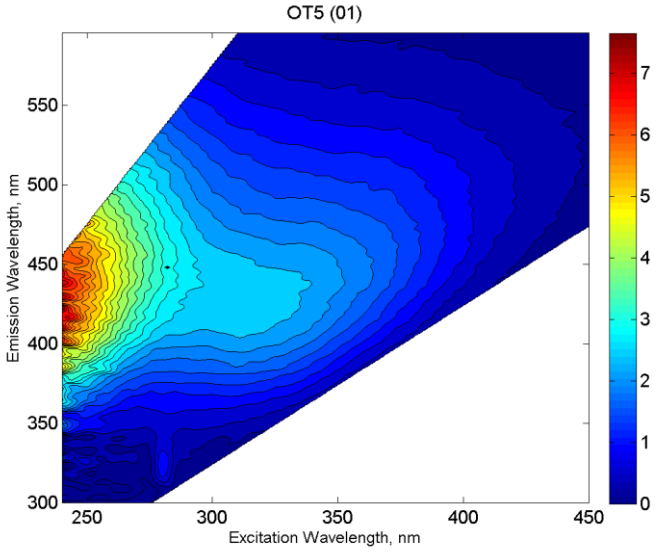
OT5 (01)
Emission Wavelength, nm
Excitation Wavelength, nm
300
350
400
450
500
550
250
300
350
400
450
0
1
2
3
4
5
6
7

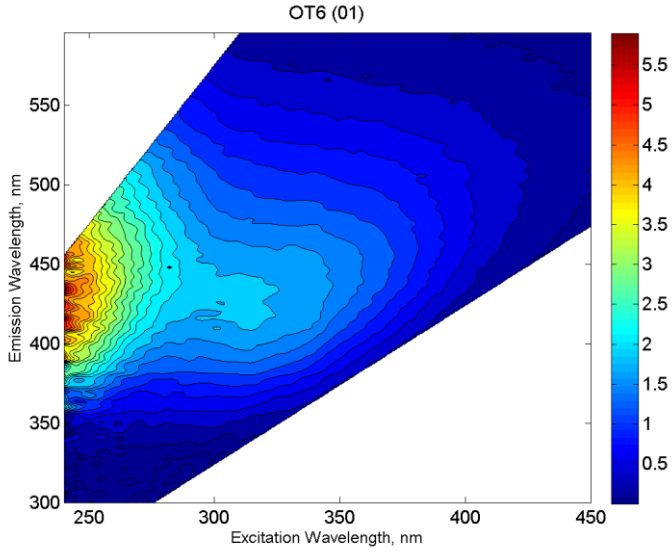
OT6 (01)
Emission Wavelength, nm
Excitation Wavelength, nm
300
350
400
450
500
550
250
300
350
400
450
0
0.5
1
1.5
2
2.5
3
3.5
4
4.5
5
5.5

Appendix D - Detailed Methods and Protocol

Gran-alkalinity titration

(Modified from Dr. Matthew Kirk's Gran Alkalinity protocol)

Equipment:

- FISHERBRAND 50ML BURETTE
- pH meter (calibrated to pH buffer 4,7, and 10)
- 25mL beaker
- Magnetic plate
- Magnetic stirrer
- 5mL micropipette

Titration procedure

1) Calibrate the pH meter. Follow the instructions in the manual.

Note that the sample needs to be the same temperature as the standards used to calibrate the meter, unless the electrode measures temperature simultaneously with pH.

2) Carefully pipet 10 mL of sample into a 25 mL beaker.
3) Put a small stir bar in the beaker and stir at moderate rpm (make sure you don't stir too fast because you will cause your sample to lose CO_2, which increases sample pH).
4) Measure and record the initial pH of the sample. You may have to wait a while for the measurement to stabilize (pH meter will display stable on the screen).
5) Start titrating the sample with acid using the digital burette. If you know beforehand that your sample has high alkalinity, use 0.2 N H2SO4. If not, use 0.02 N H2SO4. After you

add an aliquot of acid, let the pH stabilize and then record the acid volume you added and the pH. (See sample table)

6) Record about six pH and volume of acid added above pH ~4 and about six data pairs of pH and volume of acid added below pH 4.

Table D-1. Example Gran Alkalinity data

mL	pH
0.00	5.86
0.50	5.83
1.00	5.80
1.50	5.76
2.50	5.57
3.50	5.21
4.00	4.79
4.40	3.87
4.50	3.61
4.60	3.44
4.70	3.31
4.80	3.23
4.90	3.15

Don't forget to record initial pH at 0 mL acid added.

7) To do the calculations, the USGS online calculator works well: http://or.water.usgs.gov/alk/

8) Paste in the acid volume and pH data (note that you need to include the initial pH (at acid volume 0)). You also need to put in the acid concentration, temperature, sample volume, and make sure the acid concentration factor is set to 1.0, and check the Gran alkalinity box so it includes that method in the results. If you sample has high conductivity, you might also enter the conductivity data in the web-page.

9) I used the alkalinity determined from the fit of the data below pH 4 (the F1 line) (see figure below). If that line doesn't fit the titration data well, however, you can also use the fit of data above pH 4 (the F3 line).

The example data from Table **D-1**. were collected using a burette titration of a 10 mL sample at about 22°C. The acid used in the titration was 0.02N H_2SO_4. The F1 line fits the data well and indicates the sample contained **8.58 meq/L** total alkalinity. The F3 line yields a similar result, although it isn't constrained by as many data points as the F1 line so it is less trustworthy.

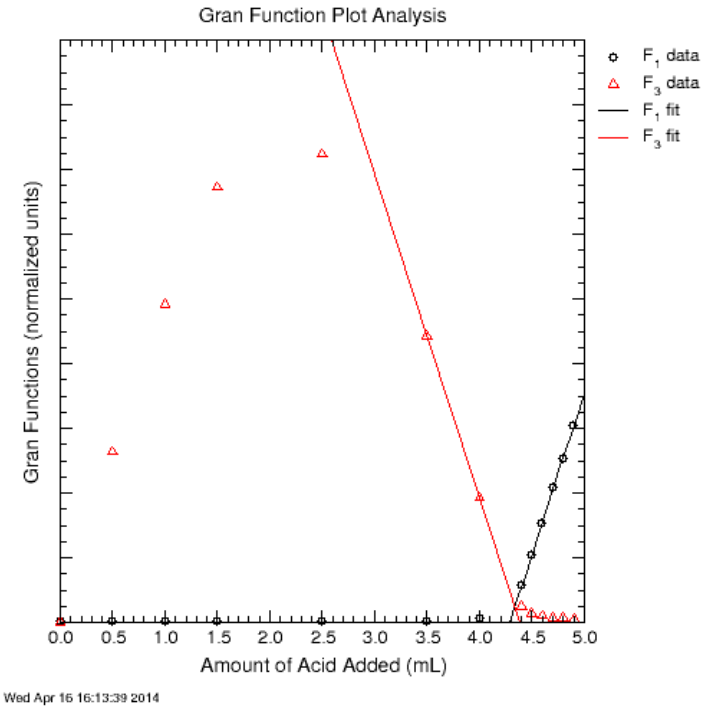

Figure D.1. Output plot from Gran-Alkalinity calculator

Additional reading

This website gives a brief description:

- http://or.water.usgs.gov/alk/methods.html
- Aquatic Chemistry by Stumm and Morgan

DNA Extraction

Modified from MoBIO Laboratories PowerSoil®DNA Isolation Kit Protocol

Equipment

- Microcentrifuge (10,000 x *g*)
- Pipettes (50 µl - 500 µl)
- Vortex
- Ethanol
- Ethanol Burner lamp

Table D-2. Component found in the MoBIO PowerSoil® DNA Isolation Kit (Kit Catalog # 12888-50) with description of each component.

Component	**Description**
PowerBead Tubes (contain 750 µl solution)	Contains a buffer that will (a) help disperse the soil particles, (b) begin to dissolve humic acids and (c) protect nucleic acids from degradation
PowerSoil® Solution C1	Contains SDS and other disruption agents required for complete cell lysis.
PowerSoil® Solution C2	Contains a reagent to precipitate non-DNA organic and inorganic material including humic substances, cell debris, and proteins.
PowerSoil® Solution C3	Second reagent to precipitate additional non-DNA organic and inorganic material including humic acid, cell debris, and proteins.
PowerSoil® Solution C4	High concentration salt solution
PowerSoil® Solution C5	Ethanol based wash solution used to further clean the DNA that is bound to the silica filter membrane in the Spin Filter.
PowerSoil® Solution C6	Sterile elution buffer
PowerSoil® Spin Filters (units in 2 ml tubes)	DNA is selectively bound to the silica membrane in the Spin Filter device
PowerSoil® 2 ml Collection Tubes	Sterile empty 2 mL tubes

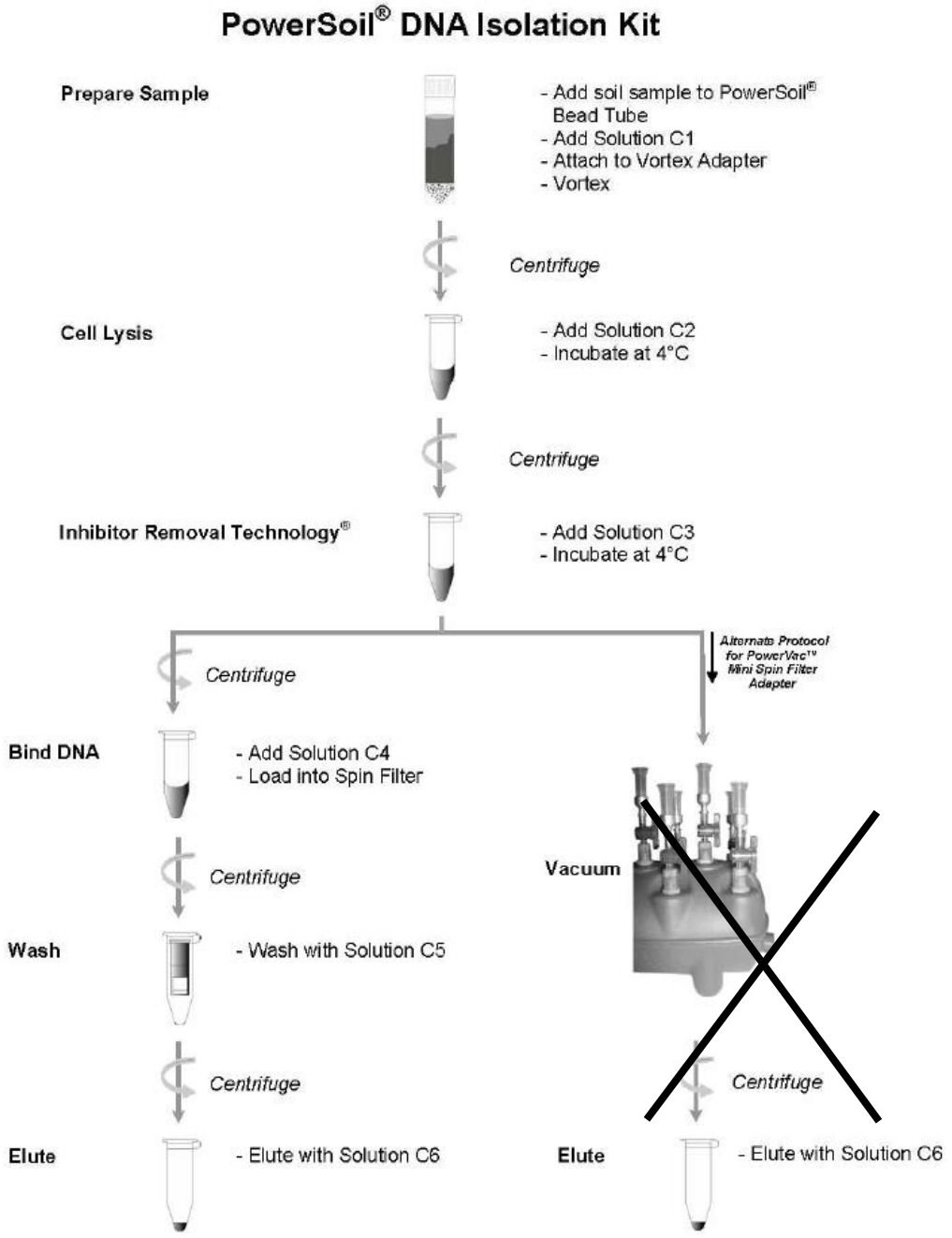

Figure D.2. Schematic diagram of DNA isolation kit protocol from MoBIO laboratories. The X mark indicates that this alternative protocol was not performed in this study.

1. Soil Sample separation

   1.1 I sterilized the anaerobic chamber with ethanol and used a sterile falcon tube for storage.

   1.2 I homogenized the soil samples by mixing it manually with spatula under anaerobic N_2 glove box at the KSU Agronomy lab. *Note: This procedure could be done outside the N_2 glove box, but I was separating the soil samples for cation analysis, which required no O_2 exposure, and microbial analysis.*

2. Modified User Protocol

   2.1 I sterilized the workspace by wiping it with isopropyl alcohol. The spatulas used to weigh the samples were sterilized by placing it over a flame (burner lamp) for a few seconds.

   2.2 To the PowerBead Tubes provided, I added ~.25 g of soil sample. **Error! Reference ource not found.** shows the weight of each sample added to the PowerBead Tubes.

Table D-3. Sample ID and weight for DNA isolation. New 5, 11, 12 and TM had double the weight specified in MoBIO protocol to ensure measurable DNA concentration.

Sample ID	Sample weight (g)
New 1	0.604
New 3	0.280
New 5	0.596
New 7	0.333
New 11	0.604
New 12	0.566
New TM WC	0.594
Camp 2	0.376
Camp 5	0.317

   2.3 I placed the mixed PowerBead Tubes with the sample in a vortex for a few seconds.

   2.4 I added 60 μL of C1 solution to the PowerBead Tube with sample using a sterile micropipette. Vortex the solution briefly.

2.5 I then incubated solution tube for 5 minutes in a water bath with ~ 70^{o}C water and vortex for 3-4 seconds. Repeat this step once.

2.6 I placed the solution mixture in centrifuge for 30 seconds using 10,000 x g setting and then decanted the supernatant (about 400 to 500 µl of supernatant) in a clean collection tube.

2.7 I added 250 µL of C2 solution, vortex for 5 seconds and incubated at 4^{o}C (using a freezer) for 5 minutes.

2.8 Centrifuge the tubes at room temperature for 1 minute at 10,000 x *g*.

2.9 I then transferred 600 µL of supernatant to a clean 2 mL collection tube.

2.10 I added 200 µL of C3 solution to the supernatant, incubated for 5 min at 4^{o}C then centrifuged for 1 min at 10, 000 x g and transfer 750 µL of the supernatant in a clean 2mL collection tube.

2.11 I added 1200 µL of C4 solution to the supernatant and vortex briefly.

2.12 I loaded ~ 675 µl of supernatant onto a Spin Filter and centrifuged for 1 minute at 10,000 x *g* and

2.13 I took the spin filter out with a sterilized tweezer and discarded the flow through.

2.14 I then added ~675 µl of supernatant step 2.11 to the Spin Filter and centrifuged for 1 min at 10,000 x *g*.

2.15 I repeated steps 2.12 to 2.14 twice until all supernatant from 2.11 were filtered through the spin filter.

2.16 I then added 500 µl of Solution C5 and centrifuge for 30 seconds at 10,000 x *g and*

2.17 I d*iscarded* the flow through from step 2.16 and centrifuged again for 1 minute at 10,000 x *g*.

2.18 I carefully placed the Spin Filter to a clean 2 mL collection tube and added 100mL of solution C6, centrifuged for 30 seconds at 10,000 x g and discard the Spin Filter.

2.19 The quality and quantity of the extracted DNA was determined using NanoDrop (from KSU Integrated Genomics Department) Spectrophotometer of 1-2uL of aliquot.

2.20 The extracted DNA was sent to MR DNA sequencing lab (Shallowater, TX) for amplicon pyrosequencing.